A SHORELINE PREDICTION MODEL

by

BOON CHER HAR
B.Sc.(Hons), The Queen's University Of Belfast, 1981

A THESIS SUBMITTED IN PARTIAL FULFILMENT OF
THE REQUIREMENTS FOR THE DEGREE OF
MASTER OF APPLIED SCIENCE

in

THE FACULTY OF GRADUATE STUDIES
Department Of Civil Engineering

We accept this thesis as conforming
to the required standard

THE UNIVERSITY OF BRITISH COLUMBIA
January 1984

In presenting this thesis in partial fulfilment of the requirements for an advanced degree at the University of British Columbia, I agree that the Library shall make it freely available for reference and study. I further agree that permission for extensive copying of this thesis for scholarly purposes may be granted by the head of my department or by his or her representatives. It is understood that copying or publication of this thesis for financial gain shall not be allowed without my written permission.

Department of Civil Engineering

The University of British Columbia
1956 Main Mall
Vancouver, Canada
V6T 1Y3

Date 2 Feb 1984

ABSTRACT

A numerical model is developed to predict shoreline changes as a function of deep water wave conditions and nearshore bathymetry. The model consists of three components, the wave refraction and shoaling component, the longshore transport component, and the on-offshore component. The refraction and shoaling component is based on the irrotationality of the wave number K, and the conservation of energy equations suggested by Noda (1974), while the longshore transport component is based on the CERC longshore transport equation. A finite difference scheme is adopted to solve both the wave refraction and the longshore transport governing equations. The third component, the on-offshore transport (beach profile change) component is based on a set of equations developed from some of the known aspects of behaviour observed by other investigators. It is also based on the results obtained from a set of experiments conducted on equilibrium profile changes, and on a proposed criteria for on or offshore sediment motion.

The model is used to simulate the shoreline changes due to a littoral barrier orientated normally to the shoreline, and to predict the changes of a beach nourishment plan. Results of these simulations show that, in addition to the longshore transport influences, the on-offshore beach modification has a large influence on shoreline retreat under more severe wave attack.

ACKNOWLEDGEMENTS

The author is very grateful to the financial support, encouragement and guidance given by his supervisor, Professor M. C. Quick.

The author would also like to thank Dr. M. Issacson for his valuable suggestions.

TABLE OF CONTENTS

LIST OF FIGURES

LIST OF TABLES

CHAPTER 1

INTRODUCTION

Over the past decade, there have been dramatic increases in the demand for coastal developments. This new demand is partly due to the increasing affluence of the people asking for more coastal recreational facilities, and partly due to the ever increasing population trying to get away from the crowded cities. In countries where land shortage is an acute problem, coastal development like sea reclaimation may prove to be the only viable solution. A good example is Singapore where reclaimed land provides not only space for housing development but recreational development as well.

Associated with this trend is the increasing demand for solutions on how to protect and manage this new economic resource. There are many questions regarding the protection of these shorelines. Among the more pressing ones are:

1. What are the causes of beach erosion, and under what situation do we expect it to occur?
2. If shore protection structures like groynes and jetties are built, what are the impacts these structures have on the beach?

3. What changes to expect when shoreline is altered for a new usage, say, building an artificial beach?

4. How to predict the extent of damage on the beach caused by storm or similar destructive waves?

This report will not try to provide the answers to all the questions above, as the nearshore processes are complex and interconnected, and many are still poorly understood. However with the existing knowledge on longshore transport, beach changes and nearshore currents, an attempt to formulate a simple model on shoreline as well as beach profile changes can be made. The use of such a model will give a 'first cut' solution to some of the above questions.

Presented in this report is the stage by stage development of such a model. Chapter three shows the wave refraction and shoaling subroutine which will be providing the prediction of nearshore wave climate from the given offshore climate. In chapter four, the longshore transport routine is developed based on the CERC transport formula. Also shown in the same chapter are the results obtained using this longshore transport routine on some typical shoreline situations.

Chapter five presents an account of the present experimental studies on beach profile changes. It also highlights some key aspects of behaviour which are used in the on-offshore transport routine which calculates the beach profile change. Chapter six shows the development of this profile change routine. The algorithms of this routine are then tested using the experimental results of chapter five. This routine is later merged with the longshore transport routine to form the complete model. Results from this final model are also shown.

Lastly, conclusions drawn from all the modelling results are given in chapter seven.

CHAPTER 2

NEARSHORE CURRENT AND TRANSPORT EQUATION REVIEW

2.1 Introduction

This chapter reviews briefly the theoretical background on the generation and evaluation of nearshore currents, as well as the resulting sand transport. The main focus is on the wave-induced longshore current and the longshore transport. A survey of the various sediment transport rate formula is also presented.

2.2 Nearshore Currents

Nearshore currents are of particular interest to coastal engineers. One of the main reasons is that these currents are believed to be the chief cause of littoral or longshore transport. These nearshore currents can be generated by wind, by tides or by wind generated waves. Of all these, the wave-induced current is the most dominant and the most important.

In the nearshore region, there exist two main types of wave induced currents. The rip current which is associated with the circulation cell and the longshore current which is due to oblique wave attacks on the shore.

Rip currents are the seaward flowing component of the circulation cell and as such its role in longshore transport is minimal. There have been many studies (Bowen, 1969; Bowen and Inman, 1969; Hino, 1975) on rip currents since it was first studied by Shepard et al (1941). Reference can be made to Dalyrmple (1978) for a review on the more recent theories on rip currents and their generation.

2.3 Longshore Currents

Longshore currents play an important part in the longshore movement of material. It is this movement which is fundamental to the formation of many coastal features. There are many early theories on the generation of longshore currents. These early theories can be categorised according to the basis of their approaches. Galvin (1967) reviewed most of the significant ones and tested some of the dozen or more predictive equations on longshore current velocity. Among his conclusions, Galvin found that none of the equations gave an acceptable prediction of the longhore current velocity. Since then, there have been new investigations, two of which will be described here, for they arrived at similar equations from different approaches.

2.3.1 Radiation Stress Approach

Longuet-Higgins (1970a) re-introduced the momentum flux approach of Putnam et al (1949). The model of Putnam was shown to have been based on erroneous assumptions, because in the model's conservation of momentum equation, Putnam equated the longshore component of the breaker velocity to the current velocity. This is wrong as it can be shown that the longshore current velocity exceeds the longshore component of the breaker velocity (Galvin, 1967).

Modifying the approach, Longuet-Higgins proposed a new method of calculating the momentum flux of the waves using the concepts of radiation stress introduced by Longuet-Higgins and Stewart (1964). The resulting equation for the mean longshore current velocity, $\overline{V}$, with respect to time is

$$[2.1] \qquad \overline{V} = \frac{5\pi}{8} \propto \frac{\tan\beta}{C_f} (gh) \frac{\sin\theta_0}{C_0}$$

where H = wave height

h = water depth

g = gravitational acceleration

$\tan\beta$ = beach slope

θ_0, C_0 = the wave angle and celerity in deepwater

and C_f = the beach bottom friction coefficient.

From equation [2.1], if C_f and $\tan\beta$ are constant,

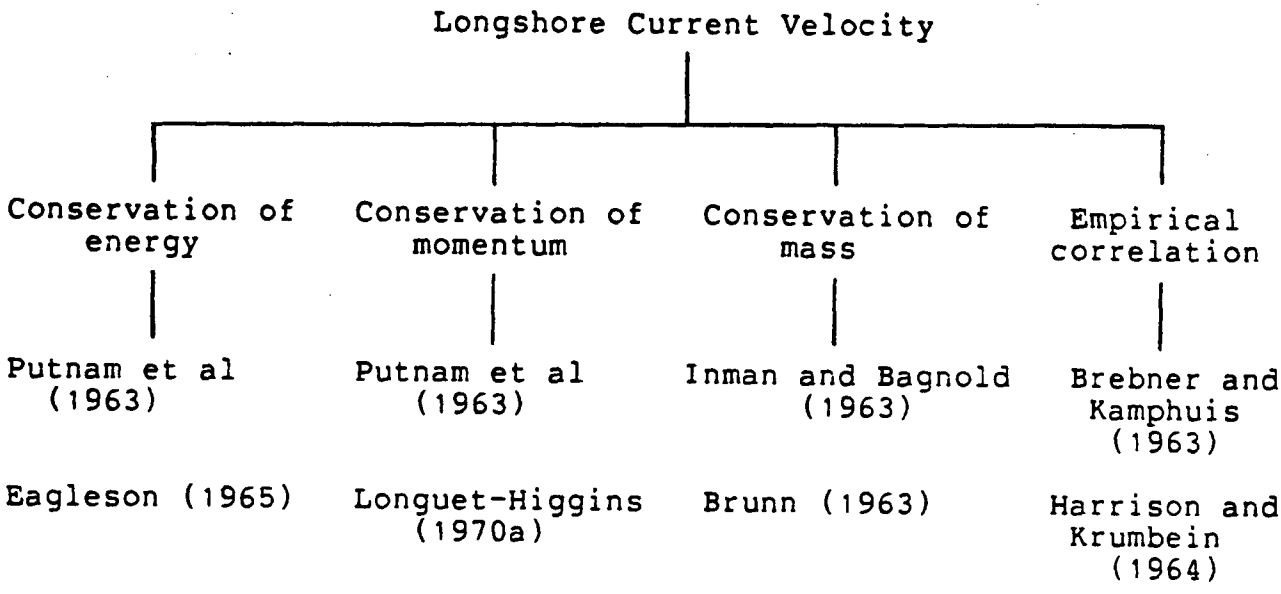

Figure 2.1 Different longshore current velocity models

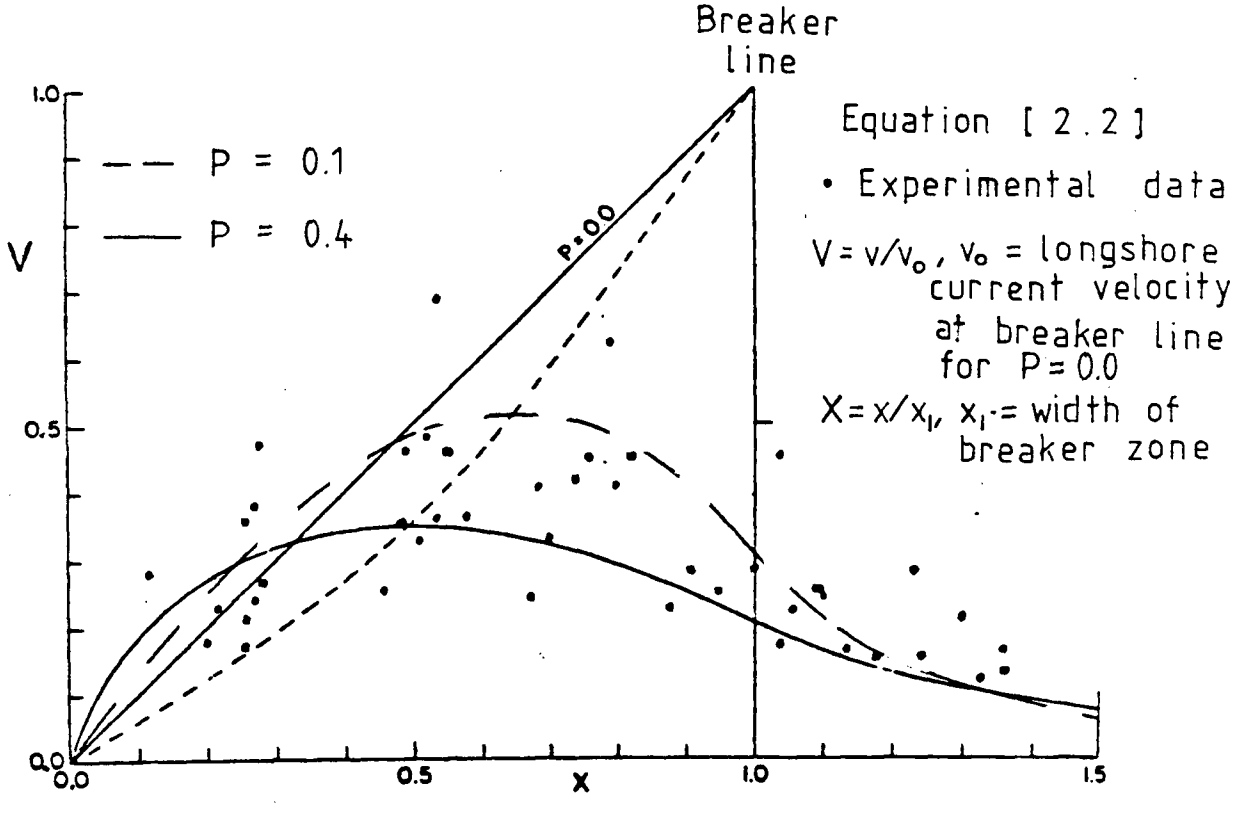

Figure 2.2 (After Longuet-Higgins, 1970b) A comparison between measured longshore current velocity and theorectical distributions

the mean longshore current velocity will vary linearly from zero at the shoreline to maximum at the breaker line. Outside the surf zone, it is assumed that there will be no wave breaking and hence no energy dissipation and no driving force for the current. Thus the distribution of the current across the surf zone is just a triangular distribution with a discontinuity at the breaker line. But laboratory and field data indicated no such discontinuity at the breaker line (figure 2.2).

One of the reasons for this difference is found to be the exclusion of horizontal mixing which is due to the horizontal eddy viscosity. In a real fluid, a discontinuity as shown in figure 2.2 cannot exist. The effect of introducing the horizontal mixing will be to flatten and smoothen the distribution profile. This will result in a better fit of the data. The maximum value of the longshore current is then no longer at the breaker line, but a little shoreward of that line which is found to be the case in the field.

Bowen (1969a) and Longuet-Higgins (1970b) introduced this horizontal mixing and obtained equation [2.2] for the longshore current velocity (see figure 2.2). P is a parameter used to indicate the degree of mixing. From a comparison with the data of Galvin and Eagleson (1965) the value of P was found to lie between 0.1 (little mixing) and 0.5 (greater mixing).

$$[2.2] \qquad V \begin{cases} A x + B_1 x^{P_1} & 0 < x < 1 \\ B_2 x^{P_2} & 1 < x < \infty \end{cases}$$

where A, B_1, B_2, P_1 and P_2 are all constants depending on P.

$$A = \frac{1}{(1 - 5p/2)} \qquad P_1, P_2 = -\frac{3}{4} \pm \sqrt{\frac{9}{16} + \frac{1}{p}}$$

[2.3]

$$B = \frac{P_2 - 1}{P_1 - P_2} \qquad B = \frac{P_1 - 1}{P_1 - P_2} A$$

Using equation [2.2] will be very tedious and requires the value of P to be known. As such, the Shore Protection Manual (1977) suggested using equation [2.4], an equation modified from the above approach, to calculate the maximum longshore current velocity in the surf zone:

$$[2.4] \qquad Vm = 20.7 \tan\beta (g h_b)^{1/2} \sin\theta_b$$

where h_b is the water depth at the breaker line.

This equation will give only the maximum current value, and not the whole variation across the surf zone, as

described by equation [2.2]. The constant 20.7 in equation [2.4] was obtained from the calibration of the equation with the laboratory data of Galvin et al (1965), and the field data of Putnam et al (1949). Also incorporated into equation [2.5] were the values of P and C_f as 0.2 and 0.01 respectively. The C_f value of 0.01 was based on the investigations by Prandtl (1952), Bretschneider (1954) and Meyer (1969).

2.3.2 Semi-Empirical Approach

From littoral transport studies, Komar and Inman (1970) introduced a longshore current velocity equation similar to equation [2.1]:

$$[2.5] \qquad \overline{V} = 2.7\ Um\ Sin\ \theta_b$$

where Um is the 'maximum orbital velocity under the wave' evaluated at the breaker line. This equation was obtained by a very different approach. Komar et al initially developed two models for longshore sand transport rate. They found that both the models agree well with field data. Prompted by this agreement, they equated the two transport equations for these apparently independent models. This leads to equation [2.6] which they have shown to be supported by field data.

The similarity of equation [2.1] and [2.5] can be seen if breaker line conditions, $C_b = \sqrt{gh}$ and $Um \doteq \alpha\sqrt{gh}$ are substituted into equation [2.1]:

$$[2.6] \qquad \bar{V} = \frac{5\pi}{8} \alpha \frac{\tan\beta}{C_f} \sqrt{gh_b} \sin\theta_b$$

Both these equations are similar, except that equation [2.5] implies the ratio $\tan\beta/C_f$ must be a constant. Komar et al presented field and laboratory data in a plot of $\bar{V}$ against $UmSin\theta_b$, and showed that the slope of the best fit line is indeed 2.7. From this they concluded that $\tan\beta/C_f$ is constant.

However, C_f was shown to have an approximate value of 0.01. Therefore, the ratio $\tan\beta/C_f$ should not be a constant for different beach slope. Longuet-Higgins suggested that this apparent constancy can be explained. With an increase in the beach slope $\tan\beta$, there would be an increase in the dissipation of energy by breaking and hence an increase in the level of turbulence. This would seem likely to effect the horizontal mixing which will indirectly bring the value of $\bar{V}$ down, and maintains an apparent constancy for the ratio $\tan\beta/C_f$ in equation [2.5].

To date, the actual relationship between the longshore current velocity and the beach slope is still relatively unknown.

2.4 Longshore Transport

Longshore transport is the movement of beach material in the littoral zone by waves and currents in the direction parallel to the shoreline. This littoral zone is usually defined as the zone between the shoreline and the breaker line. Most nearshore sedimentation studies showed that the most active part of sediment movement occurs slightly shoreward of the breaker line. Due to lateral mixing as described in the earlier section, there will also be some sediment transport seaward of the breaker line. But the amount of this movement is much smaller when compared to the total amount of movement in the littoral zone.

Figure 2.3 gives a classification of the longshore transport models. There are two main categories: those based on the wave flux approach and those based on the sediment equation approach. The equations in each category will be briefly described.

2.4.1 Wave Flux Models

The wave flux approach recognizes that energy is required to transport the sediment. Therefore, because waves possess energy or wave power, it is then possible to find a correlation between the sediment transport rate and the amount of wave power available for this transport. The equation for the transport rate has the form:

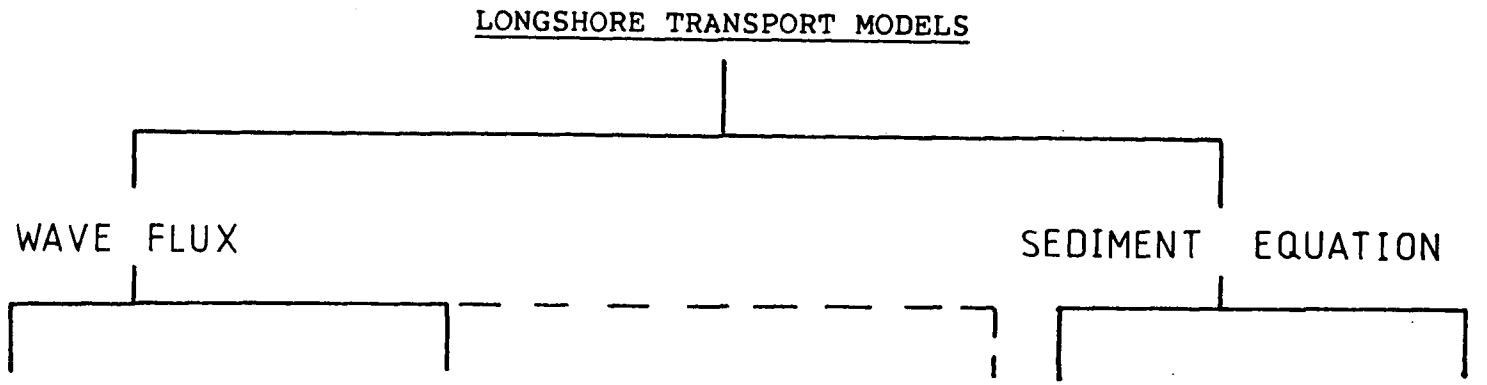

Scripp Institute of Oceanography (1947)

WATTS (1953)

CALDWELL (1956)

SAVAGE (1959)

INMAN AND BAGNOLD (1963)

KOMAR AND INMAN (1970)

GALVIN (1972)

INMAN AND BAGNOLD (1963)

BYKER (1971)

FLEMING et. al. (1976)

NIELSEN (1978)

*WILLIS (1978)

*SWART AND LENHOFF (1980)

* Adaptation of Ackers and White formula

Figure 2.3 Classification of longshore transport models

[2.7] $$S_l = A P_l^B$$

S_l is the volume transport rate and P_l is the 'longshore component of wave power' or the 'longshore component of wave energy flux'.

This value of P_l is determined at the breaker line. This is because most of the longshore transport occurs within the surf zone. By assuming conservation of energy flux in shoaling waves and using the small amplitude wave theory, it can be shown that

[2.8] $$P_l = (E C_g)_b \cos\theta_b \sin\theta_b$$

From the Airy wave theory, Cg = Cn where

[2.9] $$n = \frac{1}{2}\left[1 + \frac{2Kh}{\sin(2Kh)}\right]$$

Since n is approximately equals to 1.0 in shallow water and

[2.10] $$E = \frac{1}{8}\rho g H^2$$ ρ, = mass density of water

Equation [2.8] becomes

$$[2.11] \qquad P_l = \frac{\rho g H_b^2}{16} C \sin\theta_b$$

Equation [2.10] can be expressed in terms of parameters at the breaker line by assuming refraction by straight parallel bottom contours. A variation of equation [2.10] is thus obtained based on offshore wave parameters (SPM, 1977).

$$[2.12] \qquad P_l = \frac{\rho g^2}{64} \pi T (K_R H_o)^2 \sin\theta_b$$

where K_R is the refraction coefficient from deep water to shallow water and H_o is the deep water wave height.

Scripps Institute of Oceanography (1947) was among the first to adopt the energy flux approach in calculating the longshore transport rate. Since then there have been a number of investigators taking the same approach, but each obtained different values for coefficients A and B of equation [2.7]. Table 2.1 gives the values of the coefficients as well as the units in which they were obtained.

From table 2.1, it can be seen that the approach was slightly modified by Komar and Inman (1970). Instead of relating volume transport rate S_l, to P_l, they suggested the

$S = A P_l^B$	COEFFICIENTS		UNITS OF	
	A	B	S_l	P_l
Watts (1953)	0.0289	0.9	m^3/day	Watt/metre
Caldwell (1956)	0.0626	0.8	m^3/day	Watt/metre
Inman and Bagnold (1963)	0.0046	1.0	m^3/day	Watt/metre
SPM (1977)	0.0709	1.0	m^3/day	Watt/metre
Komar and Inman (1970) * $I_l = A P_l^B$	0.77	1.0	I_l = dyn/sec	P_l = dyn/sec

* $I_l = (\rho - \rho_s) g a' S_l$ where a' is the void ratio of beach sand

Table 2.1 Coefficients A and B of equation [2.7]

use of immersed weight transport rate I_l. This idea was initially expressed by Bagnold (1963). The advantages of this are firstly, the coefficient A becomes dimensionless giving a direct relationship between P_l and I_l, and secondly, the equation takes into consideration the sediment density.

Also noted from these equations is that the transport rate is independent of the beach slope. This independence also has supports because some of the data (Komar et al, 1970) used to find the correlation were measured on quite different beach slopes.

A comparison between the more recent equations by Komar et al (1970) and SPM (1977) indicates a difference in their prediction of the transport rate by about five percent. This shows that the empirical equations are fairly consistent with each other (Bruno et al, 1980).

Galvin (1972) proposed another empirical method in estimating the longshore transport rate. From a series of data on transport rate and observed mean breaker heights, Galvin plotted a curve

$$[2.13] \qquad S_g = 16.5\, H^2$$

where Sg is the gross longshore transport rate in units of 100,000 cubic metres per year and H is the mean breaker

height in metres. The facts that this curve reported by Galvin forms an upper limit over almost all the data points, and that the empirical equation does not consider the angle of attack, suggests that equation [2.13] may predict the longshore transport capability rather then the actual transport.

Galvin gave a physical explanation of this empirical relationship. He assumed the longshore transport occurs mostly as suspended load, and from the law of conservation of mass he obtained

$$[2.14] \qquad Q_g = [\, D K g \beta^2 c T \sin\theta_b \,] H^2$$

where c is the suspension concentration, K is the ratio of annual mean individual H^2 over square of the annual mean H, and D an empirical coefficent.

In order that equation [2.14] provides a plausible explanation to equation [2.13], those terms in the bracket will have to equal 16.5. Galvin tested this hypothesis and arrived at values which were much less than 16.5. This result is not too convincing. Furthermore, the assumption that the longshore transport occurs mostly as suspended load is subject to some dispute (Inman, 1969).

It is interesting to note that equation [2.13] can

also be obtained using a wave power approach. Combining equations [2.7] and [2.11] and assuming shallow water conditions, Cg = C = $\sqrt{gh}$ (at the breaker point), the resulting equation is

$$[2.15] \qquad S_l = A \left[\frac{\rho g^{3/2}}{16} \sin 2\theta_b \right]^B H_b^{5/2\,B}$$

Taking the coefficients A and B as given by Caldwell (table 1.1), and assuming θ_b to be approximately 4 degrees equation [2.15] becomes,

$$[2.16] \qquad S_l = 14.7\, H_b^2$$

This shows that Galvin's empirical equation is also based on the wave power approach. Inman and Bagnold's (1963) approach is also essentially a wave power method, but is derived from a sediment transport argument and so will be presented in the next section.

2.4.2 Sediment Equation Models

Unlike those in the previous section, all the models in this category are based on two relationships, one for the longshore current and a sediment transport relationship which requires the longshore current as input. Most of these models have their origin from work on sediment transport under oscillatory waves or in riverine conditions.

As all the models have been reported in the literature, the details of their formulation will not be given here, this section is a brief summary of their approaches. Table 2.2 shows the various models and their equations.

From table 2.2 it can be seen that most of the equations calculates the transport separately in terms of bed load and suspended load with the notable exceptions of Inman and Bagnold (1963) whose equation is for total load, and Nielsen et al (1978) where the transport is assumed to be totally suspended load.

Inman et al assumed that a portion of the wave energy flux $(ECn)_b Cos\theta_b$ is dissipated in placing the sediment in motion. Once the sediment is in motion, it becomes available for transport by the current which in this case is the longshore current $\overline{V}$.

Byker (1971) and Fleming et al (1976), however, adopted the approach that longshore transport consists of two components, namely, a bed load component and a suspended load component. Byker used the Frylink formula for sediment transport rate under riverine conditions for his bed load component. As for the suspended load component, Byker used the usual method which is the integration of the product of velocity and suspension concentration from the bed to the free surface. The suspension concentration is based on the Einstein-Rouse distribution of suspended material. From

	Longshore Transport Rate	Remarks
Inman and Bagnold (1963)	$I_l = K'(ECn)_b \cos\theta_b \frac{V_l}{U_m}$	$K' = 0.28$ (Komar and Inman, 1970) $U_m = (2E_b/\rho h_b)^{1/2}$
Byker (1971)	$S_l = S_b + S_s$	S_b = bed load S_s = suspended load
Fleming et. al. (1976)	$S_L = \int_0^e C\,U\,dy + \int_e^h C\,U_c\,dy$	C - sediment distribution from the bed to the free surface U, U_s - current velocity distribution of the bed load and the suspended load region e - reference point from the bed (bed load thickness)
Nielsen (1978)	$Q(t) = \int_0^h U(Z,t)\,C(Z,t)\,dZ$ Q(t) - instantaneous flux the of sediment	U(Z,t) - vertical distribution of the horizontal water velocity C(Z,t) - vertical distribution of the suspended sediment

Table 2.2 Sediment equation models

Byker's formulation, it is noted that there is no physical separation of regions between the bed load and the suspended load. Instead both are superimposed on one another and can be used quite independently.

As for Fleming's model, there are two identified regions of transport. In the bed load region, the grains are assumed to be supported by inter-particle collisions, and in the suspended load region, the grain particles are kept in suspension by the fluid turbulence. Fleming then defined a reference depth 'e' (bed load thickness) that separates the two regions. Fleming also assumed the continuity of sediment concentration and velocity between the two regions. Hence, there is actually no physical discontinuity between the two regions. Fleming then summed the two integrations from the bed to the reference depth 'e' and from 'e' to the free surface to get the total transport rate.

Nielsen et al (1978) approached the problem quite differently. From direct visual observation, they concluded that all movements of sediment occur in suspension. They assumed that a pick-up mechanism is responsible for setting the sediment into suspension. Then by arguing that the material is kept in suspension by a type of diffusion process, Nielson et al suggested that the concentration of suspended sediment satisfies the diffusion equation

[2.17] $$\frac{\partial c}{\partial t} - \omega \frac{\partial c}{\partial z} - \frac{\partial}{\partial z}\left(\varepsilon \frac{\partial c}{\partial z}\right) = 0$$

where ε is the diffusion coefficient and z is the vertical co-ordinate. From their data, Nielsen et al found that ε is constant from the bed to the free surface when waves are non-breaking, and ε increases from the bed when waves are breaking by spilling.

From the above equation, Nielsen et al were able to obtain an exact analytical solution for the time variation of the concentration profile, the instanteous sediment flux, and the net flux of sediment over a single wave period.

The last group of models is basically variations of the approach developed by Ackers and White (1973) for calculating sediment transport rate under a unidirectional flow condition. Ackers and White's method is based on the stream power approach in which the work done in moving the sediment is the product of efficiency and the stream power available for transport. Modifications of this approach have been carried out by Willis (1978) and Swart et al (1980) for use in coastal conditions. The most notable modification is the change of the original shear stress relationship of Ackers and White. This change is to compensate for the increase of instantaneous current velocity and for the difference in the initiation of threshold of motion due to the presence of waves. The

results of these modification have shown to be promising (Swart et al, 1980).

2.5 Summary

The above survey shows that there are many different approaches toward predicting longshore transport rate. Swart et al (1980) and Bruno et al (1980) have compared some of these equations to field data. They concluded that most of these equations agrees well with the data, and are fairly consistent with each other when the same set of data is used.

Also, from all the predictive equations presented, it seems that no account of particle size was taken into consideration. Since most of the equations were based on beach sand, it is felt that perhaps there was not enough variation in the particle size for its effect to be reflected in the equations.

In conclusion, there is no 'best' longshore predictive equation. However, the 'wave flux' type seems easier to use than the 'sediment equation' type. There are less variables required as input. Because of this and the fact that these wave flux equations gives good estimates (Bruno et al, 1978), it is decided that the CERC 'wave flux' equation will be use in the model described herein.

CHAPTER 3
WAVE REFRACTION AND SHOALING ROUTINE

3.1 Introduction

A model capable of predicting changes in the shoreline will require the breaking wave height and the direction of the wave along the shoreline. If these shallow water wave properties are to be obtained, the predicted incident deepwater waves must first be shoaled and refracted up to the shoreline. In addition, as the shoreline configuration changes, the wave refraction pattern also changes. This will result in a continous change of nearshore wave properties. To account for this, a wave refraction and shoaling routine is developed and incorporated into the shoreline prediction model. This chapter describes the working of such a routine.

3.2 General Description

Waves are modified as they travel from deep water toward shore. In this section, only effects due to refraction and shoaling are considered. It is assumed that wave damping, bottom friction, and any other non-linear effects are negligible.

At present, there are several methods available to draw a wave refraction diagram. The first method is known as the wave crest method (Johnson et al, 1948) in which the wave crests are obtained by drawing the envelope of circles from a preceding wave crest. The radius of the circles is proportional to the local value of the wavelength.

The second method involves the application of Snell's law of wave refraction:

$$[3.1] \qquad C_1 \sin\alpha_1 = C_2 \sin\alpha_2$$

where C, α are the wave angle and wave celerity at two different depths denoted by the subscripts 1 and 2. Based on this law, the curvature of the refracting wave orthogonals can be calculated and the orthogonals can be traced from deep water to shore. There are several variations based on this approach (Harrison and Wilson, 1964; Wilson, 1966).

The accuracy of these refraction diagrams is limited by the validity of the theory of their construction and the accuracy of the depth data on which they are based. Little error is introduced in tracing orthogonals over relatively simple hydrography, but it is difficult to calculate an orthogonal accurately over complex bottom features.

Once the orthogonals have been calculated, the wave heights can be estimated. This is done by assuming that the flux of transmitted energy is constant between a pair of orthogonals. But this assumption also means that no energy travels laterally along a wave crest. This is a reasonable assumption, but if the orthogonals bend sharply, the accuracy of the derived wave height is questionable. It should be noted that refraction effects remain small as long as the water depth is larger than L/3. Therefore, wave refraction calculations are usually carried over bottom topography shallower than such a depth.

3.3 Governing Equations

In this study, wave refraction and shoaling calculations will be based on two governing equations developed by Noda et al (1974). The first equation, given in cartesian co-ordinates, is equation [3.2]. It is derived from the irrotationality of the wave number vector, K (Phillips, 1980).

[3.2]

$$\cos\theta \frac{\partial \theta}{\partial X} + \sin\theta \frac{\partial \theta}{\partial Y} = \frac{1}{K} \left(\cos\theta \frac{\partial K}{\partial Y} - \sin\theta \frac{\partial K}{\partial X} \right)$$

The partial derivatives of K can be determined from the wave dispersion relationship:

$$[3.3] \qquad \sigma^2 = gK \ \mathrm{Tanh}\, Kh$$

where σ = wave angular velocity.

The second equation (equation [3.4]) is obtained from the steady-state energy conservation equation (Phillips, 1980):

$$[3.4] \qquad C_g (\mathrm{Cos}\,\theta)\frac{2}{H}\frac{\partial H}{\partial X} + (C_g \ \mathrm{Sin}\,\theta)\frac{2}{H}\frac{\partial H}{\partial Y} + \mathrm{Cos}\,\theta\frac{\partial C_g}{\partial X} - C_g \ \mathrm{Sin}\,\theta\frac{\partial \theta}{\partial X} + \mathrm{Sin}\,\theta\frac{\partial C_g}{\partial Y} + C_g \ \mathrm{Cos}\,\theta\frac{\partial \theta}{\partial Y} = 0$$

where Cg is the group velocity.

$$[3.5] \qquad C_g = \frac{1}{2}\left(1 + \frac{2Kh}{\mathrm{Sinh}\ 2Kh}\right) . \ C$$

By solving equations [3.2] and [3.4], the variation of wave height H and wave direction θ over the X, Y domain can be obtained. Figure 3.1 shows the definition sketch of the problem.

The main reason for choosing this approach over the other two described earlier is that this approach

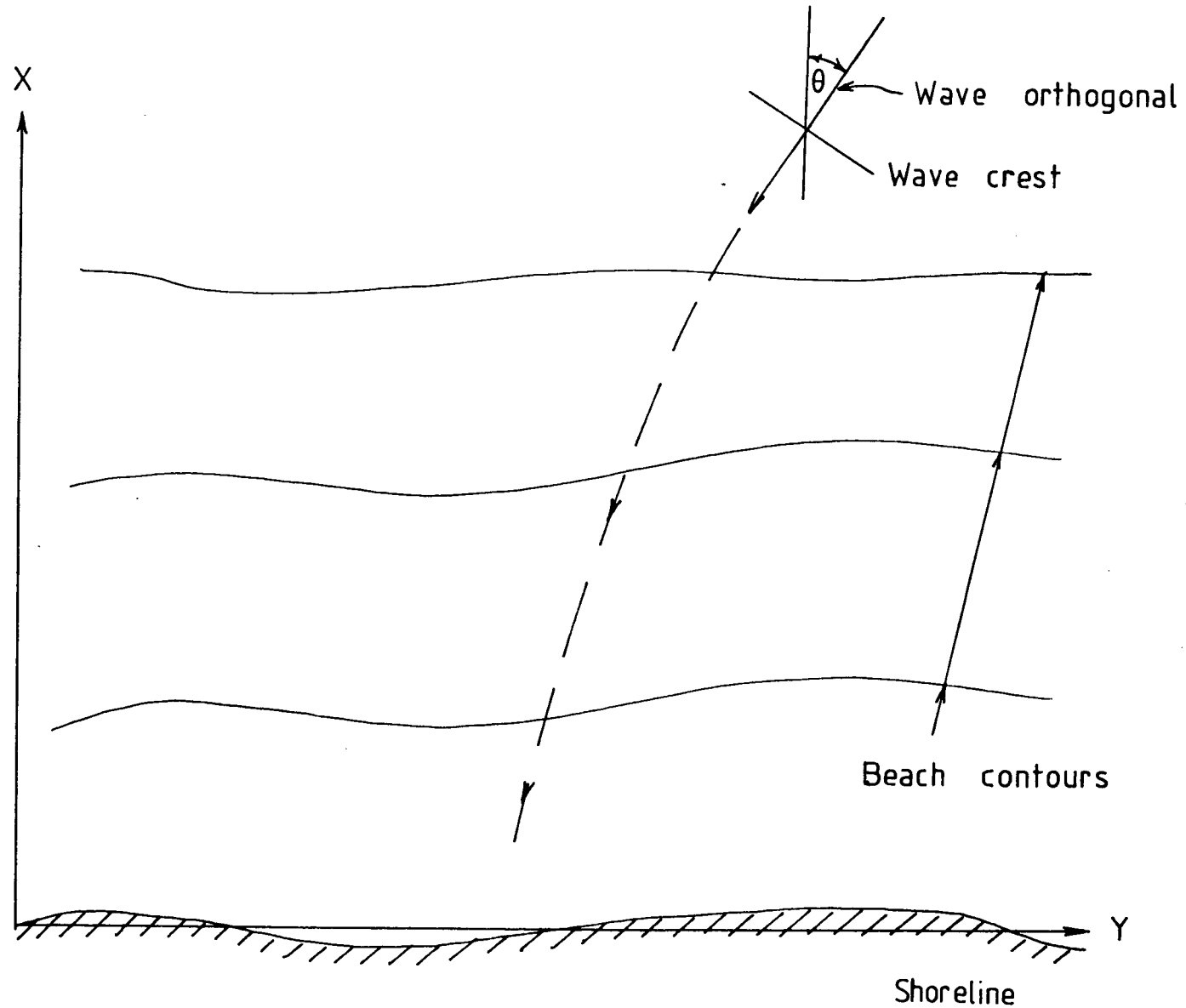

Figure 3.1 Definition sketch

predicts wave height and wave direction at each grid point (in x, y coordinates). This is very useful because this program will be integrated with the longshore transport model which is also based on a grid system.

3.4 Numerical Approach

Equations [3.2] and [3.4] are solved using a finite difference numerical method. It involves the transformation of the set of partial differential equations into a finite difference scheme. The finite difference form of equation [3.2] and [3.4] is given in equations [3.6] and [3.7] (see Appendix A for details of the formulation).

The procedure is to relax both equations [3.6] and [3.7] over the entire X, Y domain. The grid system used in this program is a rectangular/square mesh type and is shown in figure 3.2.

From the overall (global) grid, the location of each local grid point (i,j) is then established. This is done with the use of indices j, j+1, j-1, etc., for Y - direction space points, and i, i+1, i-1, etc., for X - direction space points. Figure 3.3 shows the local finite grid scheme.

3.5 Computation

A computation routine is developed and used to calculate the solution for a local grid (say at i = 3, j = 3). After that the same computation procedure is applied to the next local grid (i = 3, j = 4). The computation then proceeds step by step as shown in figure 3.2.

$$\text{Cos}\,\theta_{(i,j)}\left[\frac{\theta_{(i+1,j)} - \theta_{(i-1,j)}}{2\Delta X}\right] +$$

$$\text{Sin}\,\theta_{(i,j)}\left[\frac{\theta_{(i,j+1)} - \theta_{(i,j-1)}}{2\Delta Y}\right]$$

[3.6]

$$= \frac{1}{K_{(i,j)}}\left[\text{Cos}\,\theta_{(i,j)}\left(\frac{K_{(i,j+1)} - K_{(i,j-1)}}{2\Delta Y}\right) -\right.$$

$$\left.\text{Sin}\,\theta_{(i,j)}\left(\frac{K_{(i+1,j)} - K_{(i-1,j)}}{2\Delta X}\right)\right]$$

$$\left[Cg_{(i,j)}\,\text{Cos}\,\theta_{(i,j)}\right]\frac{2}{H_{(i,j)}}\left[\frac{H_{(i+1,j)} - H_{(i-1,j)}}{2\Delta X}\right] +$$

$$\left[Cg_{(i,j)}\,\text{Sin}\,\theta_{(i,j)}\right]\frac{2}{H_{(i,j)}}\left[\frac{H_{(i,j-1)} - H_{(i,j+1)}}{2\Delta Y}\right] +$$

[3.7]

$$\text{Cos}\,\theta_{(i,j)}\left[\frac{Cg_{(i+1,j)} - Cg_{(i-1,j)}}{2\Delta X}\right] -$$

Equation [3.7] continued,

$$Cg_{(i,j)} \operatorname{Sin}\theta_{(i,j)} \left[\frac{\theta_{(i+1,j)} - \theta_{(i-1,j)}}{2\Delta X} \right] +$$

$$\operatorname{Sin}\theta_{(i,j)} \left[\frac{Cg_{(i,j-1)} - Cg_{(i,j+1)}}{2\Delta Y} \right] +$$

$$Cg_{(i,j)} \operatorname{Cos}\theta_{(i,j)} \left[\frac{\theta_{(i,j-1)} - \theta_{(i,j+1)}}{2\Delta Y} \right] = 0$$

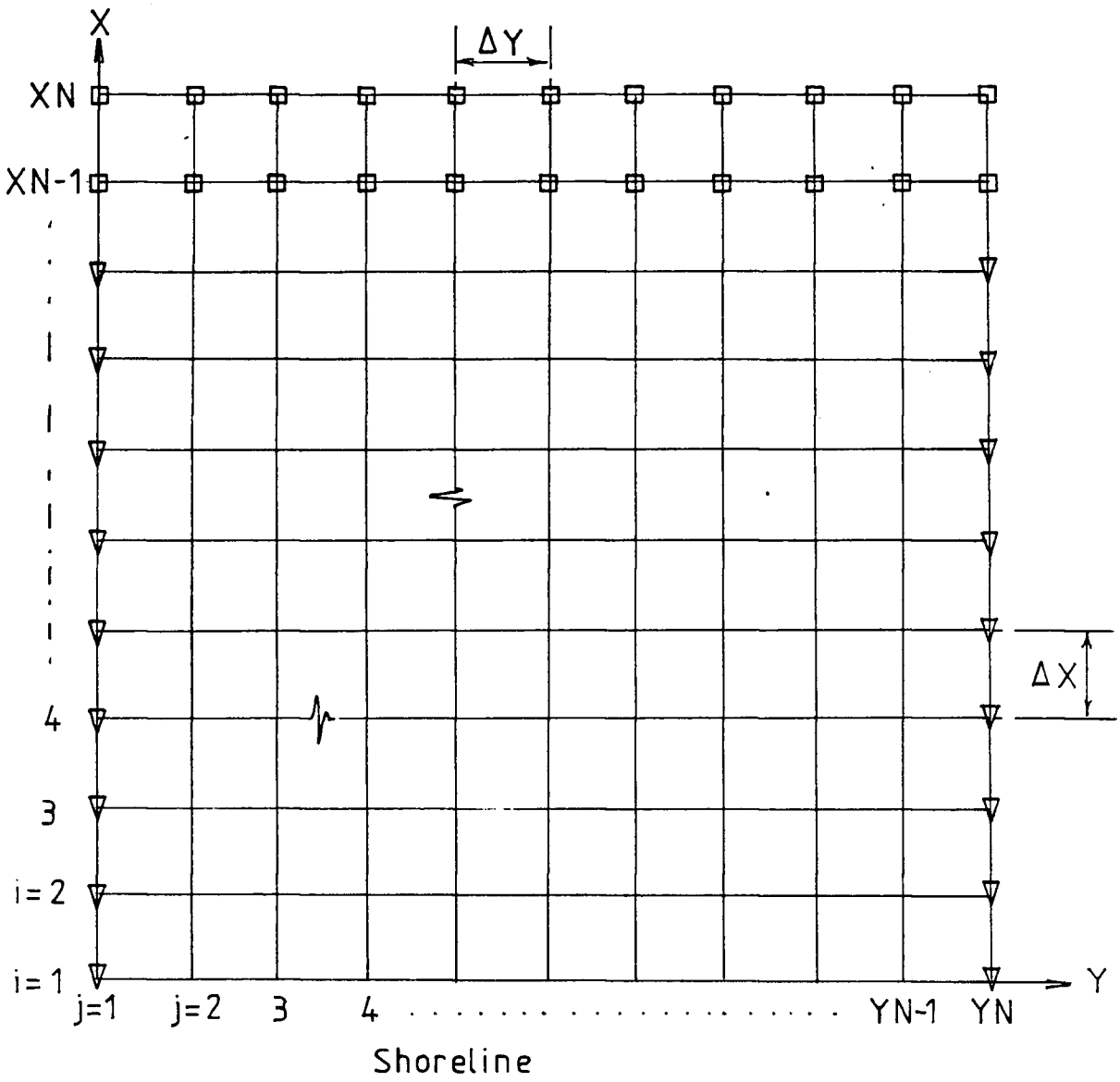

□ – Deepwater boundary condition

Δ – Side boundary condition

Computation begins with $j=1, i=XN-1$ as center of local grid. The computation then proceeds to $j=2, i=XN-1$ till $j=YN-1, i=1$.

Figure 3.2 Overall grid scheme

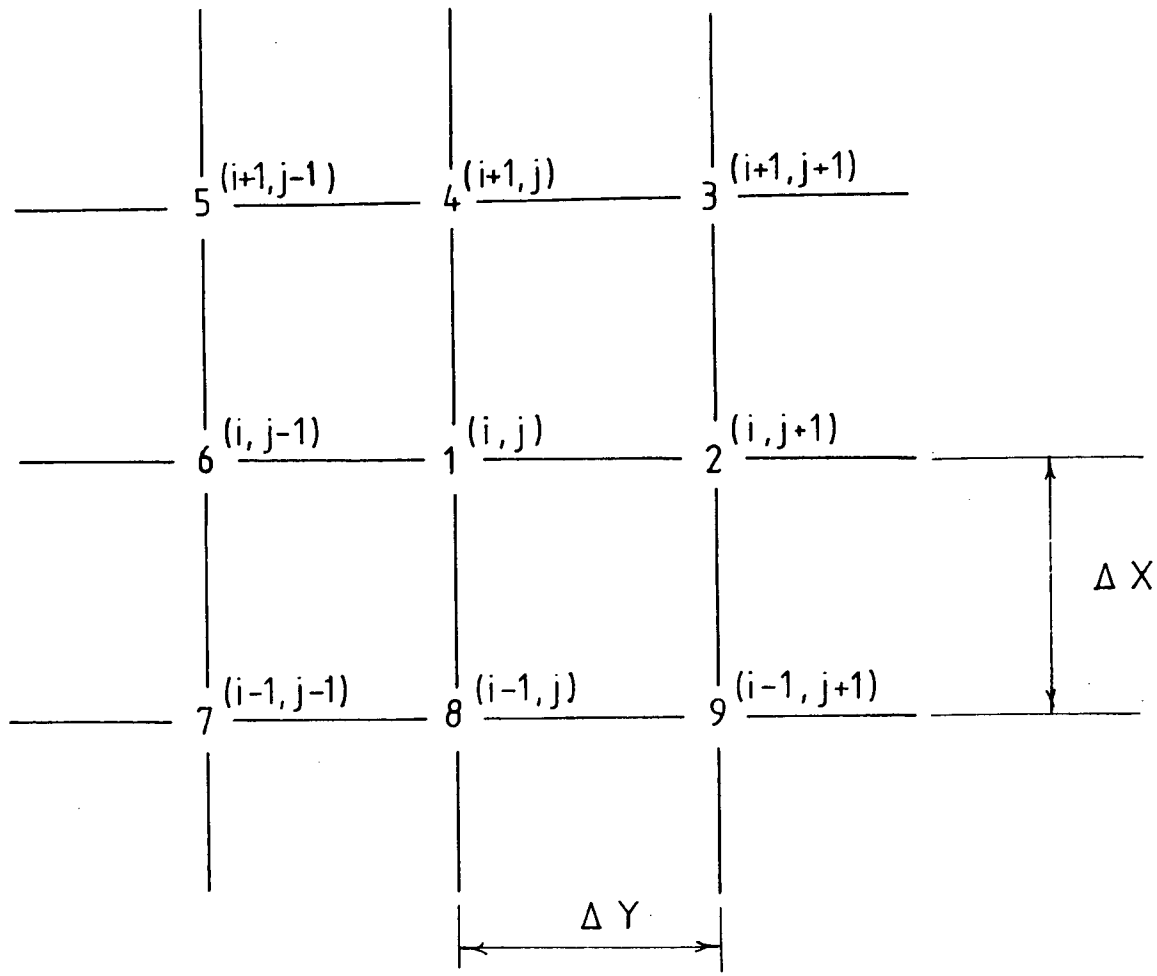

Figure 3.3 Local grid scheme

The X, Y domain of the problem area is surrounded by three sets of boundary conditions. The first is the offshore boundary given by the offshore wave conditions. The second and third are the two side boundaries of the domain (shown in figure 3.2). These side boundary conditions are usually not given in the problem, but to simplify the calculation routine, these boundaries are assumed to be far away from the area of interest in the domain, and the conditions of these boundaries to be the same as their immediate neighbour (ie solution of column j = 2 would be equated to column j = 1 and likewise for j = YN - 1 to j = YN). The details of the program and the flowchart are given in Appendix B.

3.6 Results

A few simple test runs were carried using the above procedures. The results of these are given here. Test 1 to Test 3 were to check the refraction segment of the program, while Test 4 was to check the shoaling segment.

Test No	Test conditions
1	The angle of wave incidence is 45.8 degrees (0.8 radians) to the beach normal. The beach

	slope is 1 in 10 and the wave period is 5 seconds. Figure 3.4 shows the wave crest orientation of each node as well as three wave orthogonals.
2	The waves approach a simulated headland. The deepest depth is at 3 metres, the slope of the beach is 1 in 10 and the wave period is 3.5 seconds. The result of the refraction is shown in figure 3.5.
3	A larger grid of 30 by 30 is used, to simulate a situation much more similar to field conditions. The angle of waves approach is at 0.8 radians and the wave period is 5.5 seconds. The slope is 1 in 10 and the deepest depth is 6 metres. Figure 3.6 shows the results.
4	This test is designed to test the shoaling segment of the program; as such, the waves are approaching the 1 in 10 beach normally. The wave period is set at 4 seconds and the wave height at the depth of 12 metres is 1 metre.

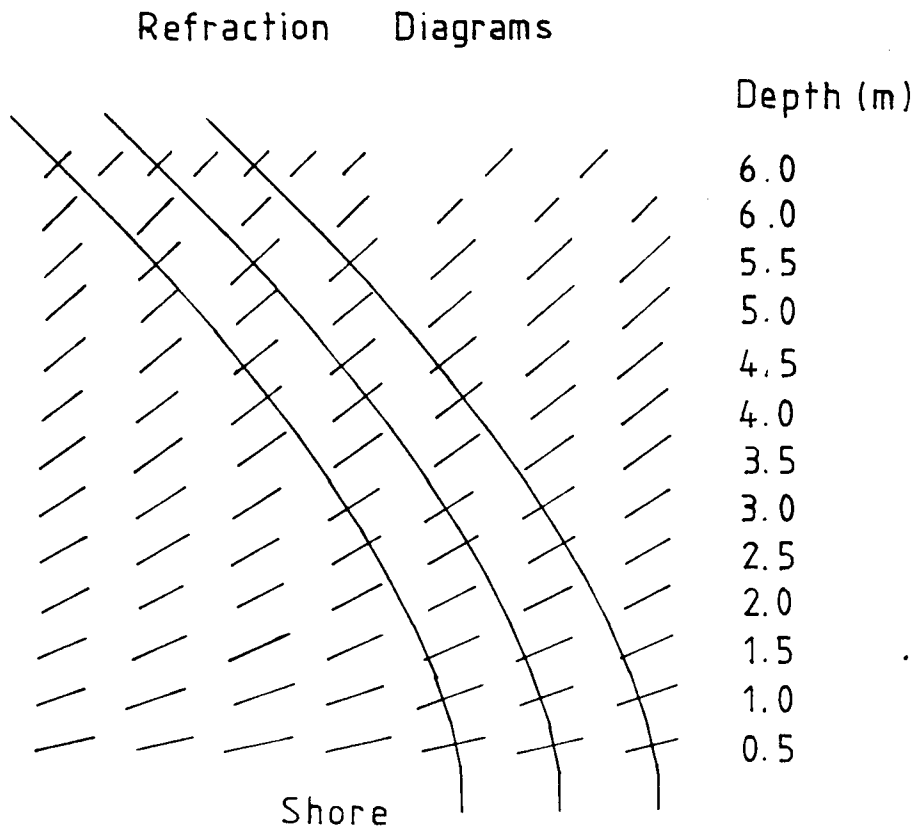

Figure 3.4 Results of test No 1 showing the wave crests

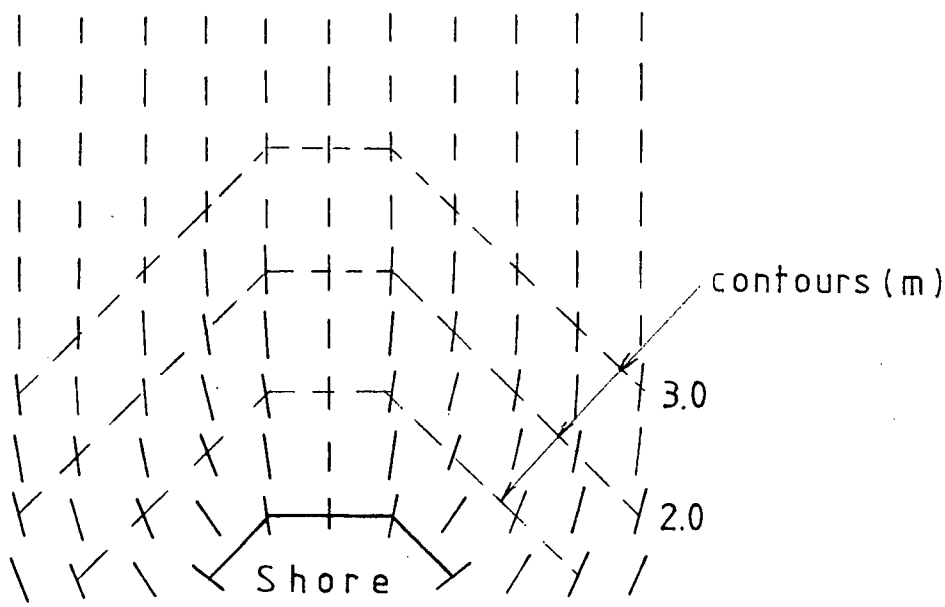

Figure 3.5 Results of test No 2 showing the wave orthogonals

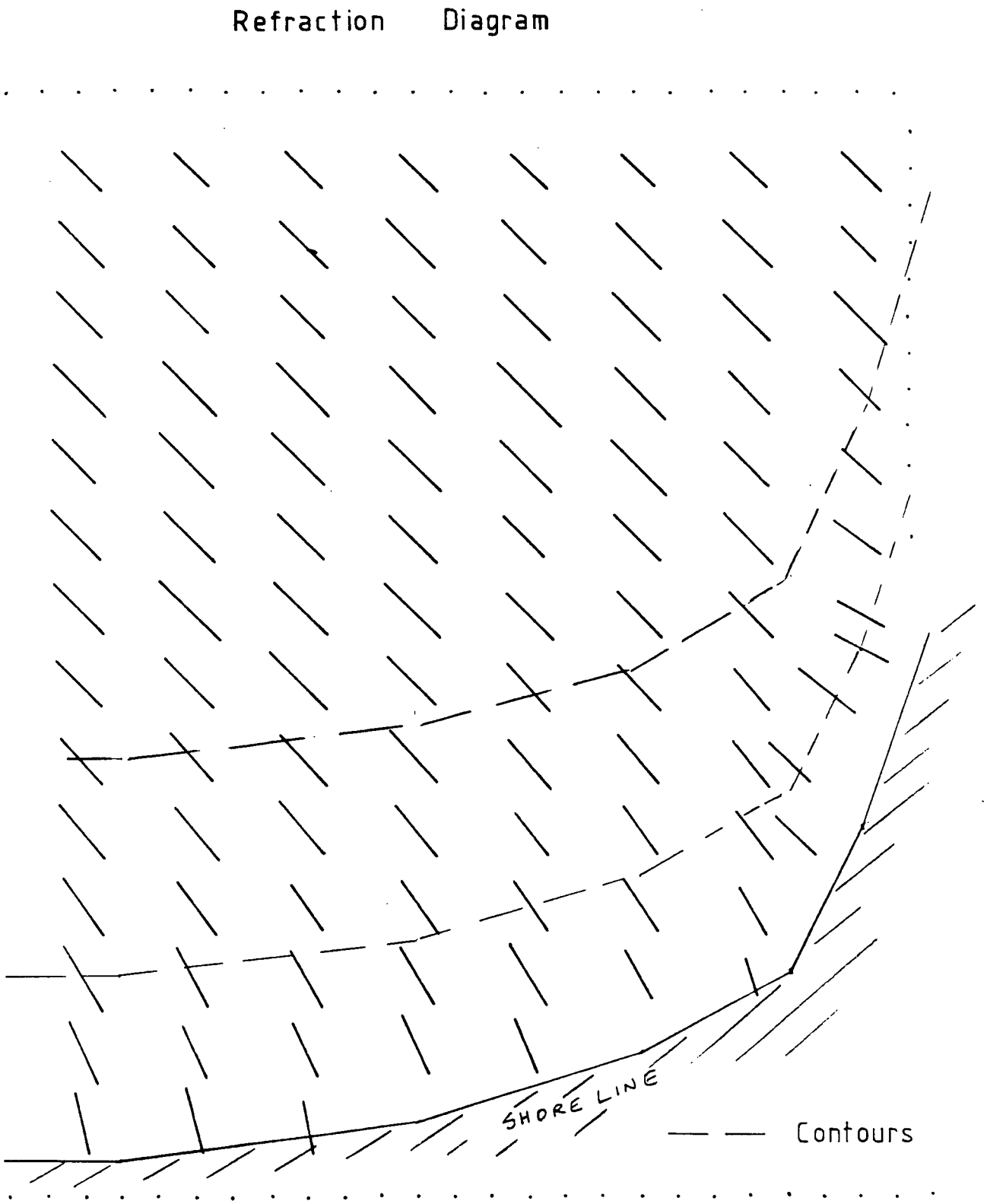

Figure 3.6 Results of test No 3 showing the wave orthogonals

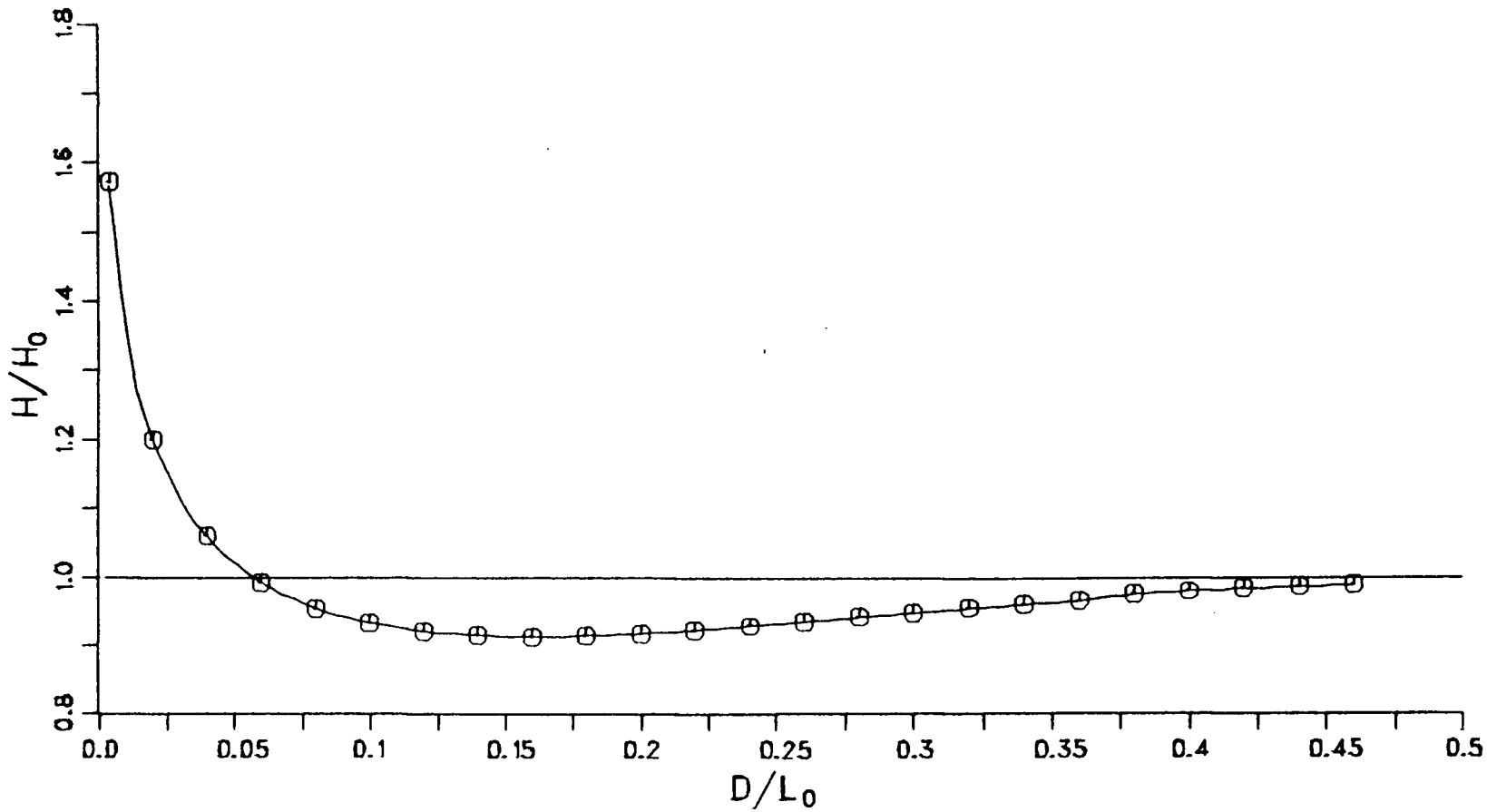

Figure 3.7 Variation of relative wave height with depth

The results from Test 1 were checked against the solution obtained by an analytical approach (equation [3.1]). The comparison showed that the results differed by only 0.2 percent. It was carried out at the depth of 3 metres. The analytical method gave the angle as 0.5761 radians, while Test 1 results gave angle at 0.5750 radians. This is considered acceptable because the uncertainties and errors from offshore wave predictions will be greater than 0.2 percent. Also, it must not be forgotten that a finite difference method is an approximation method so that the results can only be close to the true solution.

The wave height results from Test 4 also compared well with the analytical solution. The wave height at 4 metres depth using an analytical approach is 0.9235 metre, while the program gave a value of 0.9236 metre. The difference is only 0.01 percent.

The relative wave height variation with depth was plotted (figure 3.7) as a final check on the shoaling segment. that when waves approach a shore, the wave heights will initially reduce before increasing to the breaking point. Figure 3.7 shows the plot of H/H_0 against d/L_0. The subscript 'o' represents deepwater value. When it was compared with a plot obtained analytically (Le Mehaute, 1976), an almost perfect match was obtained.

In conclusion, the computation procedures of the wave refraction and shoaling program are correct, and the results are sufficiently accurate for use with the longshore transport segment to be described in the next chapter.

CHAPTER 4

LONGSHORE TRANSPORT MODEL

4.1 Introduction

From the concept of sediment budget, a section of shoreline will change its shape as a result of a net sediment movement in and out of that section. In a nearshore environment, these sediment movements can be divided into longshore and on-offshore directions. It is obvious that to have a comprehesive shoreline evolution model, the model will require considerations of net sediment movement in both directions. But the model presented in this chapter will consider only the longshore component. The on-offshore and the total longshore and on-offshore processes will be considered in chapter six.

The model will be used to simulate a beach build up due to the construction of a barrier (groyne or jetty) and to study the changes of a beach nourishment plan shape with time.

4.2 Model Review

All the existing shoreline evolution models can be classified into two groups. The first group follows the approach in which the transport rate equation and the

continuity equation are solved simultaneously. The transport rate equation used in most of the models of this group is the CERC transport rate equation. Hence, models of this group are also known as CERC models. The second group has a similar approach as the first, but with a slight variation. Instead of a using predictive transport rate equation like the CERC equation, the models in this group compute the longshore currents and then use a suitable transport theory (eg Ackers and White) to compute the sediment load. Models using this approach are known as 'current' models.

A comparison between a 'current' model and a CERC model was carried out by Willis (1977). The conclusion indicated that on the whole, the CERC models gave a better prediction of the results, in terms of the volume of sediment transported and the shoreline changes, than the 'current' models. A possible reason for the poorer prediction by the 'current' models is that there is no satisfactory theory relating the currents and the transport rates in coastal conditions. Only with more advances in this area will the 'current' models be better.

The governing equations in all the models can be solved either by an analytical or a numerical modelling method. When the analytical method is used, the resulting differential equation is complicated. The solution is impossible to obtain even with a set of simple boundary

conditions. However, the governing equations can be simplified and approximate analytical solutions can be obtained (Pelnard-Considere, 1956; Bakker et al, 1970; Walton et al, 1979). The numerical modelling method is a method where the differential equations are modelled using a numerical approximation technique. Price et al (1972) and Komar (1973) used this approach in their models. This approach will be described later in this chapter.

4.2.1 Continuity Equation

Of the two governing equations, the transport rate equation and its variations have been described in chapter two. The following section will review briefly the continuity equation of some of the early models.

Price et al in 1972 developed a CERC model for predicting shoreline changes. Equation [4.1] is the continuity equation of that model. The definition sketch of the equation is given in figure 4.1.

$$[4.1] \qquad \frac{\partial Q}{\partial X} + \frac{D}{2} \frac{\partial Y}{\partial T} = 0$$

The depth 'D' of equation [4.1] has been described differently by various authors. Willis et al (1975) suggested that 'D' be the depth beyond which longshore transport no longer takes place. From a series of

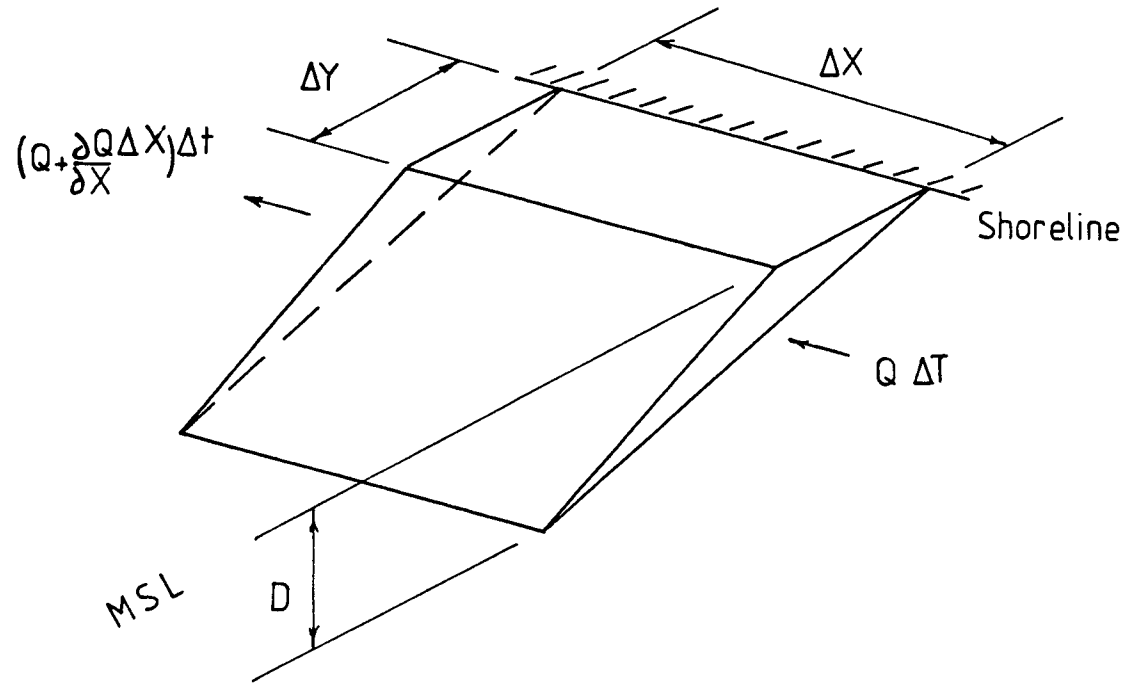

Figure 4.1 Definition sketch for equation [4.1]

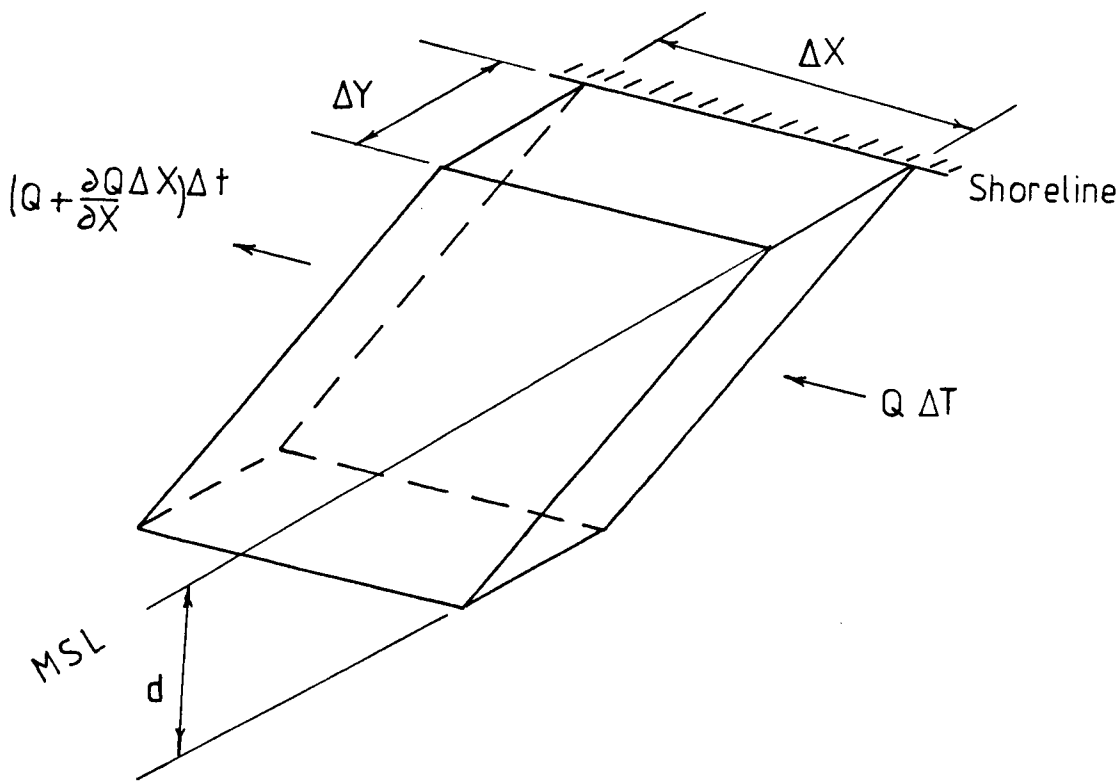

Figure 4.2 Definition sketch for equation [4.4]

observations, they concluded that a good estimate of 'D' is

$$[4.2] \quad D = 2.0 H_i$$

where H_i is the incident wave height.

Walton et al (1979) suggested a similar description for 'D'. Walton defined 'D' as the depth that encompasses the entire zone of longshore sand movement, and therefore, not only includes the depth below water to the sand movement limit, but also the depth above water of the beach. The expression for 'D' is then

$$[4.3] \quad D = 1.3 H_b + 2 a_0 + R$$

where a_0 is the maximum tidal amplitude and R is the wave run-up above the mean high tide level.

From a different approach, Komar (1976) proposed the use of a variable 'd', such that $d\Delta y$ gives the section area of the beach eroded or deposited (see figure 4.2). The resulting continuity equation becomes

$$[4.4] \quad \frac{\partial Q}{\partial X} + \frac{d\,\partial Y}{\partial T} = 0$$

The value of 'd' is obtained by calibrating the model to the prototype. This approach gives the model an added flexibility and also a better fit to the prototype.

This variable 'd' is a conceptual depth and does not have any physical significance.

4.3 Numerical Modelling

The model adopted in this report is a CERC model. The reason for adopting this model is that the 'current' models are still subjected to many uncertainties as mentioned earlier. In addition, a study by Bruno et al (1980) on the relationship between the longshore energy flux at breaking (P_l) and the immersed weight transport rate (I_l), has reaffirmed the relation $I_l = A\ P_l$ (table 2.1). With this, it is felt that the CERC model will give a more reasonable estimate of the longshore transport changes.

4.3.1 Governing Equations

There are only two governing equations for this model. The volume transport rate equation and the continuity equation. The transport rate equation used is equation [4.5] by Komar:

$$[4.5] \qquad I_l = 0.77 P_l$$

where

[4.6]
$$\begin{cases} P_l = E\, Cn \sin\theta_b \cos\theta_b \\ I_l = (\rho - \rho_s)\, g\, a'\, S_l \end{cases}$$

a' = correction factor for the pore space of beach sand = 0.6

and ρ_s = beach sand density = 2.65.

It must be mentioned that coefficient 0.77 of equation [4.5] is based on data in terms of RMS breaking wave height. Since it is common to use significant wave height values, a correction factor is used to convert equation [4.5]. The resulting volume transport rate equation is

[4.7] $$S_l = (3.85 \times 10^{-2})\, H_b^2\, Cn \sin\theta_b \cos\theta_b$$

where S_l is the volume transport rate in cubic metre per day.

The continuity equation used is equation [4.1]. The assumed beach profile change is given in figure 4.3. The depth 'D' can be calculated using equation [4.2]. However, from studies by Bakker et al (1970) on longshore sediment movement, it was found that there is virtually no sediment movement longshore at a distance of one and a half times the breaker zone width away from the shoreline. They

then proposed that this be the location for determining the depth 'D'. This approach will be adopted in the model because similar observations were also reported by Komar (1971) and Thornton (1973).

Figure 4.4 shows the distribution of sand transport rate across the width of the breaker zone. From the figure, it seems that when a barrier stops the supply of sediment downstream of a beach, a large volume of sand will be eroded at the location of the maximum transport rate and zero volume at the shoreline. This would mean no movement of the shoreline and an increase of beach slope. Obviously, this is not what happens because there must be some sediment movement along the on-offshore direction due to the orbital motion of the wave. This movement will continuously adjust the slope and cause the shoreline to recede as shown in figure 4.3.

To account for this, a distribution of sediment transport rate different from the one in figure 4.4 is adopted for the model. At present, there are two approaches:

1. Linear distribution varying from zero at depth 'D' to the maximum at the shoreline.
2. Uniform distribution from depth 'D' to the shoreline.

Both cases are contrasted with Komar's curve in figure 4.5. The area under each curve is the same.

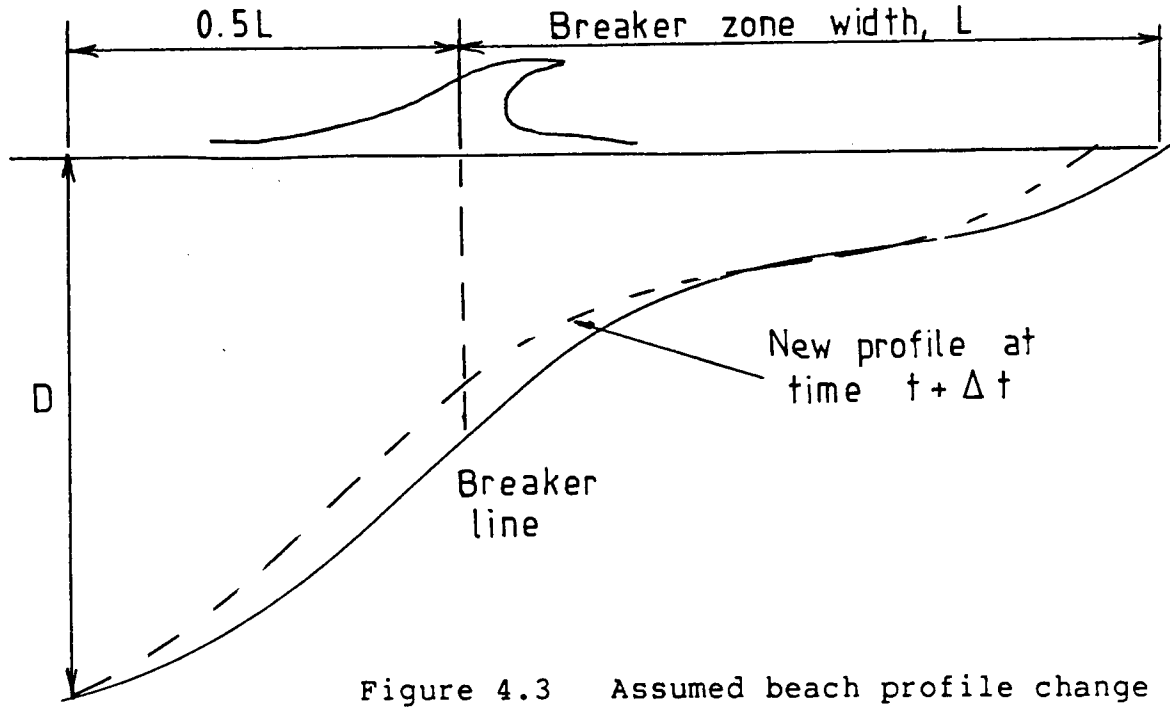

Figure 4.3 Assumed beach profile change

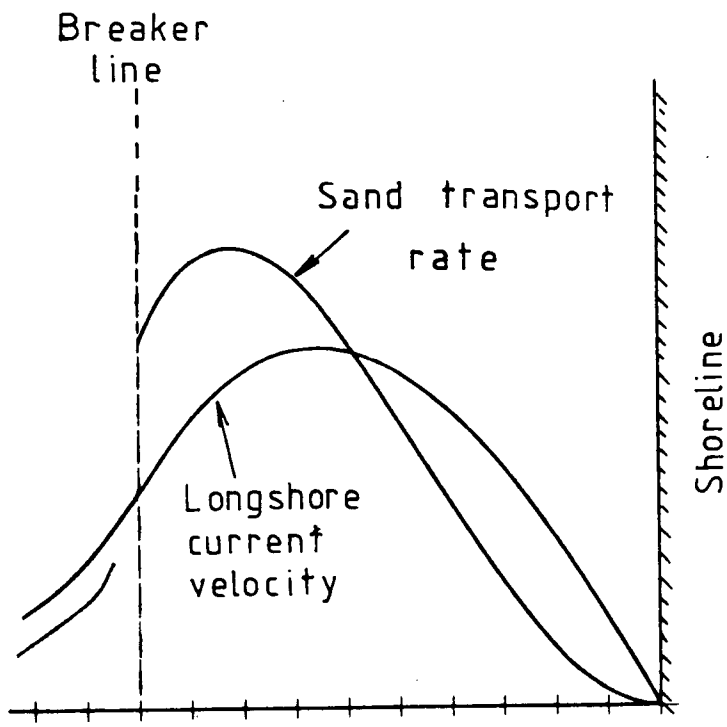

Figure 4.4 (After Komar, 1973) Distribution of sand transport rate across breaker zone

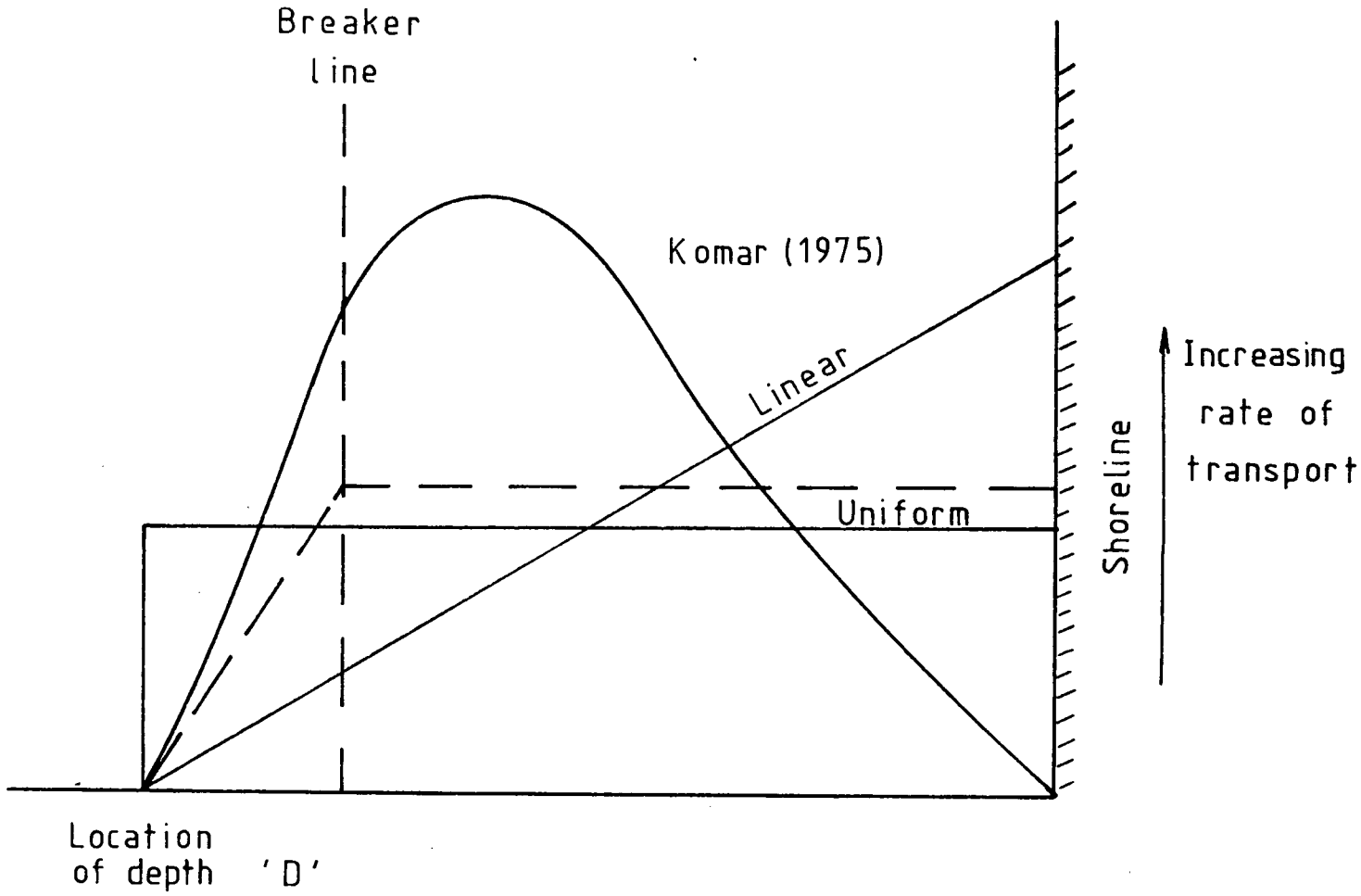

Figure 4.5 Approximated sand transport rate distribution

From the figure, it can be seen that using either of the two distributions will take into account implicitly some on-offshore movements of sediment. However, the uniform distribution will lead to the maintainence a constant profile of the beach. This is not altogether true as accretion at the barrier will tend to change the profile. On the other hand, the linear distribution seems to be grossly re-distributing the curve by Komar. In view of the disadvantages, a new distribution is proposed and used in the model. The new distribution, shown as a dashed line in figure 4.5, is actually a combination of the two earlier distributions. It assumed that a uniform rate of transport exists across the breaker zone, and it will decrease linearly after the breaker line to zero at the location of depth 'D'.

4.3.2 Computation

The governing equations are solved numerically using a finite difference scheme described below.

The shoreline in the study area is divided into a series of cells of a finite and uniform length, ΔX. This discretization is shown in figure 4.6. The transport in and out of the cell, and ΔQ can be calculated using equation [4.7] and a suitable time interval ΔT.

Before the whole procedure repeats itself with

equation [4.7] for the next ΔT, the wave refraction and shoaling subroutine is called to provide the new nearshore wave condition. A flowchart of the model is given in Appendix C.

In summary, the model performs the following:

1) Shoals and refracts deep water waves.
2) Calculates breaking wave conditions.
3) Calculates the breaker to shoreline angle.
4) Calculates the volume of acretion/erosion.
5) Distributes accretion/erosion over the beach profile.
6) Returns to (1) and re-calculates the wave shoaling and the refraction for the next iteration.

4.3.3 Boundary Conditions

The model requires suitable the boundary conditions as inputs, and these boundary conditions will have to be specified as data in a simulation run. There are three boundary conditions. Two of them are transport boundary conditions which control the rate of sediment entering and leaving the study area. The third is the shoreline boundary which under normal circumstances is assumed to be a free boundary, meaning that it is erodible. This condition is built into the model and need not be specified.

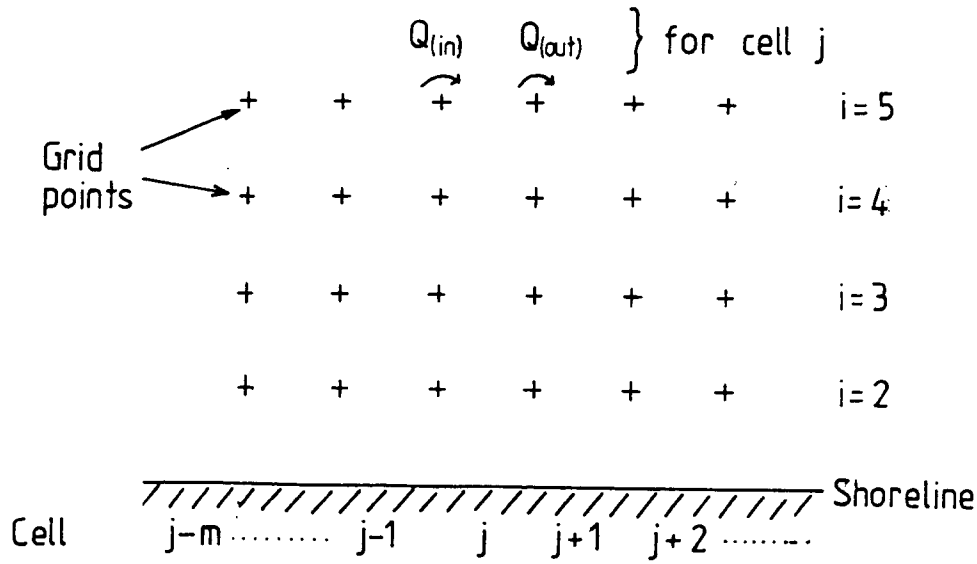

Figure 4.6 Discretization of study area

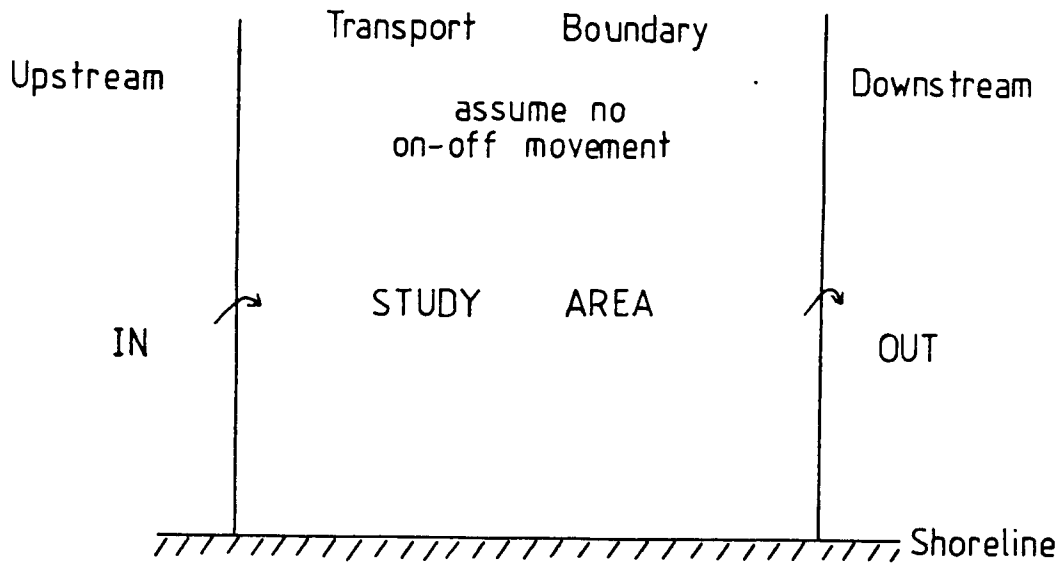

Figure 4.7 Boundary conditions

By specifying certain conditions at the two transport boundaries, the model can be used to simulate different situations. For example, in figure 4.7, by specifying no transport across the downstream boundary, it is possible to create a physical barrier at right angles to the beach. By controlling the volume of transport across the upstream boundary, it is also possible to create the situation of a river supplying more (or less) sediment than the beach requires.

4.4 Model Applications

The model is used to simulate three situations:

a) The shoreline build-up after the construction of an infinitely long impermeable barrier.

b) The shoreline build-up same as a) but with a barrier of finite length.

c) The change of a beach nourishment plan shape with time.

4.5 Results

A. Infinitely long impermeable barrier

The boundary conditions for this case are

i) The transport boundary upstream of the study area is

set to 1.0 (ie 100 percent permeable), and

ii) the downstream boundary is set to 0.0 (ie no sediment allows out of the study area).

Results of the build-up due to the barrier are shown in figure 4.8 for the particular case θ_0 = 45 degrees, tan β = 0.1, wave period T = 5.5s and H_0 = 0.6m. (Due to the effect of distortion, wave orthogonals would also be distorted and appear to be less than normal, so for figures 4.8 and 4.11, the incident wave crest direction is shown.) From the figure, the following were observed.

1. The shoreline begins its accretion in the region nearest the barrier. The rate of accretion in this region is noticed to decrease with time, while in regions further away from the barrier, the rate is fairly constant. It is believed that this is due to the decreasing angle between the breaking waves and the shoreline as it approaches the barrier.

2. The plan shape of the shoreline at any one instant is similar to the shape at any other. It is suspected that the accretion history of the shoreline to any time T can be non-dimensionalised, and a curve can be found to represent the accretion history for a specific location on the shoreline.

The growth history of the shoreline is described by three variables. They are the accretion length (Y -

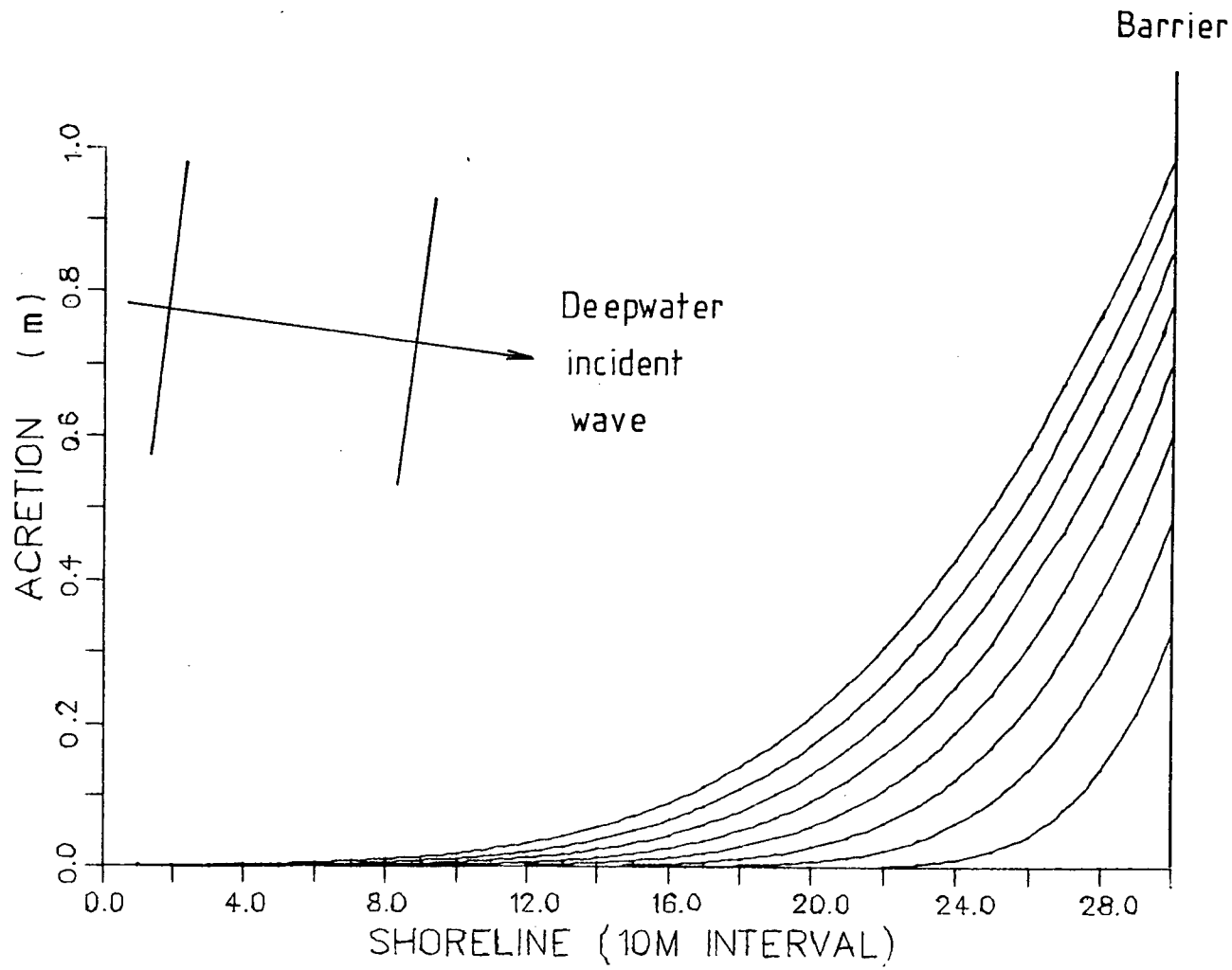

Figure 4.8 Plan view of the shoreline build-up due to infinitely long barrier

axis in figure 4.8), the location (X - axis, given as the distance away from the barrier), and the time variable T. To non-dimensionalise, a curve is chosen from figure 4.8 so that two characteristic variables, time and length, can be defined. The 'characteristic time' is the final time T of the chosen curve, and the 'characteristic length' is the maximum accretion length Lm (see figure 4.9). The definitions for the dimensionless location, time, and length ratio are also shown in the figure.

Thus, at each value of D, there is a relationship between the time ratio and the accretion ratio. The result of the above procedures is shown in figure 4.10. The variable X in the figure is the same as that defined in figure 4.9. Therefore, the curve X = 0 in figure 4.9 is the accretion history at zero distance away from the barrier. Similarly, the curve X = 2.98 would depict the accretion history at the location 2.98 times Lm distance away from the barrier. It must be noted that the six curves in figure 4.10 are from a family of infinite curves, as X ranges from 0 to infinite. These curves are also independent of the value of T_F. Appendix D shows that the same family of curves is obtained even when different values of T are used in the non-dimensionalising procedures.

Figure 4.10 shows that the accretion rates vary with location. It also shows that each curve (with the exception of X = 0), exhibits a slow, fast, and slow

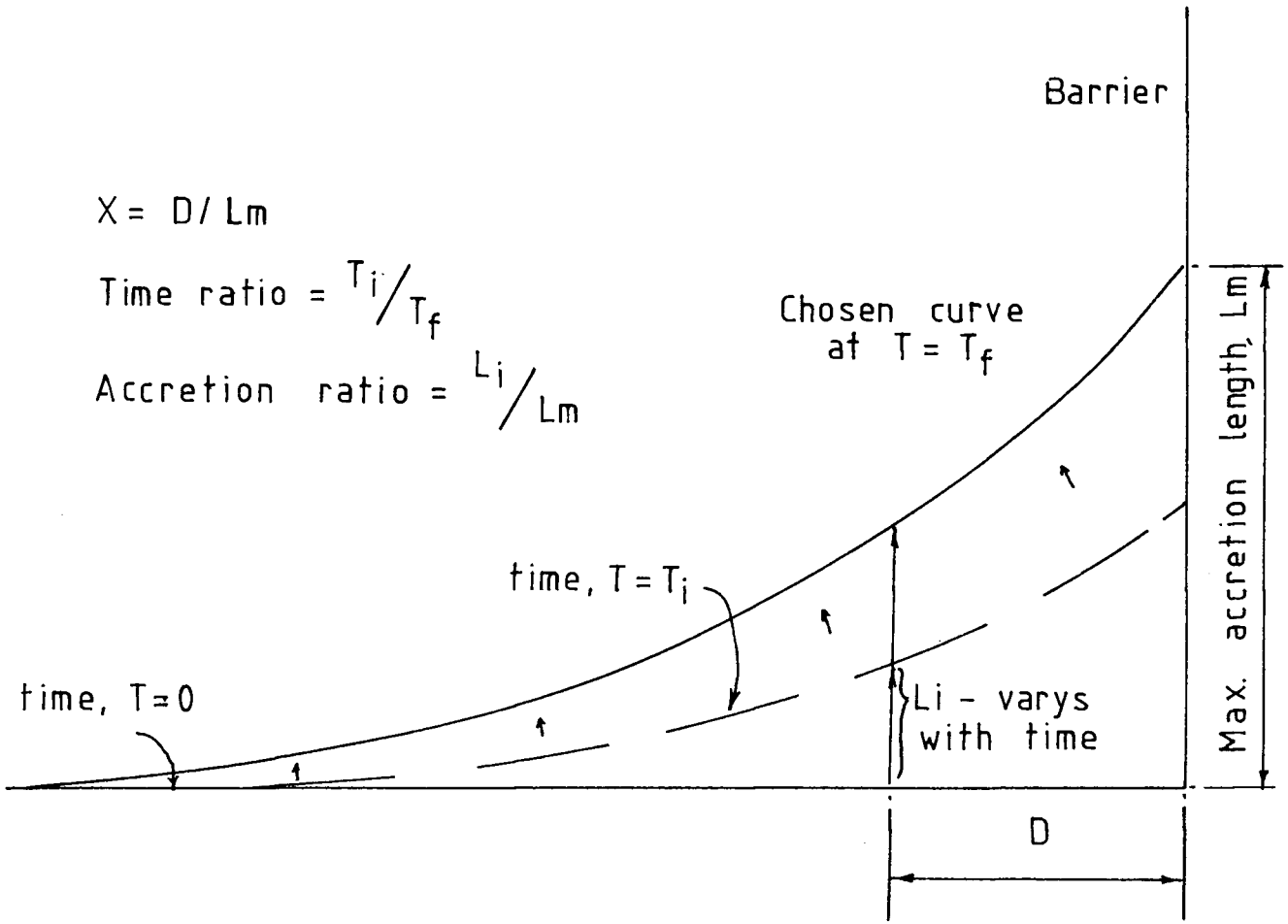

Figure 4.9 Definition sketch for non-dimensionlising procedures

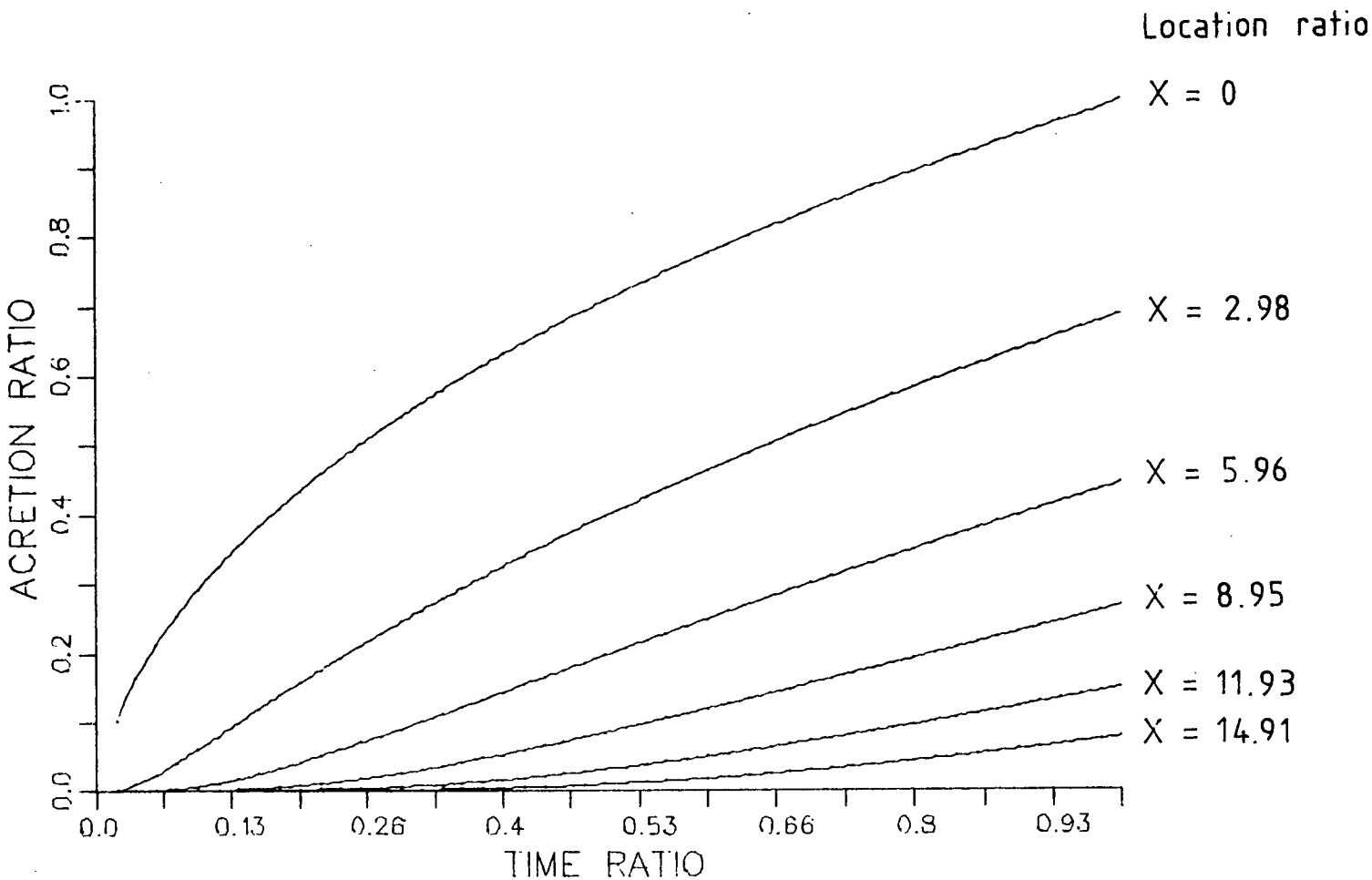

Figure 4.10 Non-dimensionalized accretion curves for infinitely long barrier

accretion rate like a 'S' curve. In addition to showing the accretion history of the various locations, figure 4.10 has a useful application in finding the minimum length of the barrier required to achieve the required sediment accummulation at a specific location within a minimum time.

Example 4.1

Find the minimum length of barrier required to achieve a 5 metres acretion at a distance 30 metres away from the barrier.

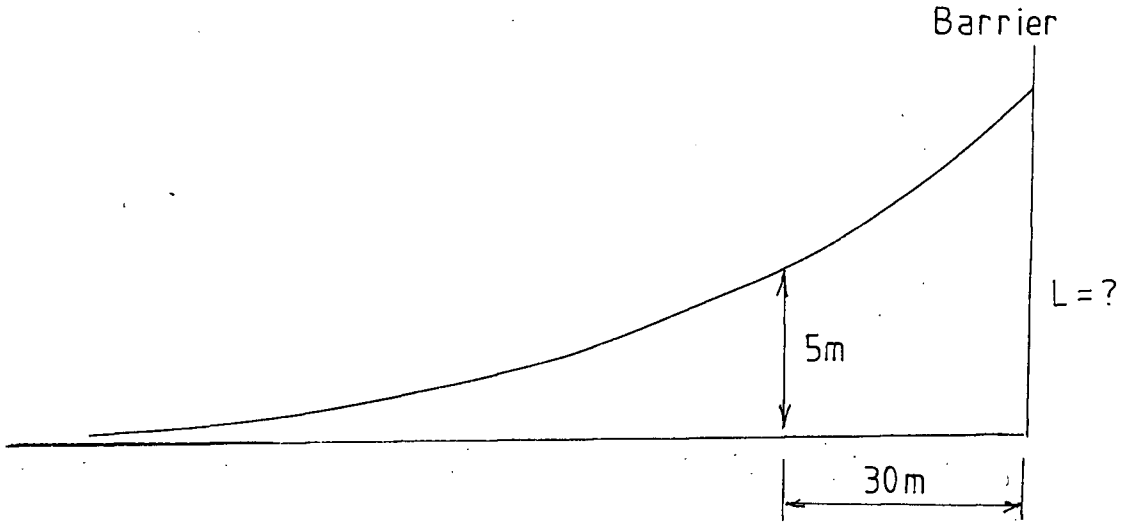

Solution

Assume the length L = 10 metres. Therefore X = 30/10 = 3.

From figure 4.11, the curve of X = 3 (by interpolation) shows the accretion history of the location 30m away from a 10 metre barrier.

The curve indicates that at the time ratio of 1, the accretion ratio is approximately 0.68. This implies that for L = 10m, accretion at 30m away is 6.8m (5.0m). To minimise the barrier length L, assume a lower value of L and repeat again.

This trial and error is carried out until accretion value of 5m is obtained for the location 30m away from the barrier. The answer to this example is approximately 8m.

This solution is for situations with the time ratio of 1.0. This means that the 5m accretion is achieved at the same time as the 8m accretion at the barrier. For values greater than L = 8m, the 5m accretion will still be achieved when the accretion at the barrier reaches 8m. Hence, a longer barrier does not mean achieving the 5m accretion at a shorter time.

B. Finite length impermeable barrier

In most situations, the barrier is not infinitely long; so a model simulating a finite length barrier would be more useful and is presented herein.

Two assumptions will have to be made in this simulation:

1. Since the barrier has a finite length, it is assumed that the sediment will start to pass the barrier after the sediment fills up the length.
2. The amount of sediment passing out of the study area will be equal to the amount passed into the last cell in the study area, so that no accretion will occur at the last cell.

The result of the finite barrier simulation is given in figure 4.11. The modelling parameters for this example is the same as those of the infinite length barrier example. The figure shows that even when the barrier

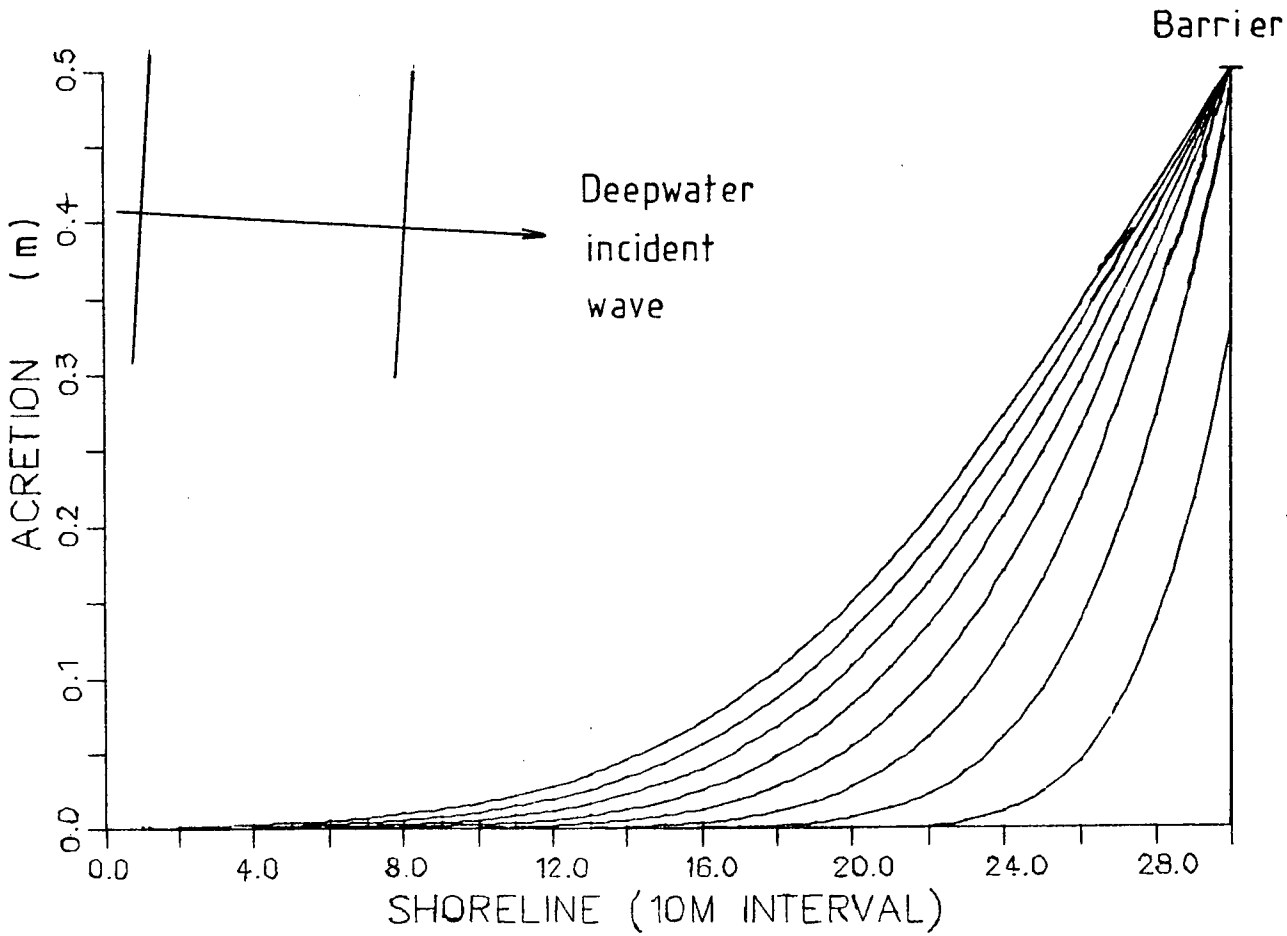

Figure 4.11 Plan view of the shoreline build-up due to finite length barrier

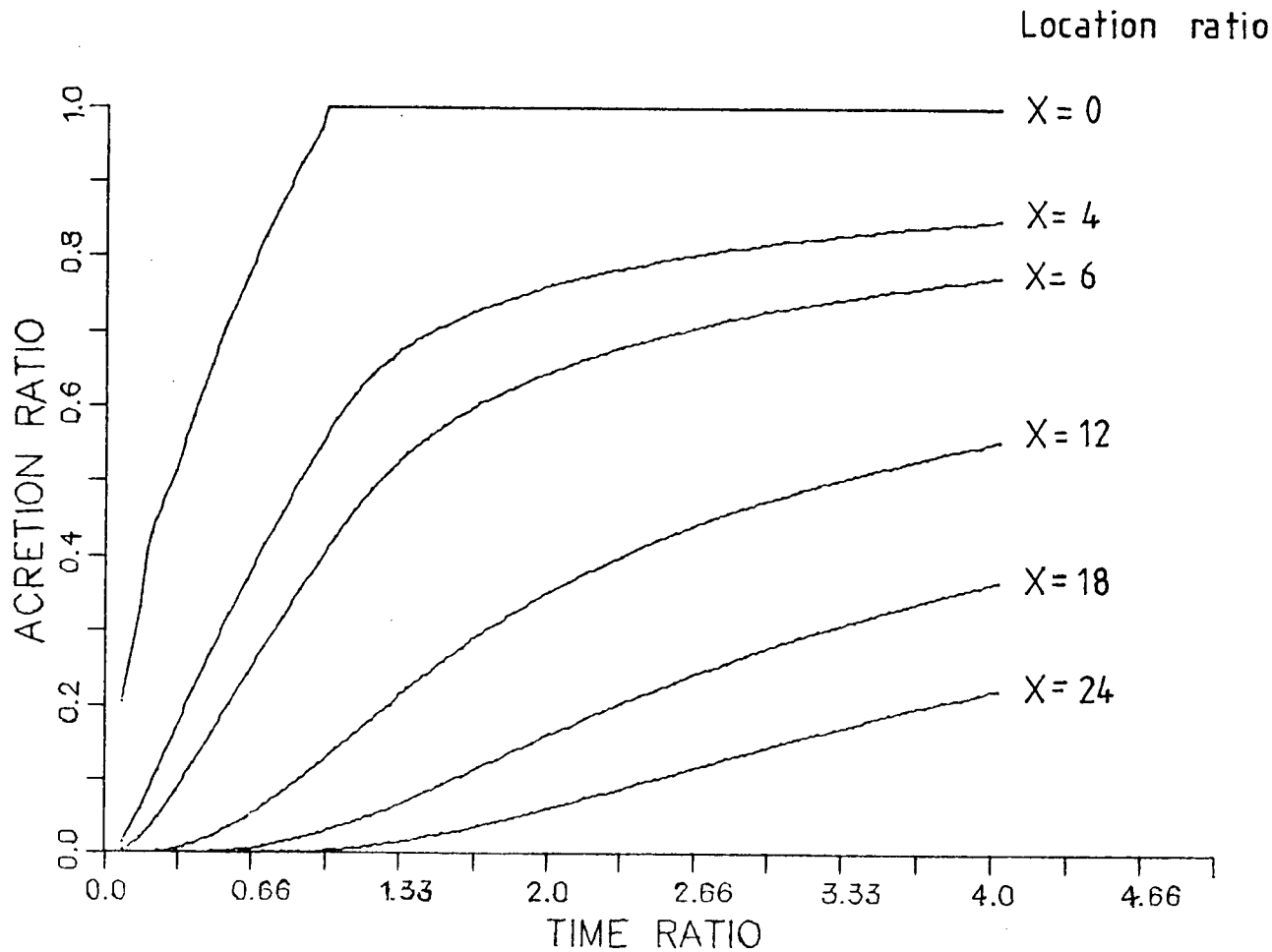

Figure 4.12 Non-dimensionalized accretion curves for finite length barrier

becomes ineffective in retaining the sediment, there is still accretion in the study area. Using a similar procedures as in the last section, a family of non-dimensionalised curves (figure 4.12) is obtained. The definition of T_F is different from before; it is now the time taken for accretion at the barrier to reach the barrier's length.

For time ratios between T = 0 and T = 1.0, the curves in figure 4.10 and 4.12 are the same. This is expected as the accretion behaviour is the same. After the time ratio exceeds 1.0, the curve X = 0 becomes a horizontal straight line. This is because there is no additional accretion at the barrier. In the other regions, the accretion continues but the rate of this accretion is noticeably reduced.

By comparing figures 4.8 and 4.11, one can see that there are two ways to achieve a desired accretion at a point. The two ways are either using a longer barrier and achieving the result in a shorter time, or a shorter barrier at a longer time. Figure 4.13 shows the two possibilities.

The solution to these two possibilities can be obtained using the following approach.

Solution

Recall that the solution for an infinitely long barrier is 8m.

Using the same approach with figure 4.12, the result

for a finite length barrier simulation is 6.2m.

This two lengths are shown as FB and FA respectively in figure 4.13.

Assume the time taken for accretion to reach B from F is T. Then from figure 4.10, the time taken to reach A from F will approximately be 0.6T. At this same instant, the accretion at E would have also reach D. From figure 4.12, the time taken for E to reach C is 4.2 (see Appendix E) times longer than for E to D. Hence the time for accretion at E to reach C will be 4.2 X 0.6T = 2.5T.

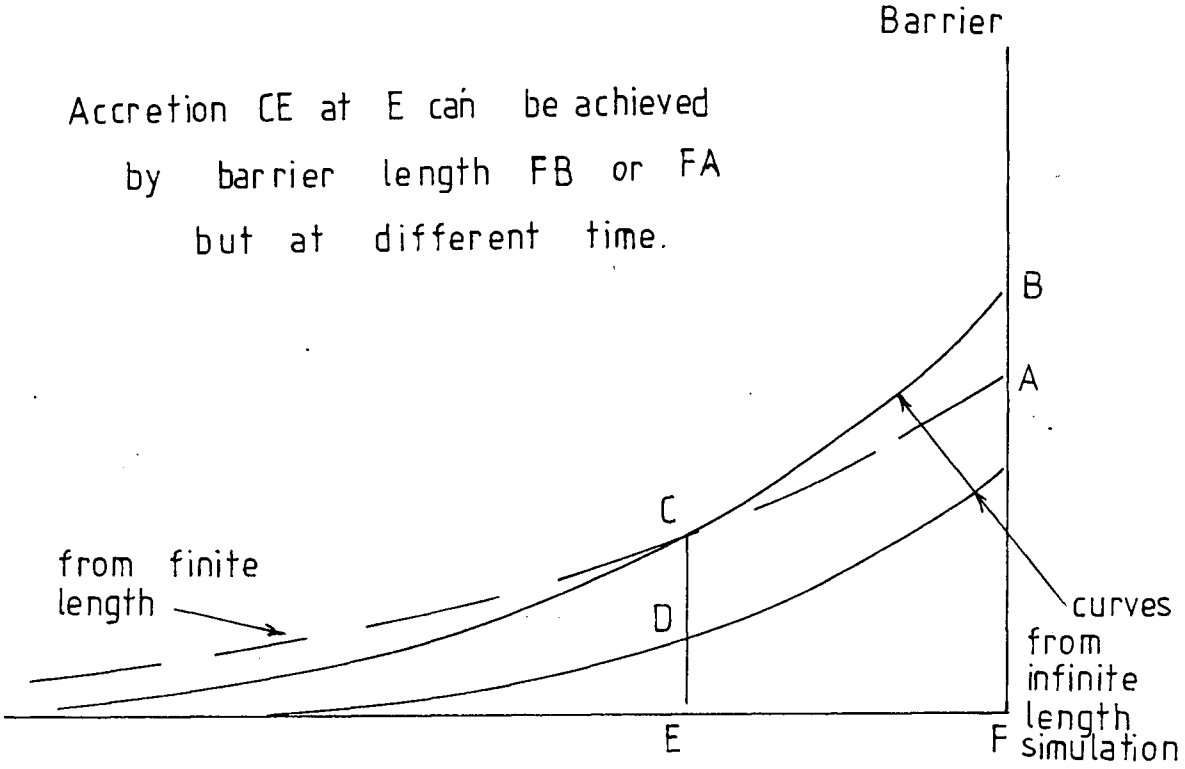

Figure 4.13 - Two possibilities of achieving a desired accretion

This implies that when using a shorter 6.2m barrier, the time taken to achieve the required accretion at the location would be 2.5 times greater than a longer 8m barrier. These two solutions are actually two extreme solutions. A whole range of solution exist between the two. Which to choose will have to depend on the restrictions

imposed on the solution. For example, if the time factor is not important as long as the required accretion is achieved, then it would make economic sense to use the shortest barrier possible.

C. Changes of beach nourishment plan

The objective of this simulation is to study the changes of a beach nourishment plan with time. The modelling parameters are the same as before except that the waves approach the shore orthogonally. The initial beach plan is triangular in shape and since symmetry is expected from the results, only half of the plan is modelled. The results of the model are shown in figure 4.14.

As expected, the sediment is eroding away from the apex of the triangular plan. The deposition occurs along the shoreline away from the apex. The time interval between each curve shown is the same. From this, it can be seen that the rate of change is slowing down.

Walton et al (1979) presented the results of the same problem using an analytical model by Pelnard-Considere. The results of the analytical model are shown in figure 4.15. A comparison of figures 4.14 and 4.15 shows many differences. However, one must look at the assumptions of the analytical model before drawing conclusions.

In order to linearise the governing equations for a simplified solution, Pelnard-Considere assumed that the breaker height is everywhere constant, and that the difference between the breaker angle and the deep water incident angle must be small at all times. These two assumptions are clearly violated in the numerical model presented in this report. This is because the refraction routine in the model will change the breaker angle and the wave height in comformity with the nearshore topograpy.

Therefore the two assumptions will have to be imposed on the numerical model to make a proper comparision. The results of the modified model with the two imposed conditions are shown in figure 4.16. For ease of comparison with figure 4.15, a non-dimensionalised version of the result is presented in figure 4.17. A comparison of figures 4.14 and 4.17 shows a satisfactory agreement. As such, the analytical model by Pelnard-Considere is essentially a model that does not consider the effects of wave refraction and wave shoaling.

The effect of wave refraction and shoaling can be seen clearly from figures 4.15 and 4.16. Due to refraction, the wave breaking angle to the shoreline will be small and approximately constant along the shoreline. Therefore, the longshore transport will be less and the rate of change of shoreline less dramatic.

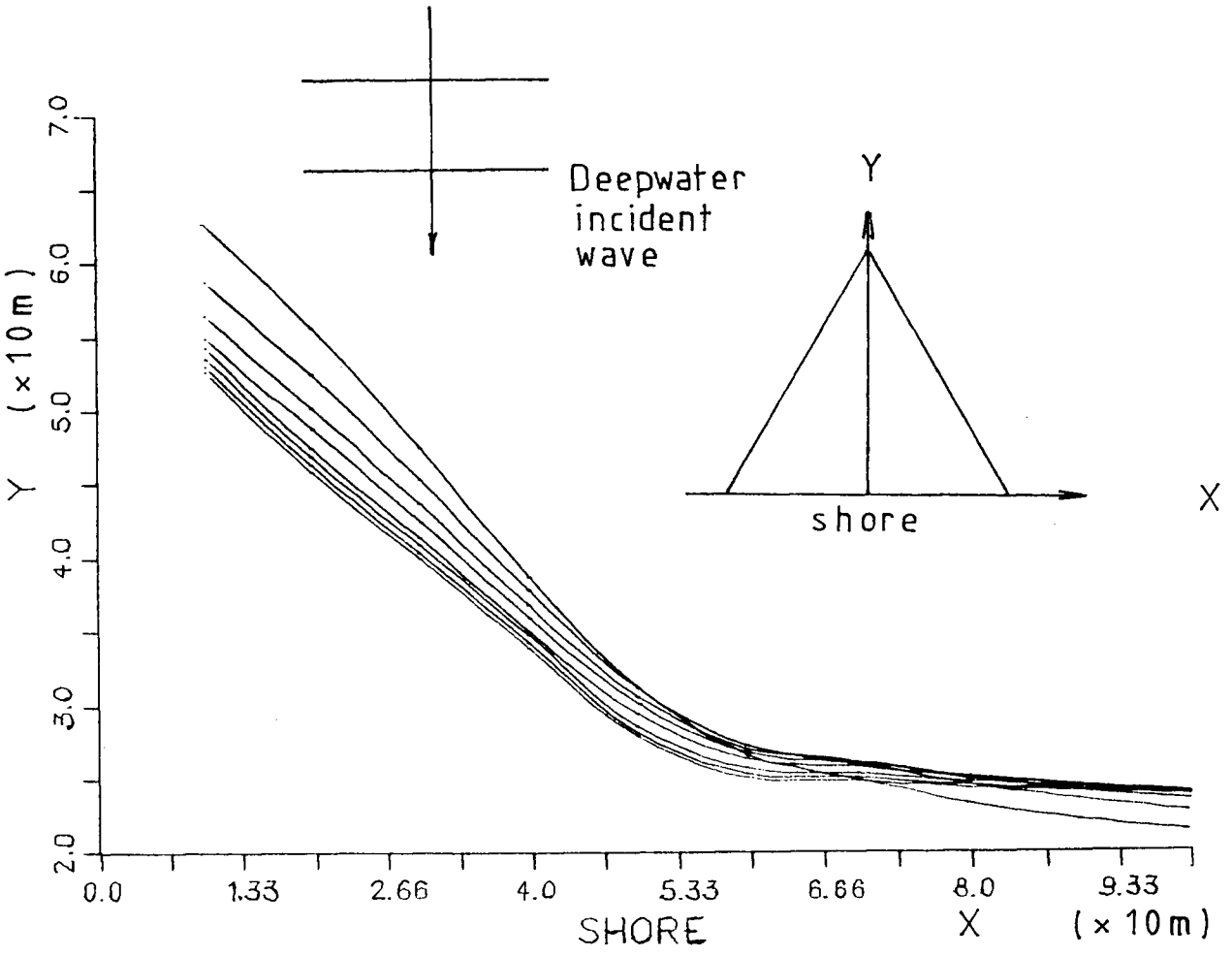

Figure 4.14 Beach nourishment plan changes
(with refraction and shoaling routine)

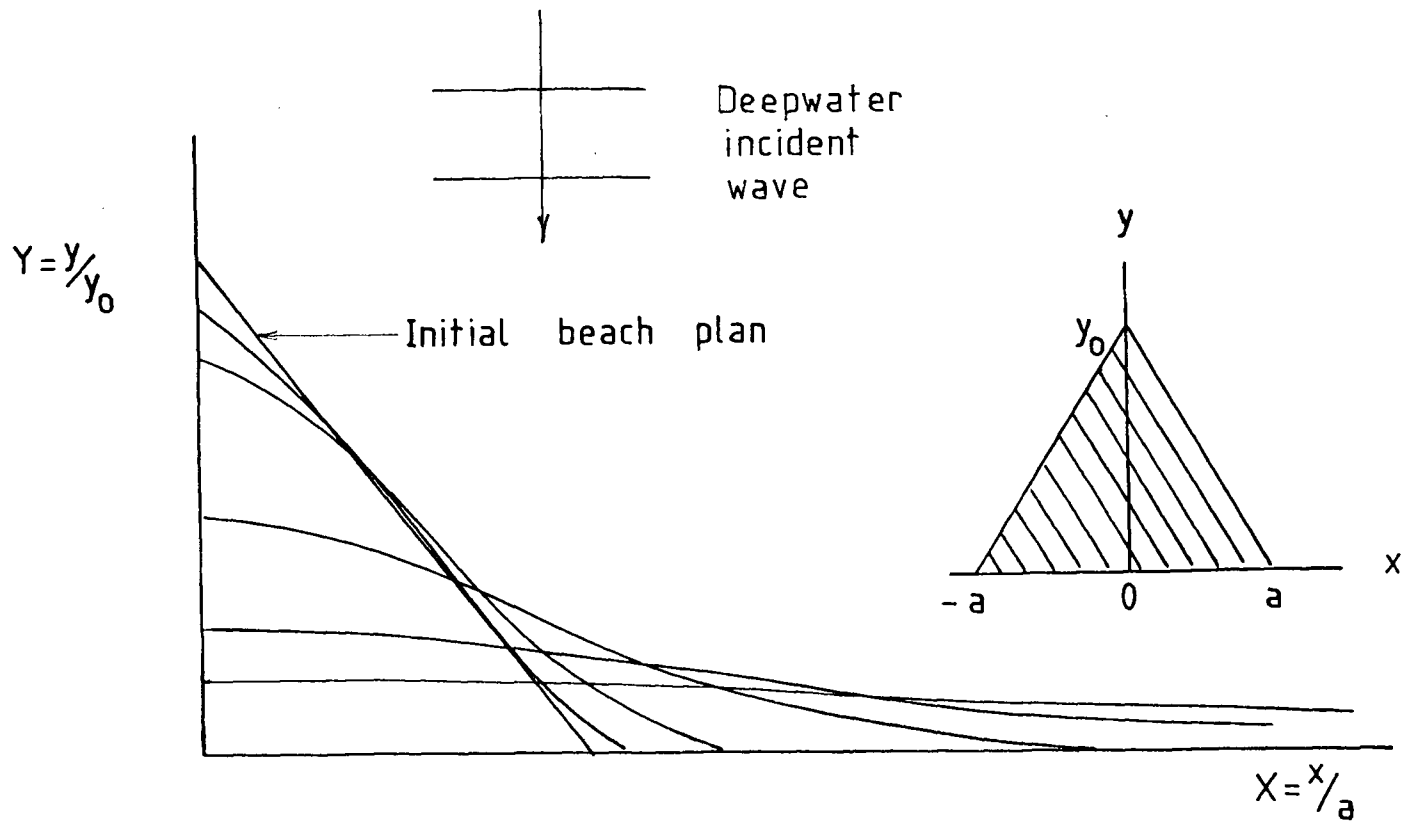

Figure 4.15 (After Walton et al, 1974) Analytical result of beach nourishment plan changes

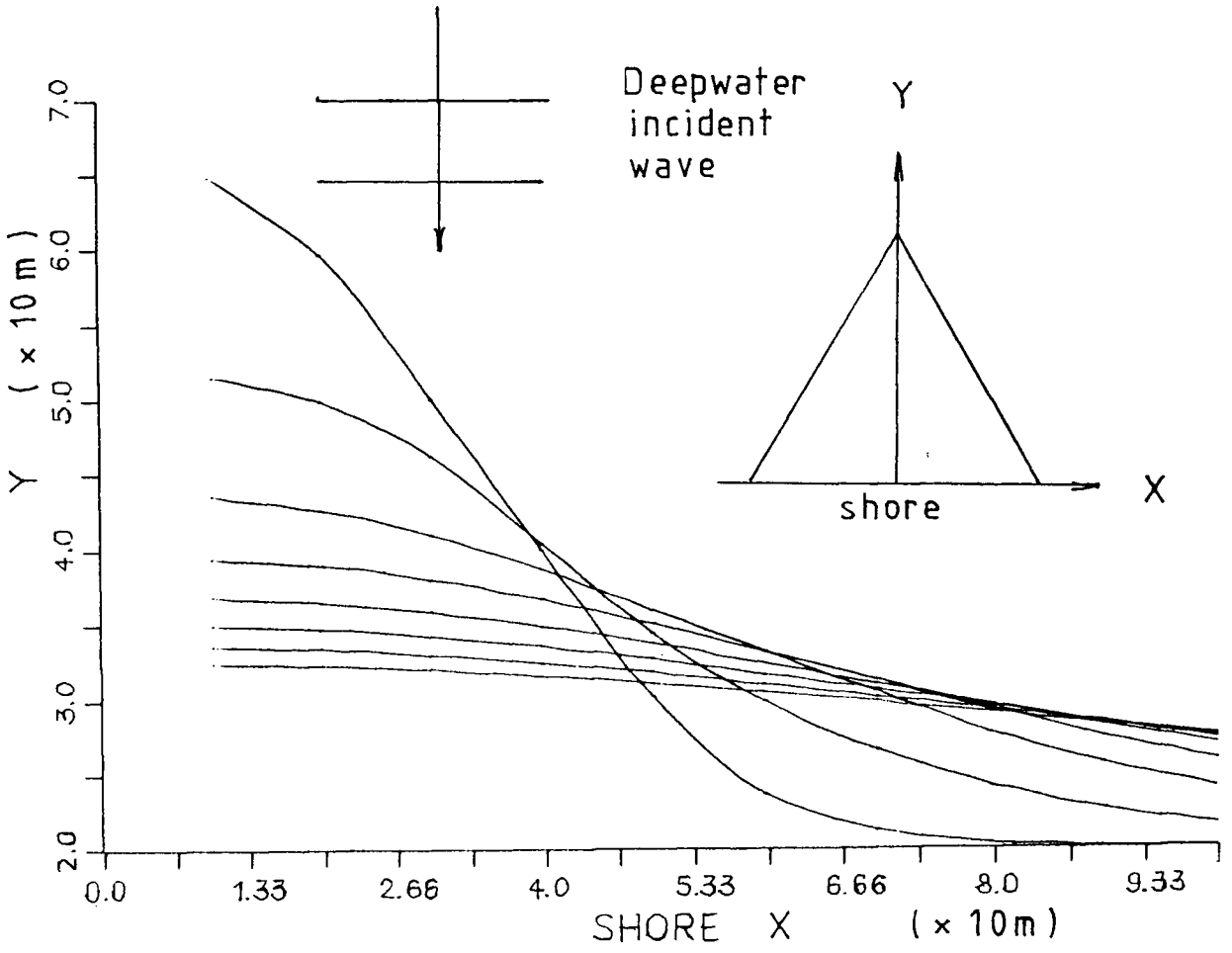

Figure 4.16 Beach nourishment plan changes (without wave refraction and shoaling routine)

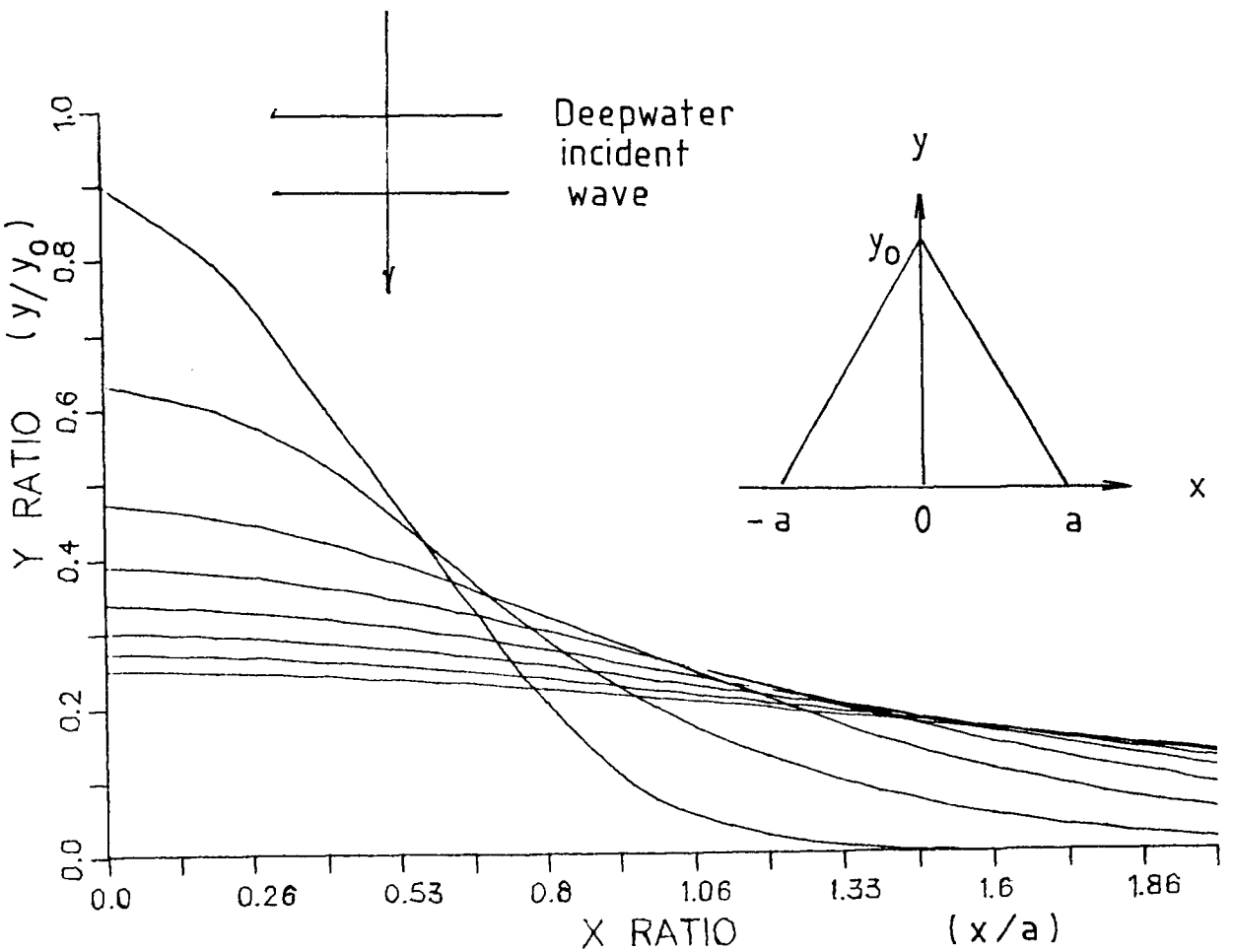

Figure 4.17 Dimensionless version of Figure 4.16

4.6 Discussion

The results presented in this chapter will have to be viewed under the light of the assumptions made in the model, the most important of which is either that there is negligible on-offshore transport, or the value of this transport is known and can be taken into account in the continuity equation. In addition to the assumptions, the model results will also be influenced by the accuracy and stability of the calculations.

As in all numerical models, the accuracy of the results will depend on modelling parameters such as the grid size, ΔX, ΔY, and model time interval ΔT. It is easy to see that if smaller values of ΔX, ΔY, and ΔT are used, the results of the model will be more accurate and detailed over the study area. However, due to the length of the computation involved, a finer grid would definitely entail more computation time and would be more costly to run. Thus there is this balance between the accuracy of the results required and cost.

In addition to the accuracy, there is the question of computational stability. Since various combinations of ΔX, ΔY, and ΔT can be used, there would exist a wide spectrum of solutions. These solutions can be of three types:

a) Inaccurate solution

b) Accurate, close to true solution

c) Oscillating, unstable solution.

The accuracy of solution as mentioned before, will improve with a finer grid mesh and a smaller time interval. However, there exist a criteria where the solution becomes unstable and oscillates.

For the calculation to be 'stable', the time-step interval, T must be small enough to ensure that the beach does not oscillate with increasing amplitude about its equilibrium position. The scheme adopted to achieve this 'stable' calculation is empirical and is determined by a trial and error technique. The condition which must be satisfied is that the net volume of transport for a cell at time 'i' must not be greater or equal in magnitude to the net volume of transport of the same cell at time 'i $+\Delta$ T'. If this condition is not met, the calculation is unstable and will not converge.

CHAPTER 5

ON-OFFSHORE TRANSPORT INVESTIGATION

5.1 Introduction

It is known from field observations that the on-off shore movement of sediment causes changes in the beach profile. The understanding of this movement and the resulting profile change is therefore important and essential in any attempt to model the on-offshore behaviour. A thorough discussion of all previous investigations on on-offshore sediment movement would be exceedingly lengthy. So this chapter will briefly mention some of the more important investigations. Also presented are the results of an experimental study on the profile change under constant wave attack.

5.2 Previous Investigations

Investigators in the 1950's descibed beach profiles brought about by different wave conditions as either winter or summer profile. A typical winter (or storm) profile has a milder slope and contains one or more offshore bars, while a summer (or swell) profile is generally steeper and smoother. This change is now

understood to be the effect of on-offshore sediment movement.

The change of direction of the sediment movement is generally believed to be related to the deepwater wave steepness (H_0/L_0). However, investigators (Johnson, 1949; King and Williams, 1949; Rector, 1954) had came up with different critical values of H_0/L_0. The differences in the values were found to be due to the dependence of the ratio H_0/L_0 on sediment grain size and scale effects (Iwagaki and Noda, 1963).

Dean (1973) presented a different model for determining the direction of movement. Dean considered the trajectory of a suspended sand particle during its fall to the bottom which is acted upon at the same time by the horizontal water particle velocity. Using the data of Rector (1954) and Saville (1957), Dean obtained the following relationship for determining the probable direction of sediment movement:

$$[5.1] \qquad \frac{H_0}{V_f T} = 0,85$$

$H_0/V_f T$ is known as the dimensionless fall velocity, where V_f is the fall velocity calculated using the median grain size, D_{50}. The coefficient 0.85 is sometimes called the fall-time parameter. Other investigators had suggested values other than the 0.85 found empirically by Dean. Kohler and Galvin

(1973) recommended the value of 0.70, while SPM(1977) suggested 1.0 to 2.0. Even though the use of this dimensionless fall velocity has proved to be very successful in the prediction of the type of profile and the direction of sediment movement, it will be shown later that equation [5.1] cannot be used alone to predict the direction of sediment movement.

5.3 Equilibrium Profile

An equilibrium profile is defined by Gourlay (1980) as 'the profile shape which when subjected to a given wave condition dissipates and/or reflects all the wave energy reaching it in such a manner that no net transport of the beach bottom sediment occurs anywhere along the profile.' A true equilibrium profile cannot exit in the field because of the changing wave conditions. However, a 'dynamic' equilibrium can be achieved if the time consideration is extended to a complete cycle of the changing season.

In a laboratory, the true state of equilibrium can be achieved under a constant, one direction monochromatic wave attack. Even though this true state of equilibrium is not achievable in the field, the concept of an equilibrium profile is extremely useful: it will enable us to understand the response of a profile to different wave conditions.

5.4 Beach Slope

Since a typical summer profile is generally steeper than a winter profile, it would then be expected that the slope of an equilibrium summer profile will also be steeper than a winter equilibrium profile. This variation of equilibrium beach slope is of interest because it is closely linked to the profile change. Among the many factors which affect the equilibrium slope, the more important ones are:

a) Mean grain size, D_{50}

b) Wave energy level, E

c) Deep water wave period, length and height, T, L_o and H_o

d) Fall velocity, V_f

e) Density of sediment, ρ_s .

Using dimensional analysis, the equilibrium slope should then be a function of

$$\left[\frac{H_o}{L_o} , \frac{D_{50}}{H_o} , \frac{V_f^2 \rho_s}{E H_o} , \frac{V_f T}{H_o} \right]$$

Most of the relationships relating the above variables and the slope were shown by Wiegel (1964) and King (1972). An experiment was conducted to affirm some of the the relationships and also to find some basis for numerical modelling in the next chapter. The descriptions and the results of the experiment are given in the next section.

5.5 Experimental design and procedures

The objectives of the experiment are to study:

1) the two types of beach profile
2) the rate of change from one equilibrium profile to another due to changes in wave conditions.

A model beach was set up in a flume 28m long 0.6m wide and 0.7m deep. The waves were generated by a wave paddle capable of varying the wave height and the wave period. 'Fraser river' sand was used as the beach sediment. The grain size distribution of the sand is shown in Appendix F. The sediment was laid over a rigid wooden base, sloping at 1 in 10, with an average thickness of about 200mm.

The instruments set up for the experiment were as follows:

1. A profiler, that reads to the nearest 0.001 feet, was mounted on a travelling carriage that can be moved along the longitudinal length of the flume.
2. Two wave probes - one fixed at a designated location and the other mounted on the same travelling carriage as the profiler.
3. A two-pen paper recorder for recording the output from the wave probes.
4. An oscilloscope for visually checking the output from the wave probes.

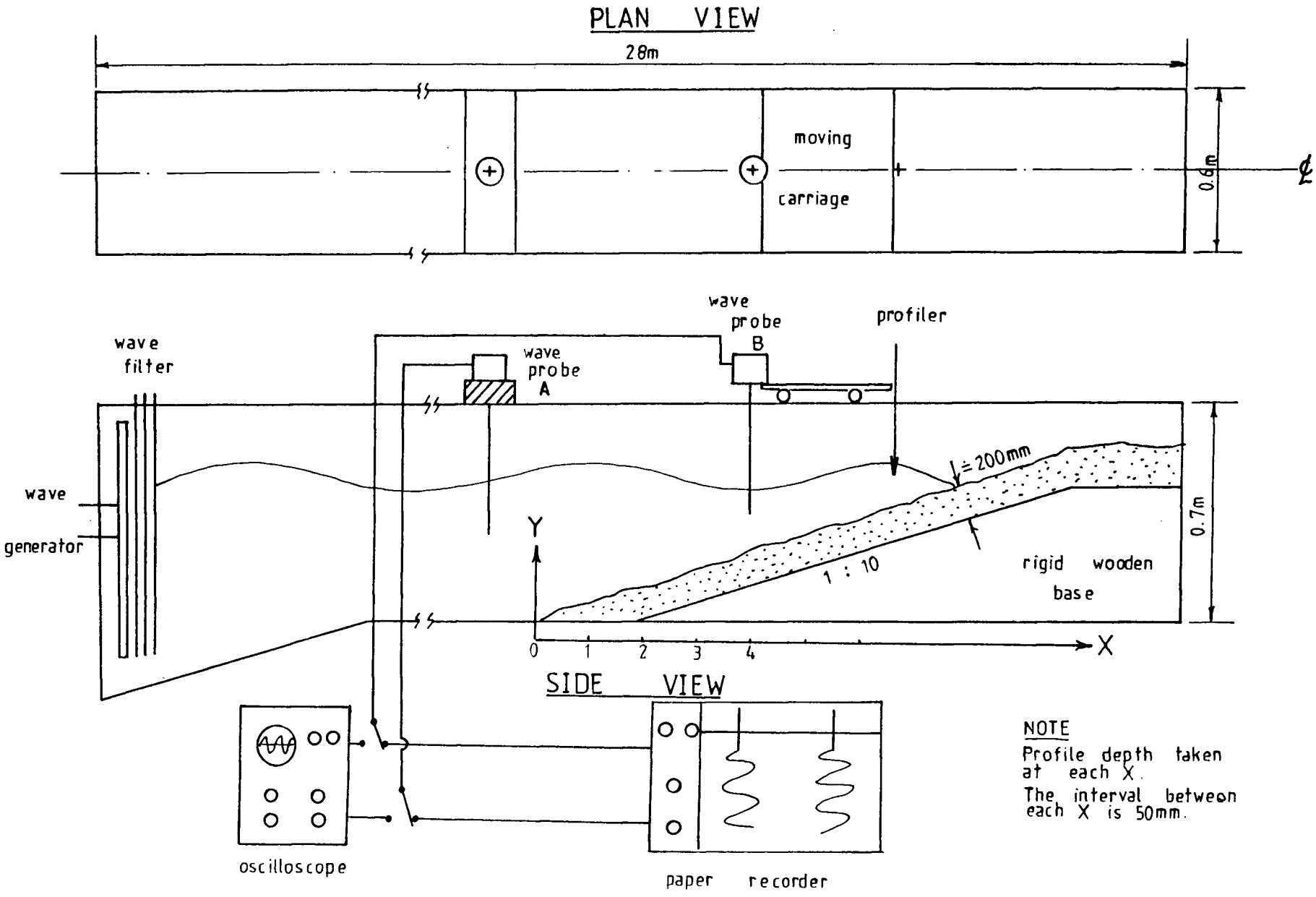

Figure 5.1 Overall experimental set-up

The overall set up of the experiment is shown in figure 5.1.

Three test were conducted, each with a different initial profile and wave condition. The different wave conditions and the schedule for data recording are shown in table 5.1. Each of the tests was performed using the same procedure as described below.

Since the main objective is to study the changes between two equilibrium profiles, it is essential that each initial profile is an equilibrium profile. Therefore before starting test 1, a certain wave condition was selected, and the beach was subjected to this initial wave action for a continuous period of about 24 hours until no significant changes in the profile were detected. The resulting profile was then designated as the initial equilibrium profile for test 1. The wave conditon for test 1 was then set and test 1 began.

At scheduled time intervals, the following data were recorded:

a) The profile of the beach from the backshore berm to the toe of the slope.

b) The envelope of the standing waves caused by the interaction between incident waves and waves reflected from the model beach.

c) The incident wave length, period, height and water depth.

TEST	IMPOSED WAVE CONDITION		Dimensionless * Fall Velocity $H_o/V_f T$	Data recording intervals	Remarks
	WAVE HEIGHT H(mm)	WAVE PERIOD T(s)			
Initial	40	1.5	0.5312 (Swell profile)		
1	58	1.12	1.0227 (Storm profile)	0 - 8 hr. @ 2 hr. 8 - 24 hr. @ 4 hr.	Total of 9 profiles recorded
2	30	1.26	0.4743 (Swell profile)	0 - 8 hr. @ 4 hr.	Total of 3 profiles recorded
3	30	2.11	0.2832 (Storm profile)	0 - 12 hr @ 4 hr.	Total of 4 profiles recorded

* The fall velocity of D_{50} for this experiment is approximately 50 mm per second.

Table 5.1 Imposed wave condition and schedule for data collection

At the end of test 1, the last profile of the test became the initial equilibrium profile for the next test. All the procedures were then repeated.

5.6 Results

Profile changes

Of the nine profiles recorded in test 1, four are shown in figures 5.2 and 5.3. Figure 5.2 shows the profile of the model beach at the beginning and at the end of the test. It can be seen that a large amount of sediment has moved offshore, as expected. Table 5.1 already showed that the profile will change from swell to storm because of the change in the dimensionless fall velocity. Most part of this movement occurred early in the test. Figure 5.3 shows the change for the first four hours at two-hour intervals. The final location for the deposition cannot be detected at these early stages; only later was it found to occur at around X = 48.0 (see figure 5.2). Other features of the profile change, like the erosion of the beach face, and the retreat of the shoreline, can also be detected from the figures.

Test 2 is essentially the reverse of test 1. The wave conditions were changed from a storm to a swell. The slope of the beach was expected to build up back towards its original condition, and from figure 5.4 in general it

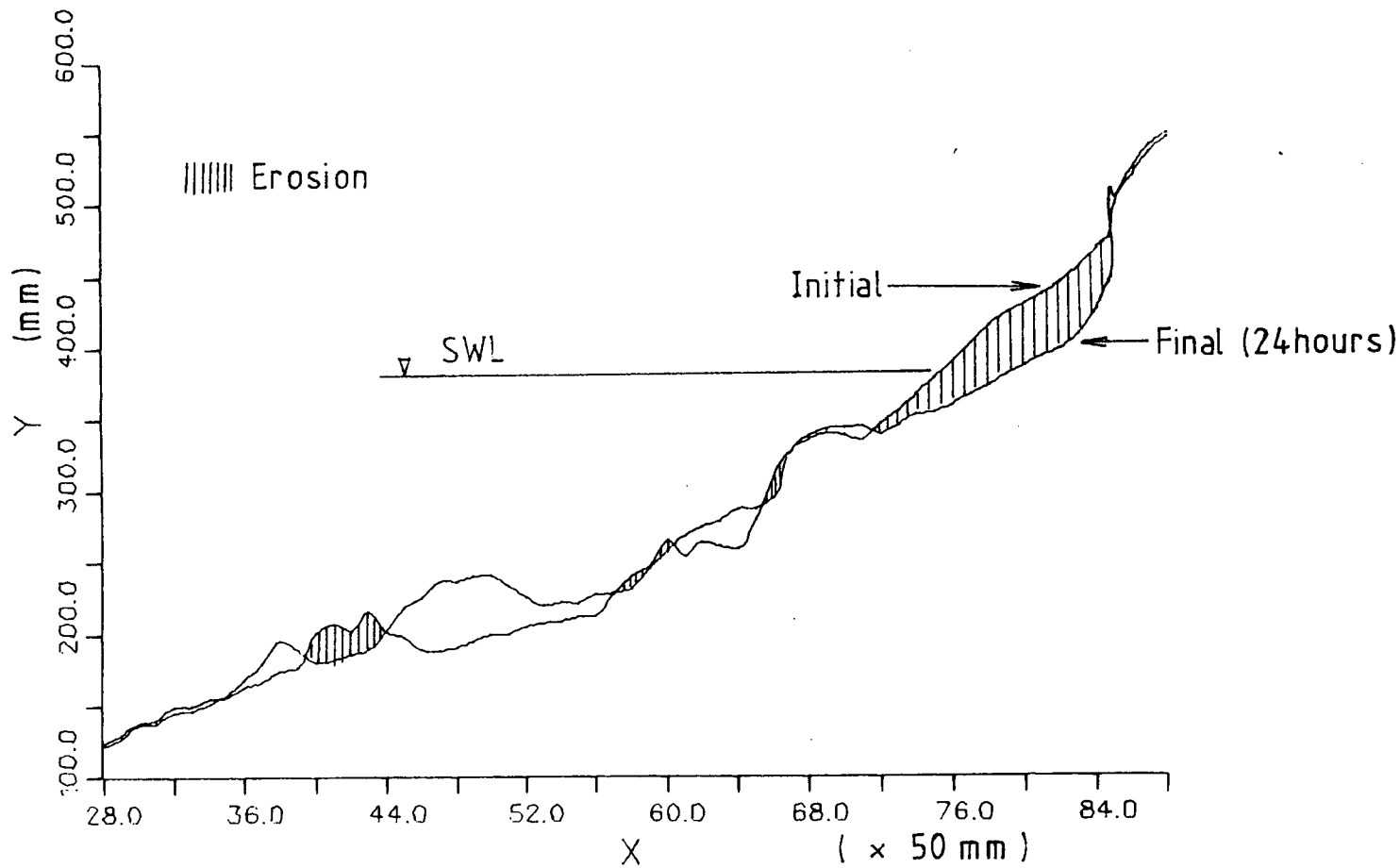

Figure 5.2 Profile changes - Test 1 (Initial and final profiles)

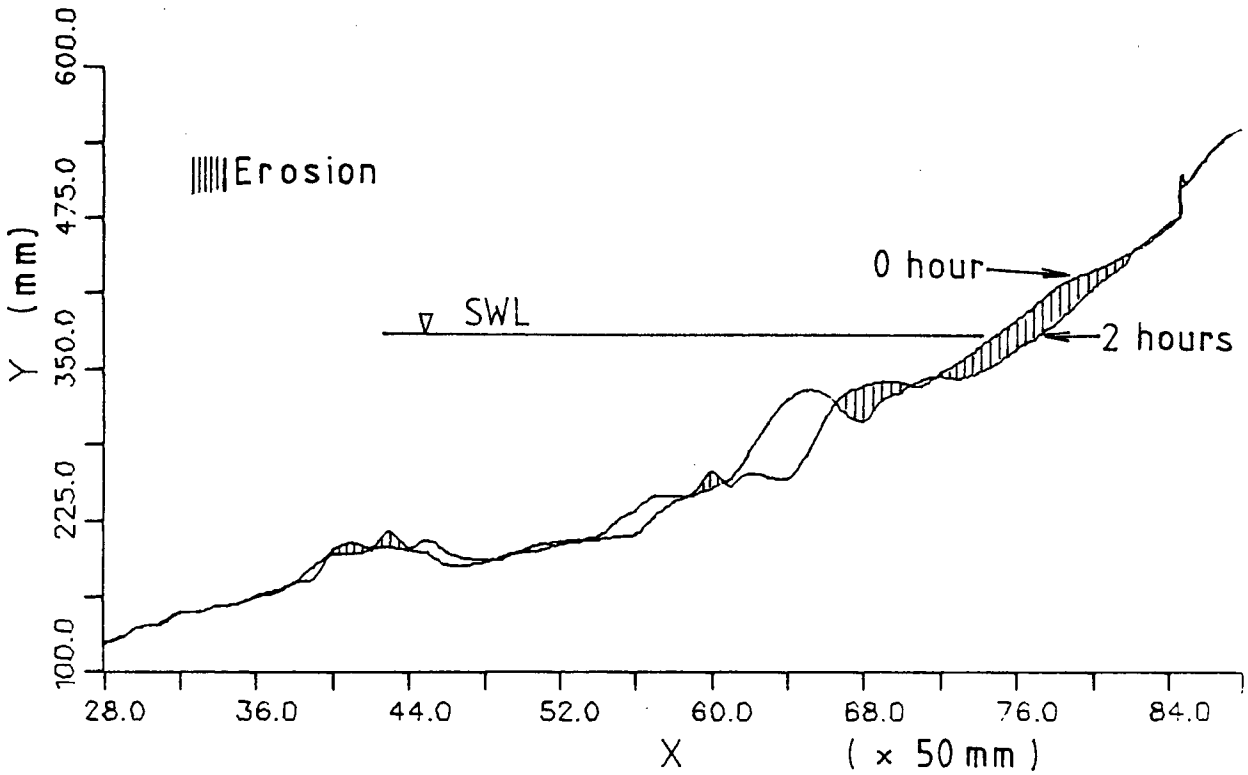

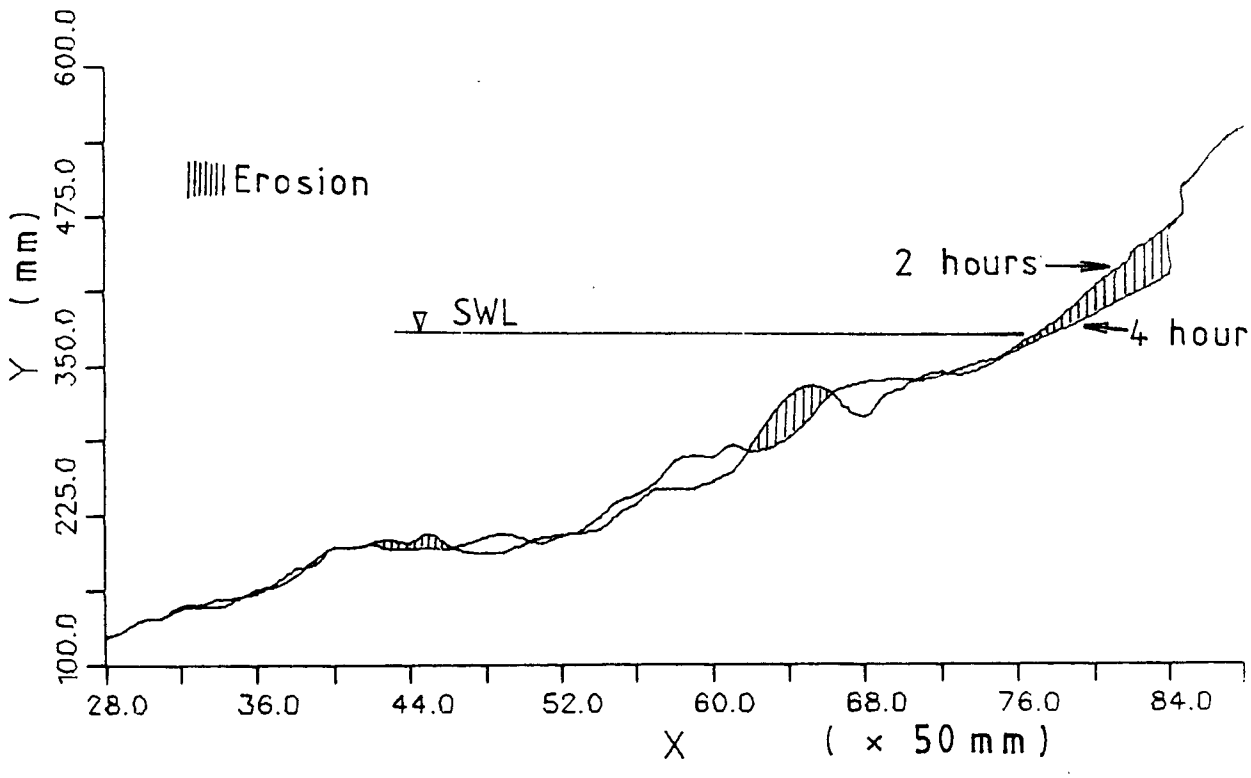

Figure 5.3 Profile changes - Test 1 (At 2 hours interval)

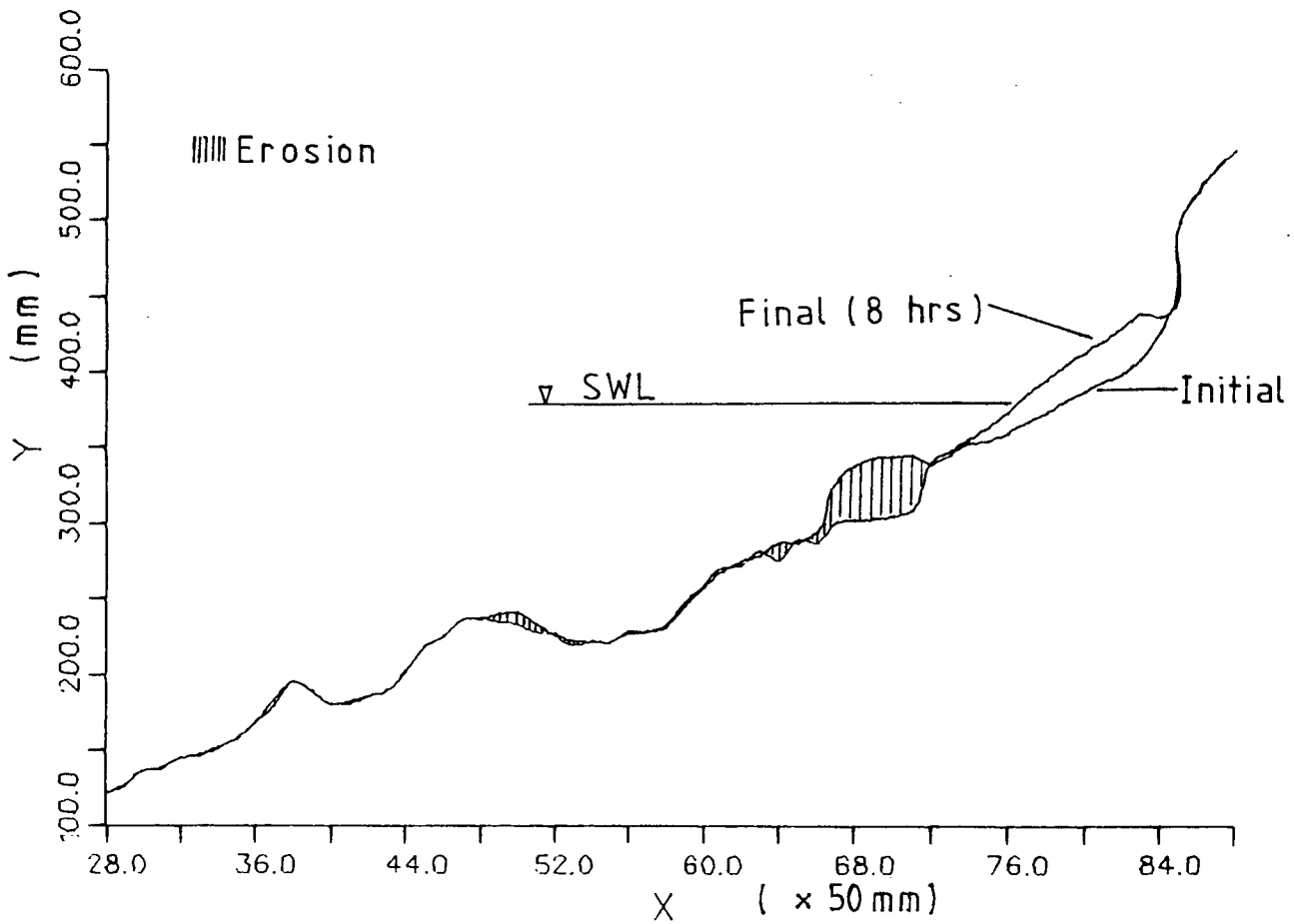

Figure 5.4 Profile changes - Test 2

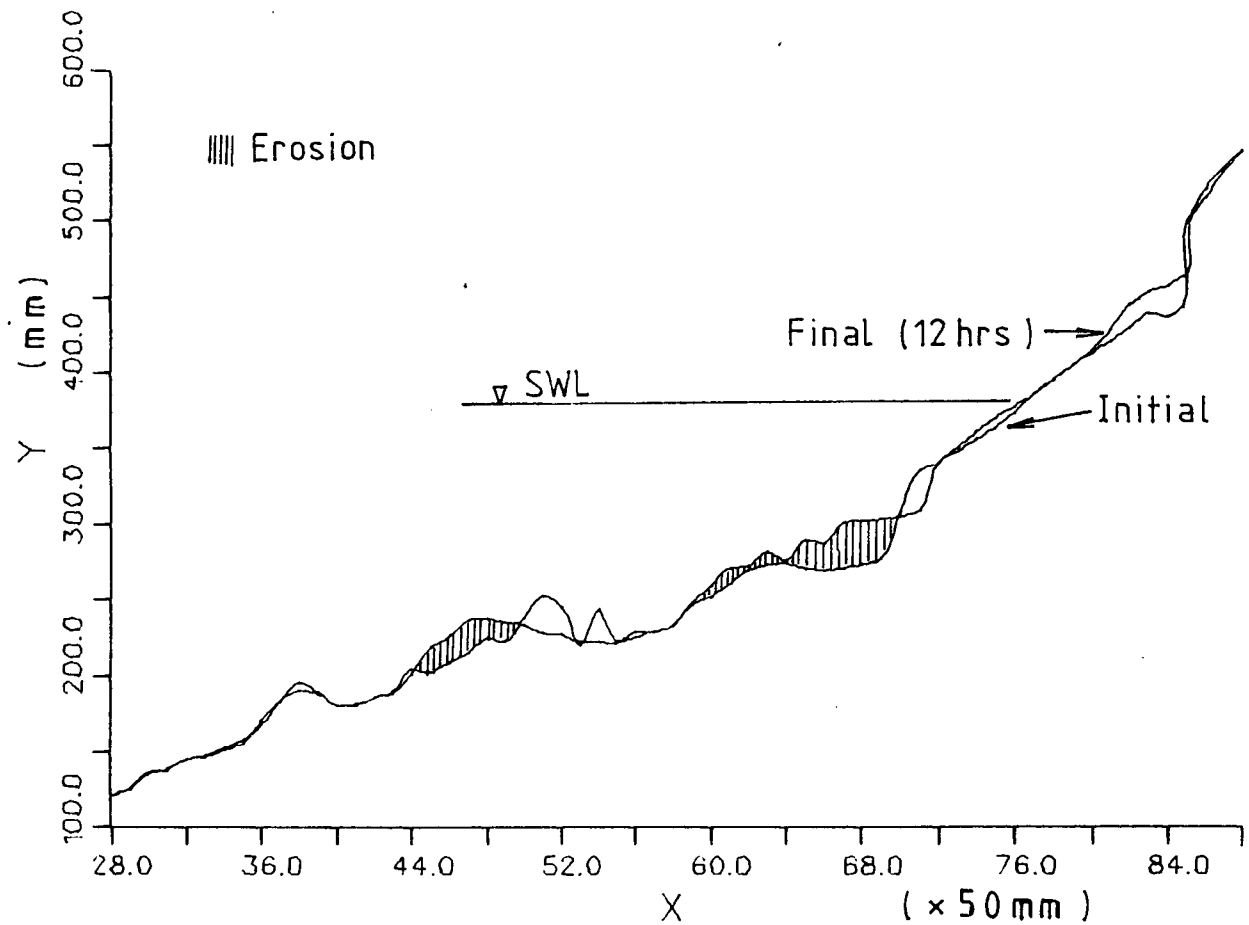

Figure 5.5 Profile changes - Test 3

clearly did. However, the process is not completely reversible because some sediment is moved offshore and smaller waves cannot move it onshore again. In the present test, a step like feature had formed at X = 70.0 and it was noticed that there was little sediment movement offshore at X = 60.0. This test was stopped after only 8 hours because of insignificant changes in the profile.

The wave conditions for test 3 were similar to test 2 except for a longer wave period. The results of the test (figure 5.5) show similarity to those of test 2. The beach slope became steeper and the step became more prominent. There was also a considerable shoreward movement of sediment at X = 48.0. This is attributed to the longer wave period which affects deeper depths and results in a wider zone of sediment movement.

From the three tests, it can be seen that beach sediment can move either onshore or offshore depending on the wave condition but not in a completely reversible manner. Sediment can sometimes be moved so far offshore by destructive waves that even an extended swell condition cannot bring them back towards the shore. When this happens, a permanent recession of the shoreline will result. Therefore it is expected that the rate of shoreline recovery after an extensive storm will be slow and incomplete.

The results of test 1 are used to find the rate of

change of profile. Figure 5.6 shows the cummulative changes of the profile (in terms of total net volume transported) against time. The figure indicates that the rate of change is decaying with time. So that changes in the profile are most detectable during the early stages. Scott (1954) obtained a similar result and suggested a logarithmic fit for the data. Figure 5.6 shows this logarithmic fit

$$Y = a + b \ln X \qquad [5.2]$$

as type I, the coefficients 'a' and 'b' of which are shown in table 5.2. Unfortunately this curve gives negative values for total volume transported when time 't' is less than 1 hour and this is physically impossible. A different approach for fitting the data is proposed here.

Assuming the change of the transport rate at a specific time is proportional to the transport rate at that time, the following equation can be written,

$$\frac{\partial(Tr)}{\partial t} = - P(Tr) \qquad [5.3]$$

where Tr is the transport rate and P a constant. The negative sign signifies that the rate of change is decreasing with time. Integrating equation [5.3],

$$Tr = e^{(k+Pt)} \qquad [5.4]$$

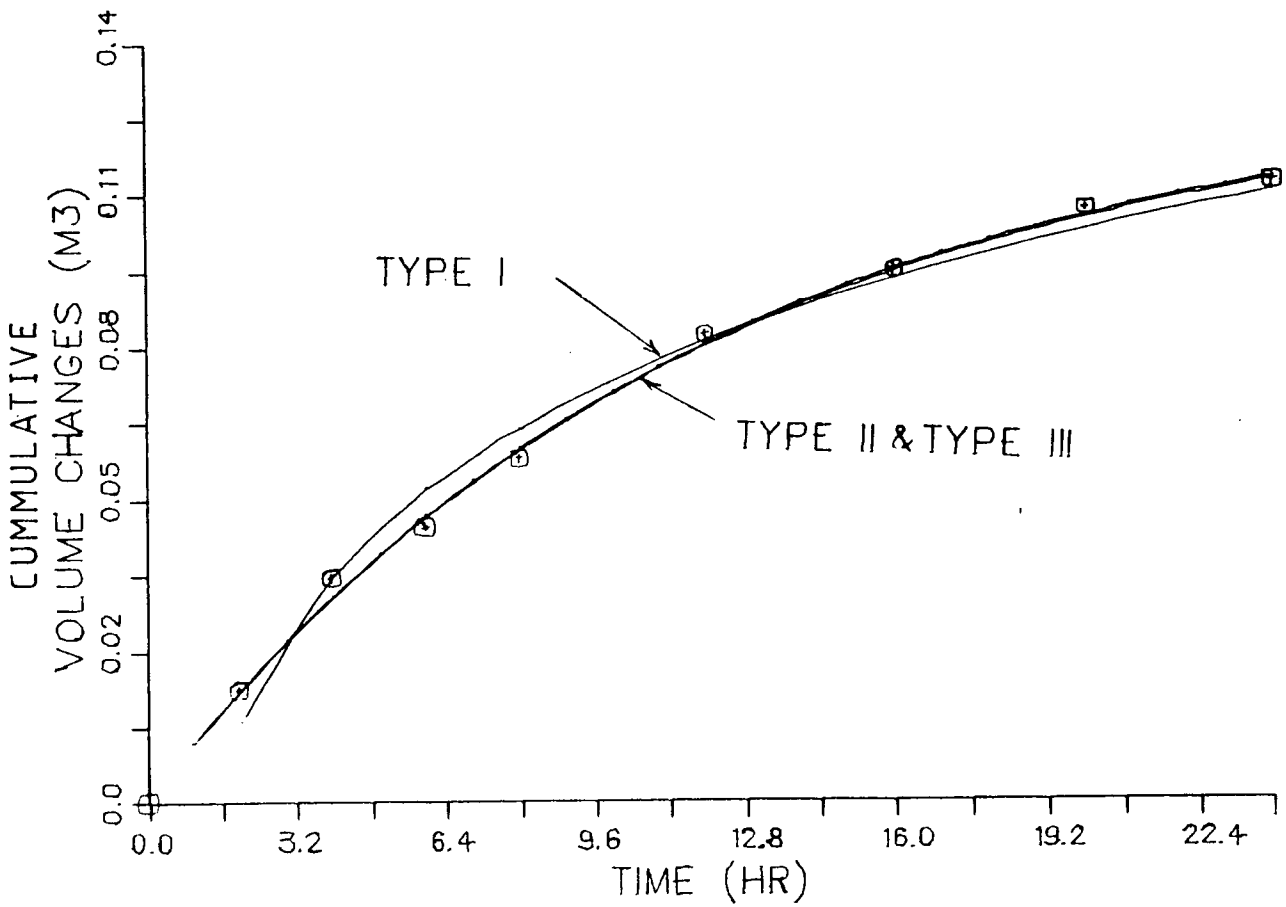

Figure 5.6 Cummulative changes of the profile against time

Since the transport rate integrate to give the volume transport over time, equation [5.4] can be re-written as

$$[5.5] \qquad Tr = \frac{\partial Q}{\partial t} = a\, e^{-Pt} \qquad \text{, where} \quad a = e^{k}$$

therefore

$$[5.6] \qquad Q = b - \frac{a}{p}\, e^{-Pt}$$

where Q is the volume transported; a and b are the integrating constants.

To fit equation [5.6] by a nonlinear least square method is difficult. However, using a computer program developed by Golub et al (1972), the coefficients of a different function, but one that is close to equation [5.6] can be obtained, (type II in table 5.2 and figure 5.6). From table 5.2, the coefficients a and b are so close that the function can be reduced to

$$[5.7] \qquad f(x) = a_1 + (a_1 + a_3)e^{-bx}$$

which is essentially the form we want.

The coefficients of equation [5.7] are obtained using a similar curve fitting procedure as above, and shown in table 5.2. The fit of this equation, shown as type III in figure 5.2, is good.

Looking again at equation [5.6] and by imposing the initial condition of zero transport at time t = 0,

$$[5.8] \qquad Q = \frac{a}{p} - \frac{a}{p} e^{-Pt}$$

From this equation, it can be deduced that when time 't' approaches infinity (i.e. approaching equilibrium), the final total volume transported is

$$[5.9] \qquad Q_F = \frac{a}{p}$$

Substituting this into equation [5.8], we obtain

$$[5.10] \qquad Q_F - Q = \frac{a}{p} e^{-Pt}$$

The left hand side of the equation represents the difference between the final volume and the existing volume. By differentiating equation [5.10] we obtain:

$$[5.11] \qquad \frac{\partial (Q_F - Q)}{\partial t} = P (Q_F - Q)$$

By intuitive reasoning, it is expected that with an increase in the wave activity and hence the wave flux, the amount of sediment transported will correspondingly increase. This suggests a relationship between Q_F and the wave flux:

TYPE	FUNCTION	COEFFICIENTS
I	$f(x) = a + b \ln x$	$a = -0.0125$ $b = 0.0395$
II	$f(x) = a_1 + a_2 e^{-b_1 x} + a_3 e^{-b_2 x}$	$a_1 = 0.1314$ $a_2 = -21.241$ $a_3 = 21.212$ $b_1 = 0.09493$ $b_2 = 0.09498$
III	$f(x) = a_1 + a_2 e^{-b_1 x}$	$a_1 = 0.1313$ $a_2 = -0.1310$ $b_1 = 0.086$

Table 5.2 Equations for the rate of profile change

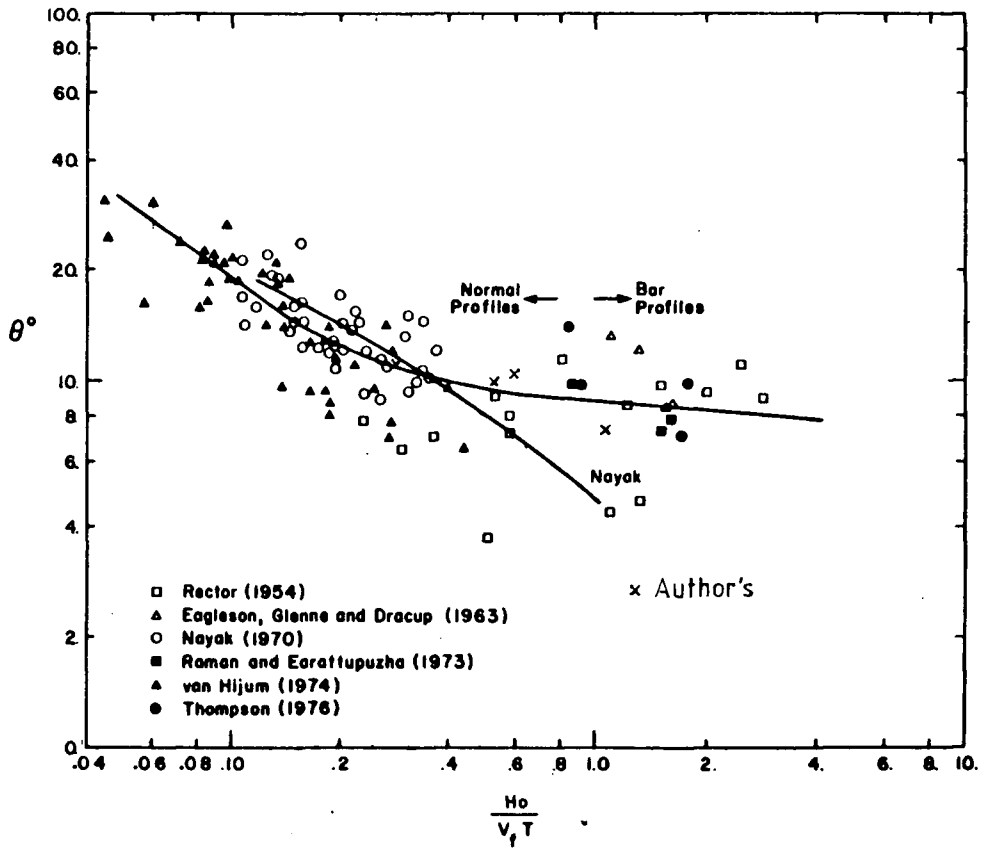

Figure 5.7 (After Dalrymple, 1976) Equilibrium slope against $H_0/V_f T$

[5.12] Wave energy flux $\propto$ $Q_F = \frac{a}{p}$

The exact relationship between these quantities cannot be determined. because insufficient data is available from the present set of experiments.

For a given wave condition, the final value of the slope is also the equilibrium slope, and as shown earlier this equilibrium slope depends on several parameters. Figure 5.7 shows a plot by Dalrymple et al (1976) relating one of these parameter, $H_0/V_f T$, to the equilibrium slope. Included in the figure are four data points from this experiment. These points show good agreement with the curve suggested by Dalrymple. This can be seen as support to Dalrymple's finding that the slope is uniquely related to the dimensionless fall velocity. Therefore, if the sediment properties and the wave condition are known, the value of the equilibrium slope can be estimated. Other than this, the curve by Dalrymple et al also provides a new way of predicting the direction of sediment movement, as suggested by Quick (1983). It is widely quoted by many investigators that equation [5.1] can predict whether the transport is onshore or offshore (Komar, 1975; Sorensen, 1978). However, by examining figure 5.7 and the experimental results, it is obvious that the direction of sediment movement depends not only on the final wave condition but also on the initial wave condition. For example, if the dimensionless fall

velocity changes from a higher value to a lower value, the slope of the beach is likely to become steeper, indicating a shoreward movement of sediment and vice versa. From this, it is apparent that a prediction of the direction of sediment movement is more appropriately based on the following relationship:

$$[5.13] \qquad \left(\frac{H_o}{T}\right)_i \frac{1}{V_f} \Big/ \left(\frac{H_o}{T}\right)_f \frac{1}{V_f} \begin{cases} > 1 & \text{for offshore} \\ < 1 & \text{for onshore} \\ = 1 & \text{equilibrium} \end{cases}$$

This new approach removes some of the problems encountered when using $H_o/V_f T$ alone, because a great range of values of $H_o/V_f T$ have been quoted by different researchers. It can also be seen from equation [5.13] that it is possible for the dimensionless fall velocity $H_o/V_f T$ to be greater than 0.85 or 2.0 (as indicated by equation [5.1]) and for the onshore movement of sediment to occur at the same time. As such, the use of $H_o/V_f T$ alone is potentially misleading, unless the profile at initial condition is at equilibrium, where $(H_o/V_f T)$ of equation [5.13] is 1.0. Therefore equation [5.2] represents just a special case of equation [5.13], and equation [5.13] is more useful as it can predict the direction of sediment movement in the profile when the wave condition changes from one non-equilibrium state to another.

CHAPTER 6

ON-OFFSHORE TRANSPORT MODEL

6.1 Introduction

The behaviour of on-offshore transport and the resulting beach profile have been studied by many investigators (Nayak, 1970; Swart, 1976; Dean, 1977). In this chapter some of these studies are discussed, and on the basis of some of these ideas a model is developed which predicts the changes of the beach profile. Thus, using this model, predictions of the shoreline retreat due to various wave conditions can be made.

This model will be incorporated into the longshore transport model presented in chapter four and the results of this combined model will also be presented.

6.2 Model Outlines and Assumptions

The model is based on the following assumptions:

1. The equilibrium beach slope can be defined if the wave condition is given. As described in chapter five, using the curve by Dalrymple et al (1976) shown in figure 5.8, the equilibrium beach slope for any wave condition can be found.

2. There is a point on the equilibrium profile where there is no net accummulation or erosion of sediment. Raman et al (1972) defined this point as a 'stable' point which 'acts as a fulcrum about which the profile swings while material is moved from one side of the point to the other.' Raman, however, did not make any attempt at predicting the location of such a point. Hallermier (1978) also conducted a similar study. He proposed that the beach be divided into two (offshore and littoral) zones. The offshore shore is characterized by relatively moderate bed agitation while the littoral zone is characterised by increased bed stresses and sediment transport. Then, by assuming the hypothetical boundary between these two zones to be the limit of intense bed agitation, Hallermier obtained figure 6.1. The variable 'd_c' of figure 6.1 is defined by Hallermier as the maximum water depth for intense bed agitation, and from laboratory tests it is also found to be the limit depth to the erosive action of the surface waves.

From the figure, it can be seen that the location of d_c is also the 'stable' point as defined by Raman. This point, even though defined as the point of no net acummulation or erosion, is also the point of maximum rate of transport. This can be shown by considering the kinematics of the sediment transported as the profile changes.

3. There exists a fixed equilibrium beach profile

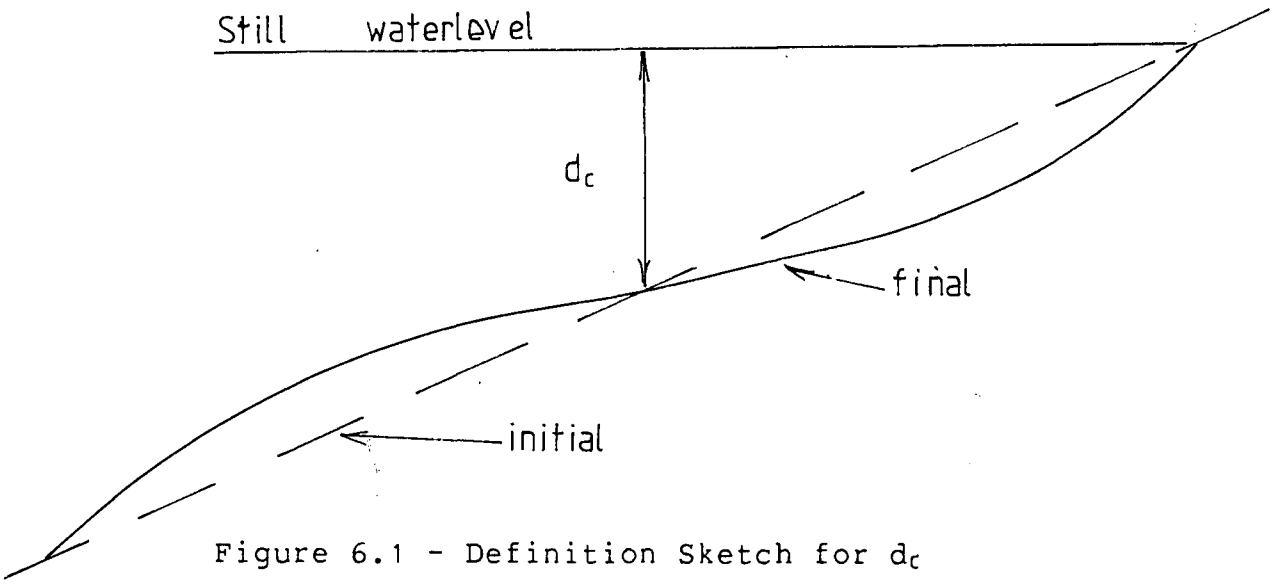

Figure 6.1 - Definition Sketch for d_c

shape corresponding to a given intensity of wave attack. Using the radiation stress theory and assuming uniform energy dissipation across the surf zone, Dean (1977) arrived at an expression, a power curve, for the equilibrium beach profile:

$$h = A x^m \qquad [6.1]$$

where h is the water depth from still water level and x is the seaward distance from the intersection of the shoreline and the waterline. In Dean's theoretical study the value of m was found to be 2/3.

Based on the above work and a similar investigation by Bruun (1954), Hughes et al (1978) fitted over 450 beach profiles to the above expression and obtained

the best 'least-squares' fit. The resulting values of A and m were analysed and the values of m were found to be normally distributed about an average value of 0.667. Their results showed that 53 percent of the values lay between 0.5 and 0.8. Because of this, they considered that m could be fixed at 2/3. This value of m is also supported by the results of Sayao (1982) and the theoretical work of Dean cited earlier. On the other hand A was found to be distributed over a wider range of values. From further investigations, Hughes et al suggested that A is primarily a function of the grain size distribution, so that its value varies from case to case.

4. The rate of profile change is assumed to follow an exponential decay. This assumption was confirmed from the experimental studies described in chapter five. Such exponential behaviour will exist whenever the rate of decay is dependent on the difference between the existing condition and the final condition. The progress of such processes is often described in terms of a half-life.

The above assumptions will be combined into a single model, and to do this it is necessary to examine the typical changes of profile (figure 6.2) due to an increase of wave activity. Under the action of wave attack, beach profile changes from profile A to profile B, which are both equilibrium profiles for their respective wave condition.

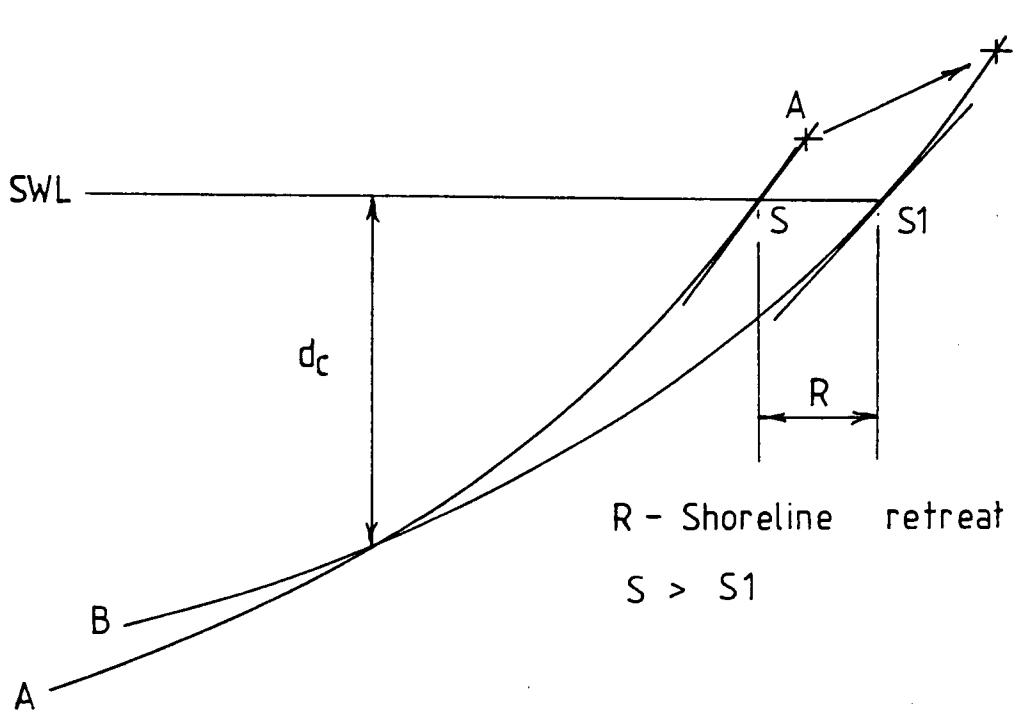

Figure 6.2 Typical profile changes

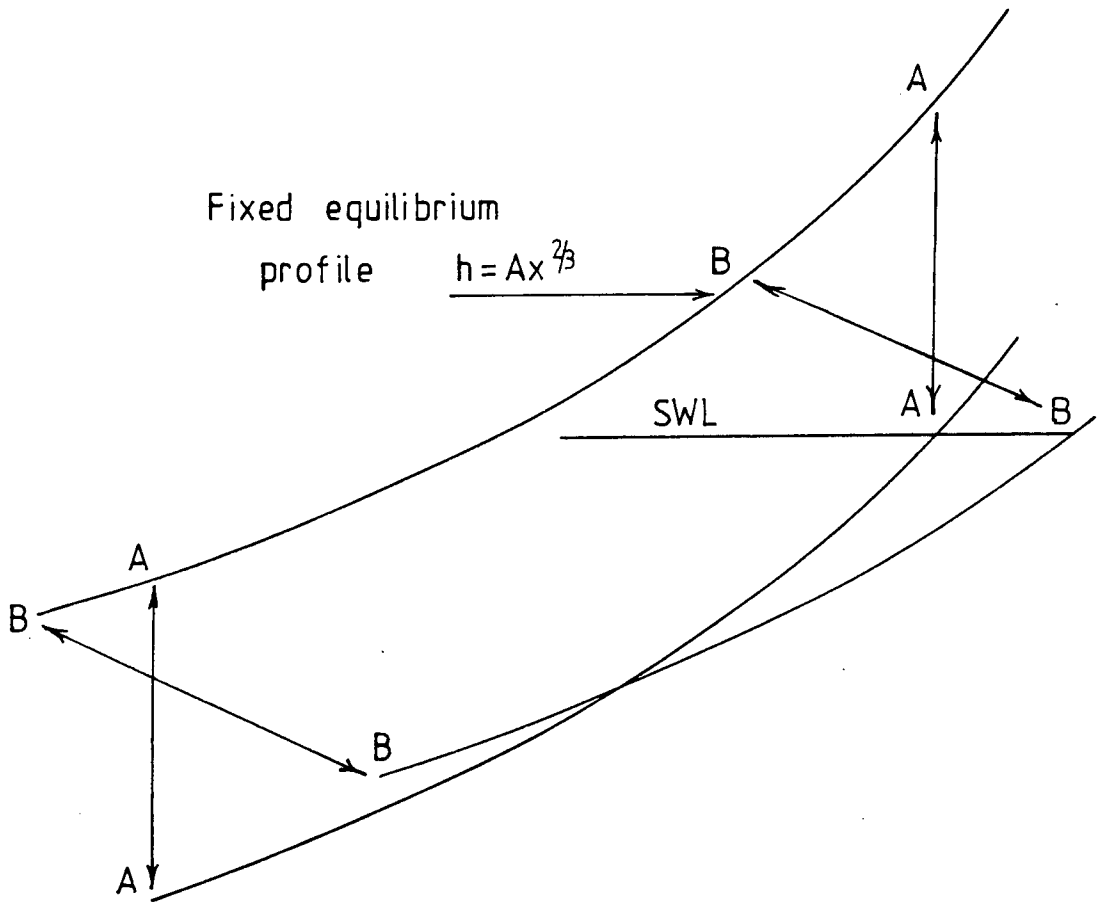

Figure 6.3 Modelling assumptions

Since equation [6.1] predicts a fixed equilibrium profile shape, it is assumed that profile A and profile B are essentially different parts of the same curve. This assumption is shown in figure 6.3. Even though this assumption is a simplification of the actual processes (it ignores offshore bar formation), the characteristic changes based on this simplified approach are still in line with those observed in the field. For example, the reduction of beach slope, the retreat of shoreline and the formation of a wider surf zone.

Figure 6.2 shows the location of d_c as the intersection point of the two equilibrium profiles. This is in accordance with the definition of a 'stable' point. The value of d_c as shown is dependent on the imposed wave condition, i.e. the wave condition that results in profile B.

With the above modelling concept, a simple model can be formed, and the following section presents the model algorithms. Later the model is tested with the results from the experiments of chapter five.

6.3 Algorithms of the Model

6.3.1 Calibrating the initial profile

As mentioned earlier, Dean and Hughes et al had arrived at an expression for the equilibrium profile. Given an initial equilibrium profile shown as in figure 6.4, the variables X, Y and A can be determined.

The value of the depth d_c can be obtained from the initial wave condition using the following formulation by Hallermier (1978):

$$[6.2] \qquad \xi \sinh^2 \xi \tanh^2 \xi \left(1 + \frac{2\xi}{\sinh 2\xi}\right) \qquad \left(329 \frac{H_o^2}{\gamma' L_o^2}\right)$$

where H_0 and L_0 are the wave height and wave length respectively in deep water and

$$[6.3] \qquad \xi = \left(2\pi \frac{d_c}{L_c}\right) \qquad , \qquad \gamma' = \frac{\rho_s - \rho}{\rho}$$

The variable L_c is the local wave length. Using linear wave theory, equation [6.3] can be written as

$$[6.4] \qquad d_c = \xi \tanh \xi \left(\frac{L_o}{2\pi}\right)$$

The variable, ξ, can be found by an iterative solution of equation [6.2], and the value of d_c then obtained from equation [6.4]. Once d_c is known, the value of X_c can be measured from the given initial profile.

There are two ways of determining the value of the initial beach profile slope, S. It may be measured from the given initial profile and related to the preceeding wave history. Alternatively, the curve by Dalrymple et al (1976) can be used, and it is then necessary to know the values of the sediment fall velocity V_f, and the wave period T, which are usually known. In the paper by Dalrymple et al, no equation was given to represent the curve, so in the present study a set of approximate equations are derived from the curve and are given here,

$$[6.5] \quad \begin{cases} 0.5928 - 0.6945 \left(\log \frac{H_o}{V_f T}\right) & \frac{H_o}{V_f T} \leqslant 0.1548 \\ 0.9438 - 0.0087 \left(\log \frac{H_o}{V_f T}\right) + 0.3343 \left(\log \frac{H_o}{V_f T}\right)^2 & 0.1548 < \frac{H_o}{V_f T} \leqslant 0.6 \\ 0.9383 - 0.0828 \left(\log \frac{H_o}{V_f T}\right) & 0.6 < \frac{H_o}{V_f T} \end{cases}$$

It remains to find the varibles X, Y and A before the initial profile can be uniquely defined. It must be noted that the resulting curve must pass through d_c and have a slope of S at the still water level (figure 6.4). Using these facts the following three equations are obtained:

$$[6.6] \quad S = \frac{2}{3} A (x)^{-1/3}$$

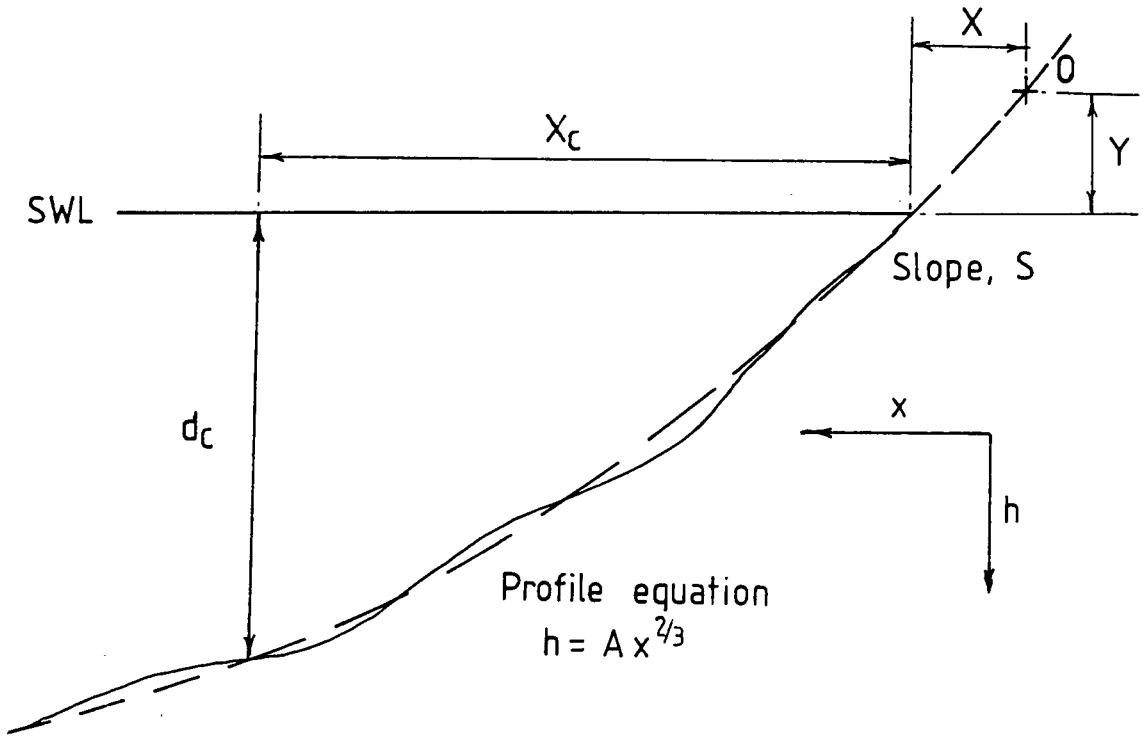

Figure 6.4 Initial profile calibration

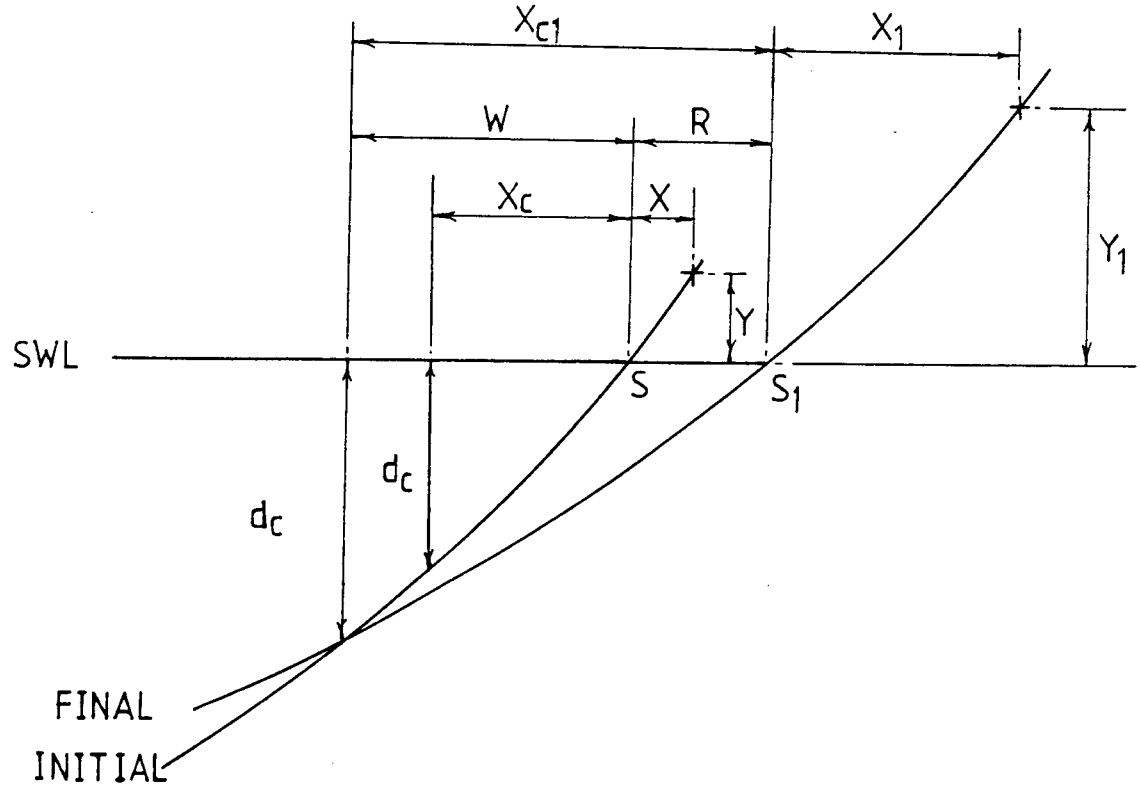

Figure 6.5 Initial and final profiles

[6.7] $$Y = A(x)^{2/3}$$

[6.8] $$d_c + Y = A(X_c + x)^{2/3}$$

Solving the above three equations simultaneously will yield the unknown variables X, Y and A.

6.3.2 Final profile

Figure 6.5 shows the change of the profile from the initial condition to the final condition. To determine the unknown variables X_1, Y_1 and X_{c1} of the final profile, the approach for calibrating the initial profile can be used, but with a change. Instead of finding the coefficient A, this coefficient is now known and X_{c1} is the new unknown variable. The value of d_{c1} is obtained through the same procedures as mentioned before, and the slope S_1 must be obtained from Dalrymple's curve using the new wave condition.

By solving the same set of equations ([6.6] to [6.8]), the value of X_{c1} is obtained. Once X_{c1} is known, the value for the shoreline retreat R can be determined.

This shoreline retreat R is the retreat from one equilibrium profile to another. According to the exponential rate of change of profile, this will be achieved only at an infinite time. Therefore to obtain intermediate

values of the shoreline retreat, the following expression is used:

$$[6.9] \qquad R_{(t)} = [\, 1 - e^{-b(t)} \,] R$$

where $R_{(t)}$ is the shoreline retreat at time t, and b is the coefficient of decay.

6.4 Model Testing

The model was checked using the results of the experiments described in chapter five. The model was first calibrated to the initial condition of test 1, and then used to predict the retreat of the shoreline when a new wave condition was imposed. The notation of the variables used here will be the same as that shown in figure 6.5. The results of the calibration to the initial condition of test 1 are:

A = 1.4282
X = 89.875 cm
Y = 28.656 cm

Thus the equation of the equilibrium profile is

$$[6.10] \qquad h = 1.428\, x^{2/3}$$

where h and x are both in centimetres.

Using the given new wave condition, the new

critical depth d_{c_1} and the new beach slope S_1 are calculated. They are 11.44 cm and 0.1522 respectively. Using these values, the calculation for X_{c_1} is carried out as outlined in the algorithms of the model. The value of X_{c_1} is found to be 78.86 cm. From equation [6.10] the value of W is 58.85 cm. Therefore the retreat of the shoreline R (= X_{c_1} - W) is 20.01 cm. As noted earlier, this value of shoreline retreat is achieved only when time approaches infinity. To obtain the intermediate values, equation [6.9] is used. These results are then compared to the results from the experiment.

Figure 6.6 shows a comparison of the profiles from the experiment and the profiles from the model. These profiles show that the prediction of the shoreline retreat after 24 hours agrees well with that of the experiment. The model predicted a retreat of 17.5 cm while the experimental results gave 18.6 cm, an error of -6 percent. However, the results obtained from the model are not too satisfactory when the variation of the shoreline retreat with time is considered (see figure 6.7). In view of the possible data scatter from the experiment, the error between the experiment and the model may not be as great as shown.

From the comparison, it can be seen that the model gives reasonable predictions. The model manages to predict the trend of the profile changes. It also shows that the various different aspects of profile behaviour can be

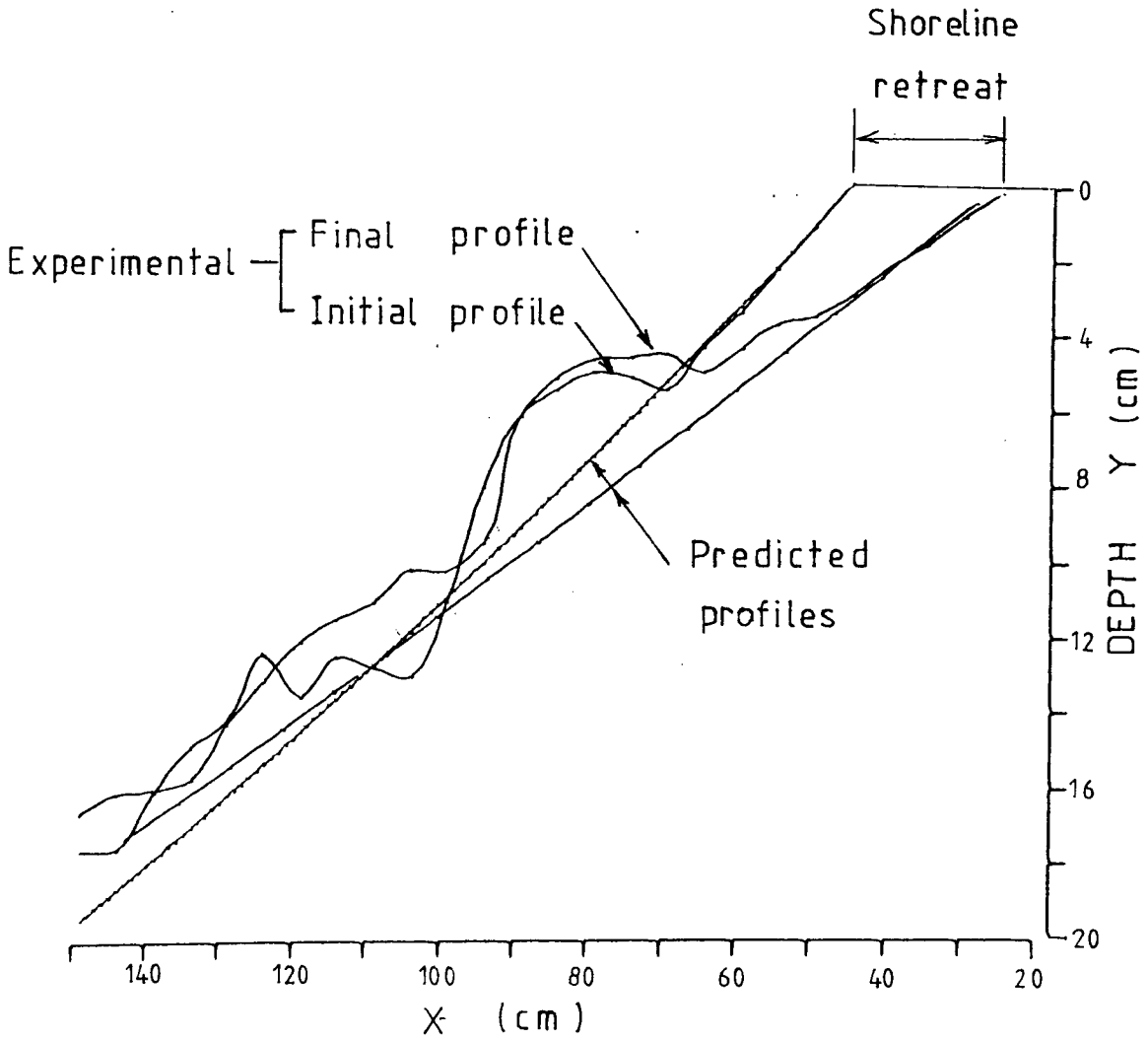

Figure 6.6 Comparison between measured profiles and model's results

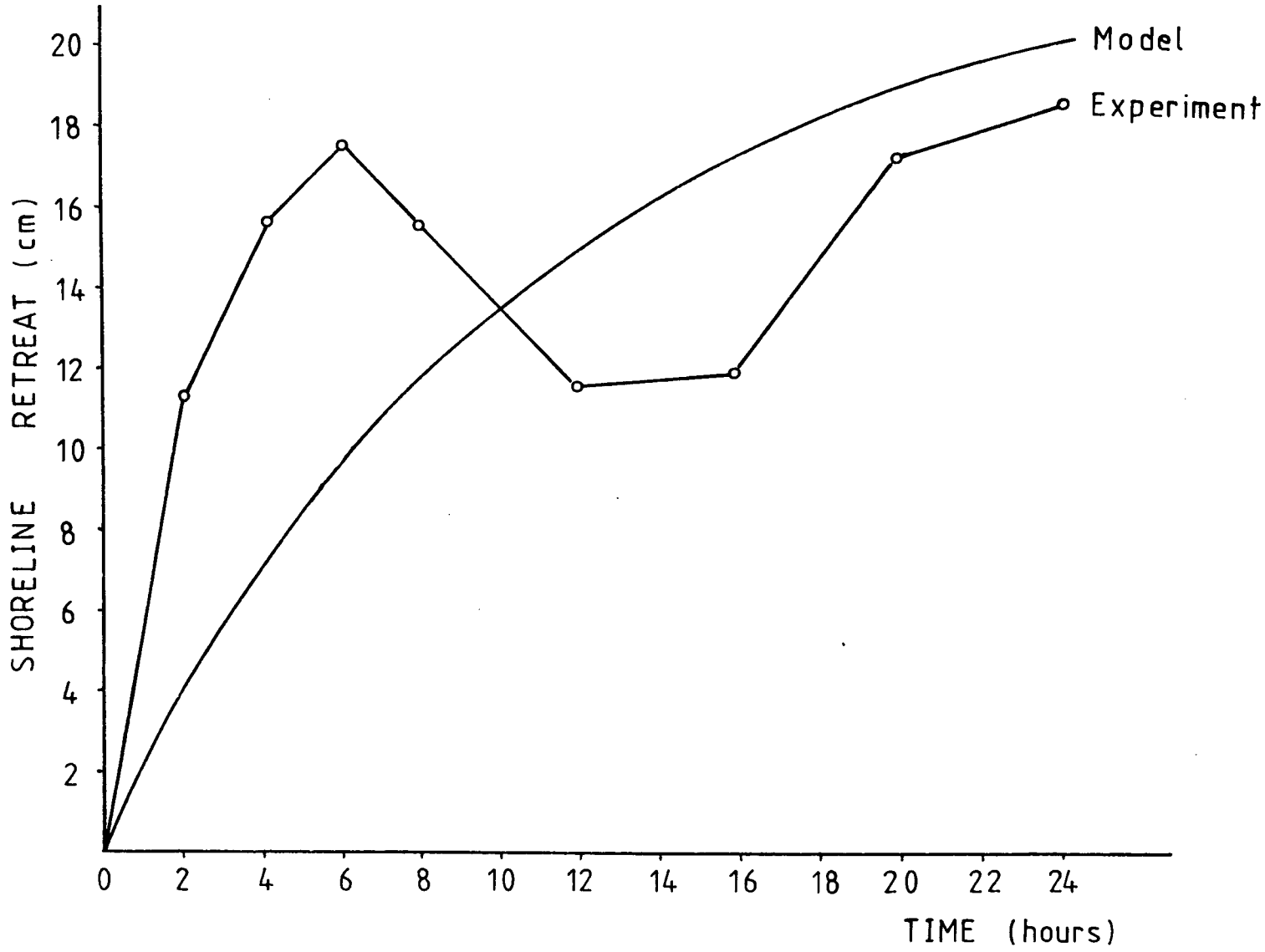

Figure 6.7 Variation of shoreline retreat with time - Comparison between experiment and model's results

brought together and related to one another. This should be especially noted because the slope, the critical depth and the profile are determined in ways which are different and independent of each other. It therefore appears that this simple model works quite well and makes acceptable predictions of shoreline and profile changes.

6.5 Combining the Longshore and On-offshore Transport Routines

In this section, the profile change routine is merged with the longshore transport routine. This combined model will be used to simulate four simple field situations. For each simulation, the modelling conditions which have to be specified are, the modelling parameters, the initial wave condition and the final wave condition. The combined model is then used to predict the corresponding adjustment of the beach profile to these different wave conditions. The four simulation examples are briefly described here.

1. As an initial test to check that the on-offshore routine has been correctly incorporated, the angle of wave attack is set equal to zero and no littoral barrier is included. The initial wave height in this case is specified to be lower than the final wave height. Essentially what is being modelled here is the effect of direct wave attack on a beach. The shoreline changes that occur should be due only to profile changes which resulted from on-offshore transport. Figure 6.8 shows the results of the shoreline retreat.

2. The purpose of this example is to compare the results obtained by the combined and the pure longshore transport model. The result of the pure longshore transport model is

shown as curve 2 in figure 6.9. The initial and final wave conditions for the combined model are specified to be approximately the same as that for the pure longshore transport model. The result of this combined model is shown as curve 3 in figure 6.9. From the figure, it can be seen that the inclusion of the on-offshore routine resulted in a significantly different final shoreline. Curve 2 (pure longshore model) shows that there is only accretion of the shoreline, nowhere along the shoreline can any shoreline recession be found, because there is no on-offshore transport. Therefore, even when a wave condition exists which will result in a change of profile and a shoreline retreat, the pure longshore transport model cannot produce this effect, and the inclusion of the on-offshore component is essential (curve 3). The difference in the two shorelines, curve 2 and 3 is especially noticeable closer to the barrier. The reason for this is because the profiles near the barrier are steeper, as a result of the accmmulation of sediment from the longshore component of the model. Therefore, when the on-offshore component is also considered, the on-off transport changes in these regions will be additionally magnified because of this steeper initial profile, resulting in a greater final shoreline difference as shown in figure 6.9.

3. The third example is to simulate the effect of an increase of incident wave height on the beach shoreline.

The increase of wave height is kept small, as the intention here is to simulate a heavier sea condition but not as extreme as for storm waves. The resulting change of the shoreline is shown as curve 4 in figure 6.9. By comparing this curve with curve 3 in the same figure, it can be seen that more shoreline erosion takes place at some regions while more accumulation at others. This shows that a slight increase of the wave height does not necessarily mean that a destructive effect on the shoreline will occur when a barrier is present.

4. This last example is intended to simulate the effect of storm waves on an existing accumulation of sediment. The wave height is increased by 75 percent of the initial wave height. The results show some interesting features (figure 6.10). The length of shoreline where erosion occurs increases as compared to curve 4 of figure 6.9. The amount of accumulation is small and when compared with erosion at the other regions, the net effect on the shoreline can be seen as destructive. This, in comparison with example 3, shows that the overall effect on the shoreline is determined not only by the increase of wave height, but also by the amount of such an increase.

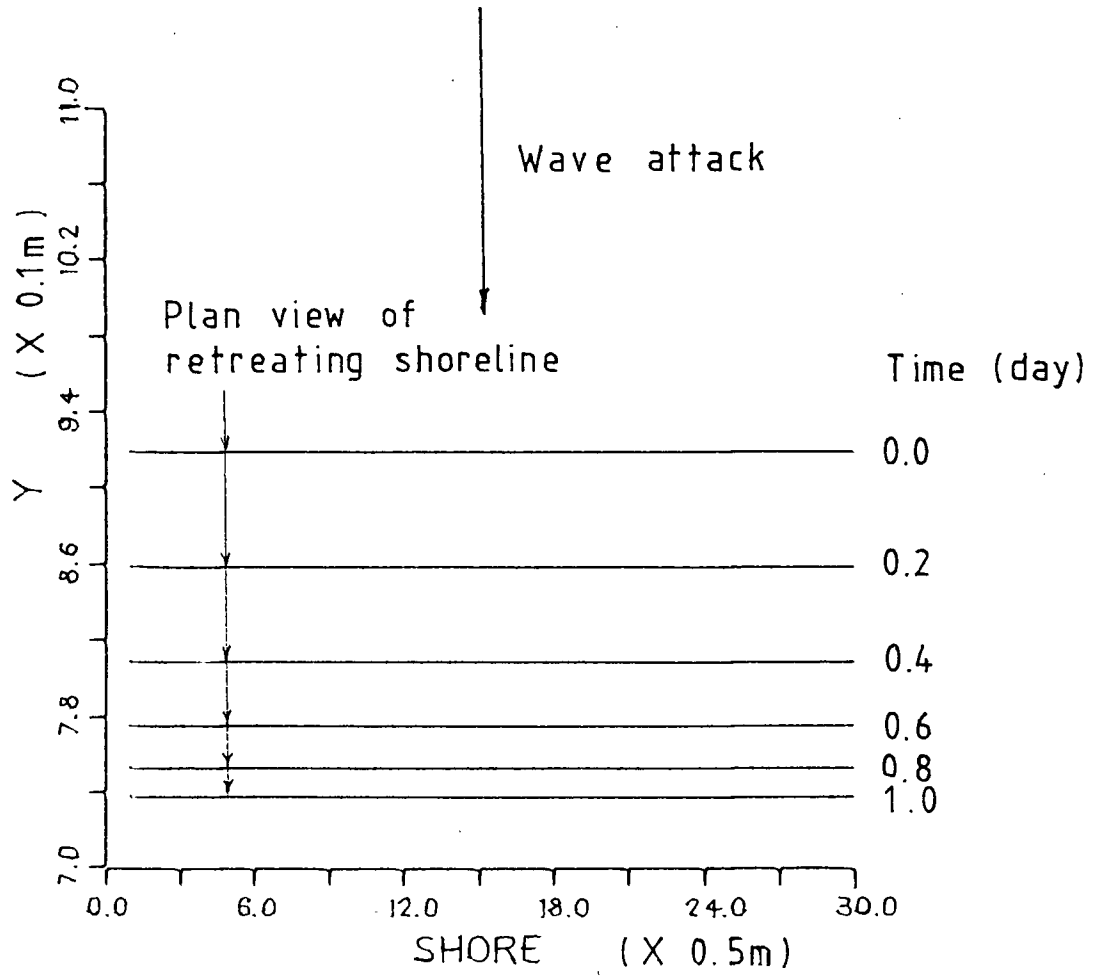

Figure 6.8 Beach plan - Retreat of shoreline due to wave approaching beach orthogonally

Curve 1 - Initial shoreline.
Curve 2 - Final shoreline when only the longshore transport component is modelled.
Curve 3 - Final shoreline when both the longshore and on-offshore components are modelled.
Curve 4 - Final shoreline with conditions similar to that for curve 3, except with an increase of incident wave height.

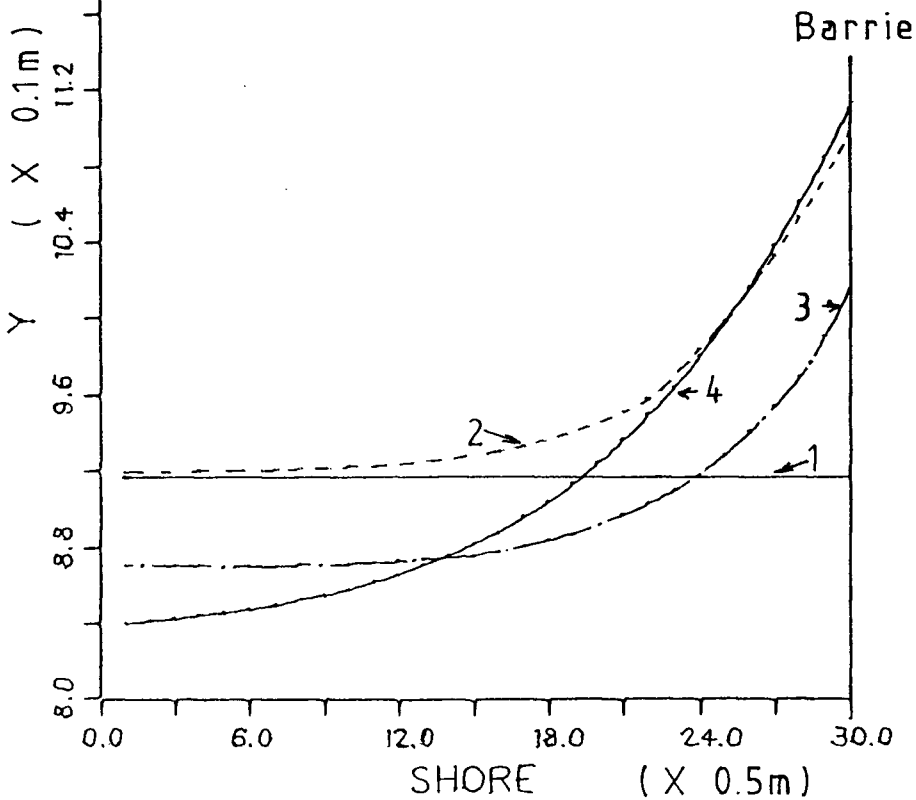

Figure 6.9 Beach Plan - Combined on-offshore and longshore simulations

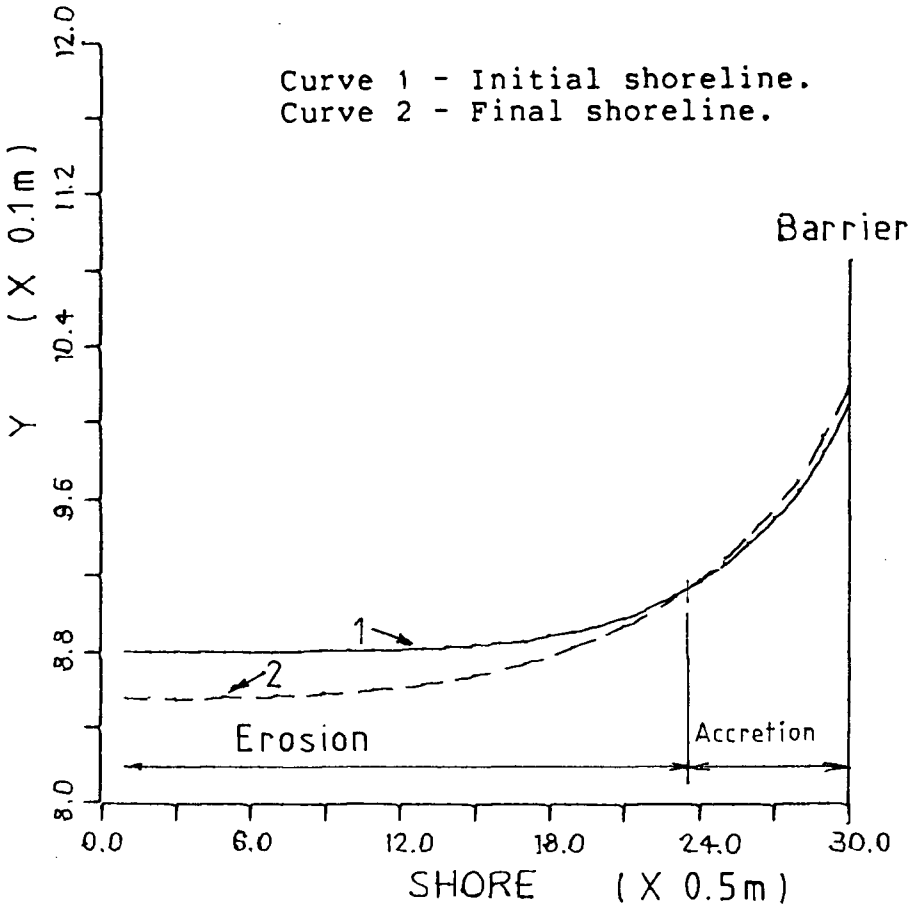

Note the net destructive effect of the storm wave.

Figure 6.10 Beach plan - Storm waves simulation

6.6 Discussion

From the above simulations, several general observations can be drawn. It has been seen that whether the longshore or the on-offshore component of transport is dominant depends on the situation. From the results of example 1, it can be seen that if no barrier is present to obstruct the longshore flow of sediment, then an increase in wave height will only produce a shoreline retreat which is due to the adjustment of profile resulting from the on-offshore transport. However, if a barrier is introduced as in example 3, the results show a combination of two effects. At regions far away from the barrier where the longshore flow of sediment remains relatively unhampered, the resulting effect is the same as those of example 1 (ie an exponential retreat of the shoreline). But at regions nearer the barrier where the longshore movement of sediment is restricted ,the longshore accumulation effect becomes dominant. This is shown by the accretion of the shoreline.

In the event of a large storm, the larger storm waves with longer wave period and higher wave height will begin to refract further off-shore. When these waves reach the shore and break, the wave orthogonals will tend to be more normal to the beach. This means the angle of wave attack is very small and most of the energy will be expended in causing on-offshore transport rather than longshore transport. These effects are seen in the results of example

4 where the dominant transport is on-offshore, causing a net retreat of shoreline.

Lastly, the results of the longshore model (chapter 4) and the combined model show the following differences.

1. When using only the longshore transport model, there is no shoreline retreat anywhere along the shore. This is because the longshore model does not account for sediment loss through on-offshore movement.

2. With the inclusion of the on-offshore routine, an accmulation behind the barrier can still be observed. But the amount of this accmulation is less than that obtained from the longshore transport model. Therefore the inclusion of the on-offshore routine reduces the accretion effect of the longshore transport model.

It can therefore be concluded that to have a complete simulation of coastal sediment movement, both the longshore and the on-offshore routines will have to be taken into consideration.

CHAPTER 7

SUMMARY AND CONCLUSIONS

This report has presented the step by step development of a shoreline prediction model. The following is a summary of this development.

A brief review of the longshore current and transport equation was conducted before the formulation of the model. In the review, it was noted that both the radiation approach by Longuet-Higgins and the semi-empirical approach by Komar yielded similar equations. The equation by Longuet-Higgins is based on the conservation of momentum of the waves. This approach is believed to be the most suitable as momentum is conserved when waves break, whereas the energy is not. Both the equations were shown to be consistent with experimental data but the equation by Komar requires the constancy of the ratio $\tan\beta/C_f$. Even though supporting data were presented, this constancy is still unexplained.

From the review on the transport rate equation, it was shown that there is no 'best' predictive equation available. It was found that most of the 'wave flux' formulations have similar approaches yielding a general equation of the form:

[7.1] $$S_l = A P_l^B$$

However, there is no such similarity in the 'sediment equation' approaches. Even though predictions by these 'sediment equation' were shown to be in agreement with the data, there is still an apparent lack of agreement on the mode of the longshore transport. In general, the application of 'wave flux' equations are easier and require less inputs than the 'sediment equation.'

After the review, the CERC transport rate equation was selected for use in the longshore transport component of the model. A finite difference scheme was adopted to solve the wave refraction and shoaling equations as well as the transport and continuity equations. The model was used to study the accretion behaviour due to an infinite length and a finite length barrier. In addition, the model was also used to predict nourishment beach plan changes with time.

An experimental study on the on-offshore was presented after the longshore model. The purpose of the study was to highlight some of the key aspects of behaviour in the profile changes and to find the rate of change of the profiles. Equations were developed which define a characteristic depth, beach slope and shape for a given set of wave parameters. The model based on these equations was then tested against the experimental results. Lastly, this on-offshore component model was combined into the longshore

numerical model and the combined results are presented.

The following were observed from the various modelling results and the experimental study:

a) It was shown that the inclusion of wave shoaling and refraction (or wave deformation) routine had a dramatic effect on the transport and the resulting shoreline changes. (see figures 4.14 and 4.16). The reason for this was found to be the nonlinear effects which this wave deformation routine introduced into the results. This is concluded from the comparision of the modelling results and the results from Walton's paper on simplified analytical solution. In Walton's model, the governing equations were linearised for ease of solution. The results obtained were found to be very similar to those of the model without the wave deformation routine, suggesting that the nonlinear effects of the model are due to the wave shoaling and refraction routine.

b) The results of the model also indicated that accretion behaviour due to a barrier can be non-dimensionalised to form a set of dimensionless accretion curves for a given wave direction. These curves proved to be useful in the estimation of the barrier length required to achieve a desired accretion at a specific location. These non-dimensionalised curves also showed that a desired accretion can be achieved either with a longer length barrier at a shorter time or a shorter length barrier at a

longer time. Hence, there is not a single solution, but several, and the most suitable solution will have to depend on additional factors, such as cost.

c) From the experimental study of on-offshore behaviour, it was seen that the beach profile will change as a result of a change in wave activity. If the wave height is increased, the beach slope will reduce and the beach shoreline will retreat. The rate of this change was found to be decaying exponentially with time, implying that most of the expected changes will occur in the early stages. It was also shown that there is a relationship between the wave energy flux of the incoming wave and the total amount of sediment transported. However, due to insufficient data, no definite relationship was given.

d) The experimental results also supported Dalrymple et al's findings on the unique relationship between the dimensionless fall parameter H_0/V_fT and the equilibrium beach slope. This unique relationship suggested that the direction of sediment movement in the on-offshore direction is not predicted by using only the value of the dimensionless fall parameter derived from the imposed wave condition as suggested by Dean and others.

Dalrymple et al's findings showed that for each wave condition, there is a unique equilibrium beach slope associated with it. As such, when wave conditions change from one state to another, the direction of sediment

movement due to this wave condition change will have to depend on the relative change of the associated equilibrium beach slope. It was suggested by Quick (1983) that the more appropriate expression in determining the direction of sediment movement would be the ratio of the initial to the final value of the dimensionless fall parameter (shown as equation [5.13]). This relationship is supported by the experimental results.

e) From the results of the combined model, it was seen that there is a definite interaction between longshore and on-offshore transport. The dominant transport component can either be longshore or on-offshore depending on the wave height and direction. Prediction of shoreline changes will be inaccurate unless both the components are incorporated into the model, because the on-offshore transport can produce large profile changes which the pure longshore model cannot reproduce.

This report has used the littoral barrier example quite extensively because data and other studies exist for this situation. Whether a littoral barrier is an appropriate solution for an eroding beach depends on the nature and the extent of the problem, not to mention the economic and enviromental constraints. The total consequences of installing a littoral barrier must be examined with care, especially the downstream consequences. In nearly every instance, littoral barriers are designed to

interrupt the longshore movement of sediment and therefore starving adjacent downdrift beaches of its supply, and causing shoreline recession to occur.

Though this report also showed that a beach is eroded by storm waves and may later be restored by swell waves, this recovery of offshore sediment is not always complete. Erosion and accretion patterns may occur seasonally, but the long range condition of the beach - whether eroding, stable or accreting will depend on the net movement of material. It is believed that the rate of beach restoration during swell condition is much slower than beach erosion during storm conditon. Therefore one large storm can offset many seasons of swell restoration.

Lastly, it must be mentioned that there are several factors which have not been considered in the model. They are wave diffraction, wave setup, wave runup and tide action. Wave diffraction is due to the distribution of energy along the crest of the wave and is dominant in the shadow of a barrier. Since the model in this report is used to simulate the effect upstream of a barrier, the wave diffraction effect is assumed to be insignificant. As for wave runup, it is felt that little is known about its effect on sediment transport. In most of the wave runup studies, the experiments were conducted on steep, plane and impermeable slopes, so that application of the results on sand beaches is inappropriate. While for wave setup, even

though there are theories to account for many of the principal processes, these theories contain factors that are often difficult to specify in practical problems. For example, wave setup in a simplified plane beach can be estimated using radiation stress theory (Longuet-Higgins and Stewart, 1964), but for a non plane beach, there is still no solution except using estimation that requires considerable judgement. As to the tide action, the inclusion of it in the model requires a more complicated algorithms because the tide level in the model will have to vary with time. In order to simplify the problem, a model using only one constant tide level is adopted. This simplification will not cause a significant change in the results if it is assumed that the sediment transport due to wave action is significantly greater than that due to tide action. Since this constant tide model can be used at any tide level, the model can be used to simulate the most destructive situation for a beach, in which the destructive wave attack occurs at the same time as the highest tide. The results obtained will be conservative compared to those of a variable tide model. This is because as the tide level drops after reaching the highest level (in a variable model), the destructive effect of the waves will not be able to reach the same distance inshore as during the highest tide level. Therefore, to keep the overall model simple, it is assumed that the above neglected factors are insignificant compared to those already considered in the model.

BIBLIOGRAPHY

Ackers, P., and White, W. R. (1973). Sediment transport: new approach and analysis. Journal of the Hydraulics Division, ASCE, HY11, pp. 2041 - 2060.

Bagnold, R. A. (1963). Mechanics of marine sedimentation. In 'The Sea', edited by M. N. Hill, Vol. 3, pp. 507 - 528. Interscience, NY.

Bakker, W. T., Klein Breteler, E. H. J., and Roos, A. (1970). The dynamics of a coast with a groyne system. Proceedings, 12th Coastal Engineering Conference, pp. 1001 - 1020.

Bowen, A. J. (1969). Rip currents, 1 : theoretical investigations. Journal of Geophysical Research, Vol. 74, pp. 5467 - 5478.

Bowen, A. J. (1969a). The generation of longshore currents on a plane beach. Journal of Marine Research, Vol. 37, pp. 206 - 215.

Bowen, A. J., and Inman, D. L. (1969). Rip currents, 2 : laboratory and field observations. Journal of Geophysical Research, Vol. 74, pp. 5479 - 5490.

Bretschneider, C. L. (1954). Field investigation of wave energy loss of shallow water ocean waves. U.S. Army Corps of Engineers Beach Erosion Board, Technical Memo. No. 46.

Bruno, R. O., Dean, R. G., and Gable, C. G. (1980). Longshore transport evaluations at a detach breakwater. Proceedings, 17th Coastal Engineering Conference, pp. 1453 - 1475.

Bruun, P. (1954). Coast erosion and the development of beach profiles. U. S. Army Corps of Engineers, Beach Erosion Board, Technical Memo. No. 44.

Byker, E. W. (1971). Longshore transport computations. Journal of the Waterways, Harbours and Coastal Engineering Division, ASCE, WW4.

Coastal Engineering Research Center (1977). Shore Protection Manual (SPM). Superintendent of Documents, U. S. Government Printing Office, Washington, D. C. 20402, 3 Volumes.

Dalrymple, R. A. (1978). Rip currents and their causes. Proceedings, 16th Coastal Engineering Conference, pp. 1414 - 1427.

Dalrymple, R. A., and Thompson, W. W. (1976). Study of equilibrium beach profiles. Proceedings, 15th Coastal Engineering Conference, pp. 1277 - 1296.

Dean, R. G. (1973). Heuristic models of sand transport in the surf zone. Conference on Engineering Dynamics in the Surf Zone, Sydney, Australia.

Dean, R. G. (1977). Equilibrium beach profiles : U. S. Atlantic and Gulf Coasts. Ocean Engineering Report No. 12. Department of Civil Engineering, University of Delaware, Newark, Delaware.

Fleming, C. A., and Hunt, J. N. (1976). Application of a sediment transport model. Proceedings, 15th Coastal Engineering Conference, pp. 1184 - 1202.

Galvin, C. J. (1967). Lonshore current velocity : a review of theory and data. Reviews of Geophysics, Vol. 5, No. 3, pp. 287 - 304.

Galvin, C. J. (1972). A gross longshore transport rate formula. Proceedings, 13th Coastal Engineering Conference, pp. 953 - 970.

Galvin, C. J., and Eagleson, P. E. (1965). Experimental study of longshore currents on a plane beach. U. S. Army Coastal Engineering Research Center. Technical Memo. No. 10, pp. 1 - 80.

Golub, G. H., and Pereyra, V. (1972). The differentiation of pseudoinverses and nonlinear least squares problems whose variables separate, STAN-CS-72-261, Computer Science Department, Stanford University.

Gourlay, M. R. (1980). Beaches : Profiles, processes and permeability. Proceedings, 17th Coastal Engineering Conference, pp. 1320 - 1339.

Hallermeier, R. J. (1978). Uses for a calculated limit depth to beach erosion. Proceedings, 16th Coastal Engineering Conference, pp. 1493 - 1512.

Harrison, W., and Wilson, W. S. (1964). Development of a method for numerical calculation of wave refraction. U. S. Army Coastal Engineering Research Center, Technical Memo. No. 6.

Hino, M. (1975). Theory on formation of rip current and cuspidal coast. Proceedings, 14th Coastal Engineering Conference, pp. 901 - 919.

Hughes, S. A., and Chiu, T. Y. (1978). The variations in beach profiles when approximated by a theorectical curve. Report TR-039, Coastal and Oceanographic Engineering Laboratory, University of Florida, Gainsville, Florida.

Johnson, J. W. (1949). Scale effects in hydraulic models involving wave motion. Transactions of the American Geophysical Union. Vol. 30, No. 4, pp. 517 - 525.

Johnson, J. W., O'Brien, M. P., and Isaacs, J. D. (1948). Graphical construction of wave refraction diagrams, Hydrographic Office, Navy Department, Publication No. 605.

King, C. A. M. (1972). Beaches and Coasts. 2nd edition, St Martin's Press, NY.

King, C. A. M., and Williams, W. W. (1949). The formation and movement of sand bars by wave action. Journal of Geology, Vol. 113, pp. 70 - 85.

Kohler, R. R., and Galvin, C. J. (1973). Berm - bar criterion. Unpublished memorandom for the record, U. S. Army Coastal Engineering Research Center, Washington.

Komar, P. D. (1971). The mechanics of sand transport on beaches. Journal of Geophysical Research, Vol. 76, No. 3, pp. 713 - 721.

Komar, P. D. (1973). Computer models of delta growth due to sediment input from rivers and longshore transport. Geological Society of America, Bulletin, Vol. 84, pp. 2643 - 2650.

Komar, P. D. (1976). Beach processes and sedimentation. Prentice-Hall, Englewood Cliffs, NJ.

Komar, P. D., and Inman, D. L. (1970). Longshore sand transport on beaches. Journal of Geophysical Research, Vol. 75, No. 30, pp. 5914 - 5927.

Le Mehaute, M. (1976). An introduction to hydrodynamics and water waves. Springer-Verlag, NY.

Longuet-Higgins, M. S. (1970a). Longshore currents generated by obliquely incident sea waves, 1, Vol. 75, No. 33, pp. 6778 - 6789.

Longuet-Higgins, M. S. (1970b). Longshore currents generated by obliquely incident sea waves, 2, Vol. 75, No. 33, pp. 6790 - 6801.

Longuet-Higgins, M. S. (1972). Recent progress in the study of longshore currents. In 'Waves on beaches', edited by R. E. Meyer, pp. 203 - 248. Academic Press, NY.

Longuet-Higgins, M. S., and Stewart, R. W. (1964). Radiation stresses in water waves; a physical discussion, with applications. Deep-Sea Research, Vol. 11, pp. 529 - 562.

Meyer, R. E. (1969). Note on wave run-up. Journal of Geophysical Research, Vol. 75, pp. 687 - 690.

Nayak, I. V. (1971). Equilibrium profiles of model beaches. Proceedings, 12th Coastal Engineering Conference, pp. 1321 - 1339.

Nielson, P., Svendsen, I. A., and Staub, C. (1978). Onshore-offshore sediment movement on a beach. Proceedings, 16th Coastal Engineering Conference, pp. 1475 - 1492.

Noda, E. V., Sonu, C. J., Rupert, V. C., and Collins, J. I. (1974). Nearshore circulations under sea breeze conditions and wave-current interactions in the surf zone. Tetra Tech, Inc., Report TC-149-4.

Pelnard-Considere, R. (1956). Essai de Theorie de l'Evolution des Formes de Rivage en Plages de Sable et de Galets. 4th Journee de l'Hydraulique, Les Energies de la Mer, Question III, Rapport No. 1.

Phillips, O. M. (1980). The dynamics of the upper ocean. Cambridge University Press, Cambridge.

Prandtl, L. (1952). Essentials of fluid dynamics. Haffner, New York, NY.

Price, W. A., Tomlinson, K. W., and Willis, D. H. (1972). Predicting changes in the plan shape of beaches. Proceedings, 13th Coastal Engineering Conference, pp. 1321 - 1329.

Putnam, J. A., Munk, W. H., and Traylor, M. A. (1949). The prediction of longshore currents. Transaction of the American Geophysics Union, Vol. 30, pp. 337 - 345.

Quick, M. C. (1983). Personal Discussion.

Raman, H., and Earattupuzha, J. J. (1972). Equilibrium conditions in beach wave interaction. Proceedings, 13th Coastal Engineering Conference, pp. 1237 - 1256.

Rector, R. L. (1954). Laboratory study of the equilibrium profiles of beaches. U. S. Army Corps of Engineers, Beach Erosion Board, Technical Memo. No. 41.

Saville, T. (1957). Scale effects in two dimensional beach studies. Transactions of the 7th meeting of the Association of Hydraulic Research, Lisbon, Portugal, pp. A3-1 - A3-9.

Sayao, O. S. F. M., and Kamphuis, J. W. (1982). Wave action on beaches. CE Research Report No. 77. Department of Civil Engineering, Queen's University, Kingston, Ontario.

Scott, T. (1951). Sand movement by waves. U. S. Army Corps of Engineers, Beach Erosion Board, Technical Memo. No. 48.

Scripps Institution of Oceanography (1947). A statistical study of wave conditions at five sea localities along the California coast. University of California Wave Report No. 68, La Jolla, California.

Shepard, F. P., Emery, K. O., and LaFond, E. C. (1941). Rip currents : a process of geological importance. Journal of Geology, Vol. 49, No. 4, pp. 337 - 369.

Swart, D. H. (1976). Predictive equations regarding coastal transports. Proceedings, 15th Coastal Engineering Conference, pp. 1113 - 1132.

Swart, D. H., and Fleming, C. A. (1980). Longshore water and sediment movement. Proceedings, 17th Coastal Engineering Conference, pp. 1275 - 1294.

Thornton, E. B. (1973). Distribution of sediment transport across the surf zone. Proceedings, 13th Coastal Engineering Conference, pp. 1049 - 1068.

Walton, T. L., and Chiu, T. Y. (1979). A review of analytical techniques to solve the sand transport equation and some simplified solutions. Coastal Structures 79, Waterways, Port, Coastal and Ocean Division, ASCE, pp. 809 - 837.

Wiegel, R. L. (1964). Oceanographical Engineering. Prentice-Hall, Englewood Cliffs, NJ.

Willis, D. H. (1977). Evaluation of alongshore transport models. Proceedings, 5th Symposium of the Waterway, Port, Coastal and Ocean Division, 'Coastal Sediment 77', ASCE, pp. 350 - 365.

Willis, D. H. (1978). Sediment load under waves and currents. Proceedings, 16th Coastal Engineering Conference, pp. 1626 - 1637.

Willis, D. H., and Price, W. A. (1975). Trends in the application of research to solve coastal engineering problems. In 'Nearshore sediment dynamics and sedimentation', edited by Hails and Carr, pp. 111 - 121, John Wiley and Son Ltd.

Wilson, W. S. (1966). A method for calculating and plotting surface wave rays. U. S. Army Coastal Engineering Research Center. Technical Memo. No. 17.

Appendix A

Finite difference formulation

The concept of finite difference method is to assume that there exist a solution surface (say for wave height, H) over the entire X,Y domain, as shown in figure A1.

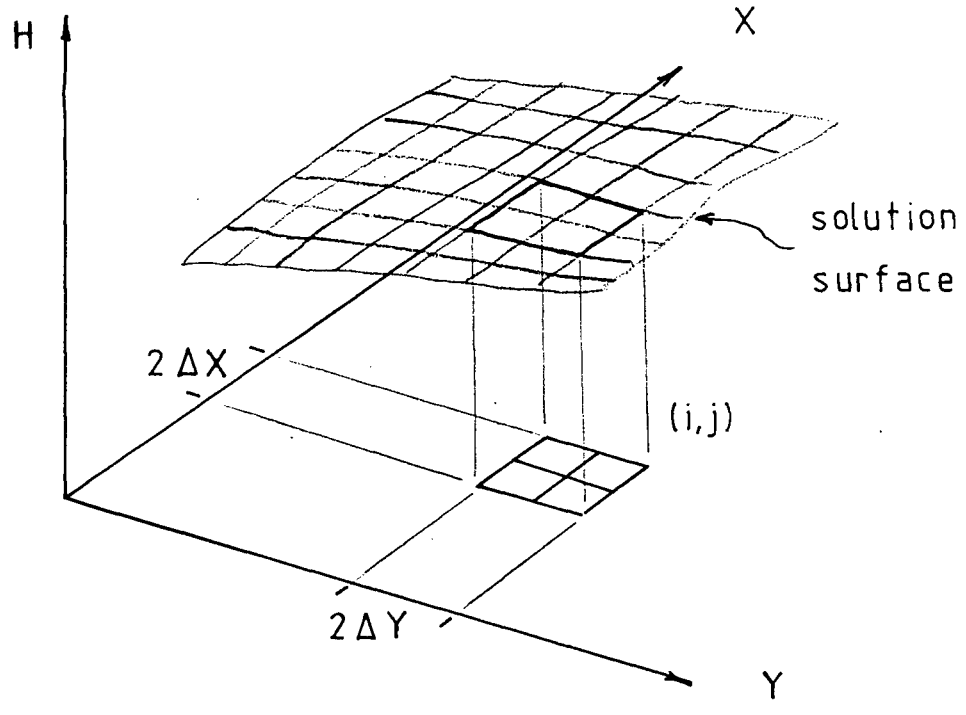

Figure A1

To approximate the derivative of $\partial H/\partial X$ at point (i,j), there are three basic methods:

1. Forward difference $$\frac{\partial H}{\partial X} \doteq \frac{H_{(i+1,j)} - H_{(i,j)}}{\Delta X}$$

2. Backward difference $$\frac{\partial H}{\partial X} \doteq \frac{H_{(i,j)} - H_{(i-1,j)}}{\Delta X}$$

3. Central difference $$\frac{\partial H}{\partial X} \doteq \frac{H_{(i+1,j)} - H_{(i-1,j)}}{2\Delta X}$$

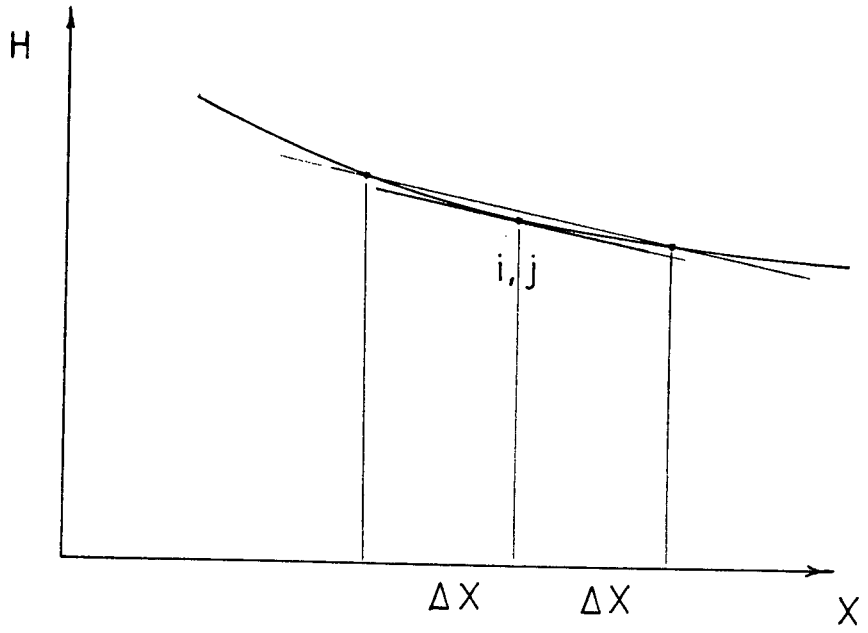

Figure A2

The method chosen for the refraction and shoaling program is based on the central difference method of approximation.

Appendix B

Flowchart for wave refraction and shoaling routine

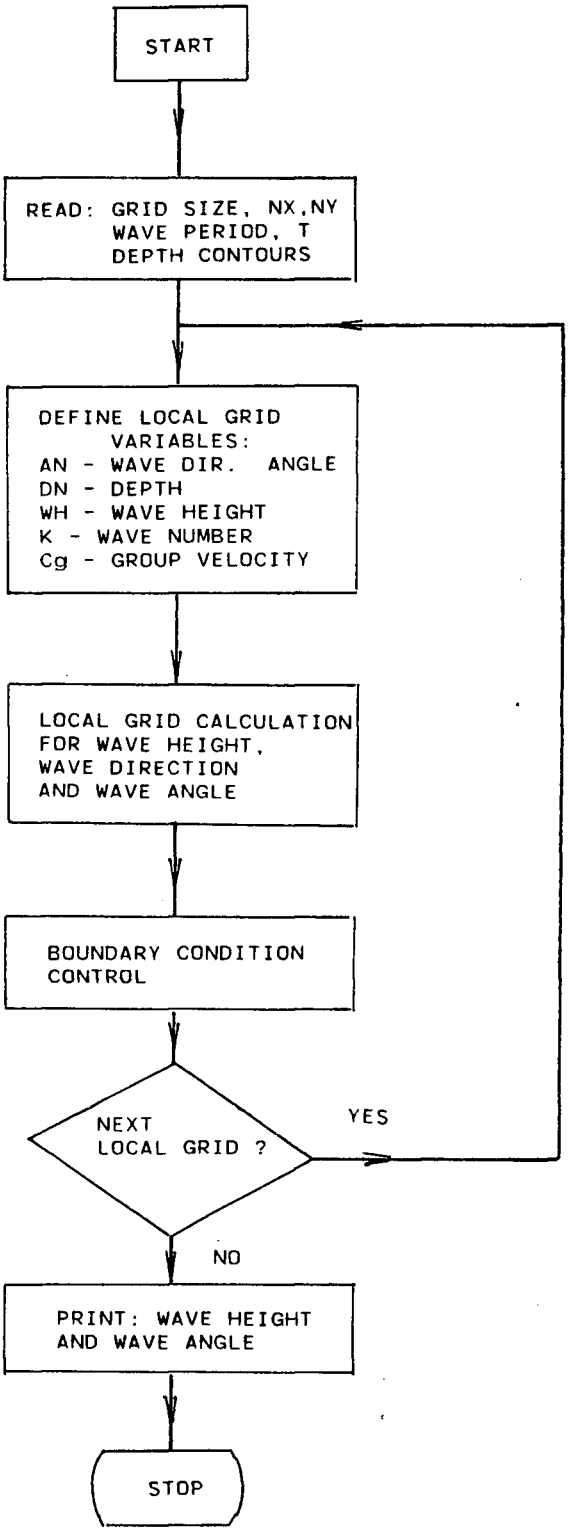

Appendix C

Flowchart for longshore transport model

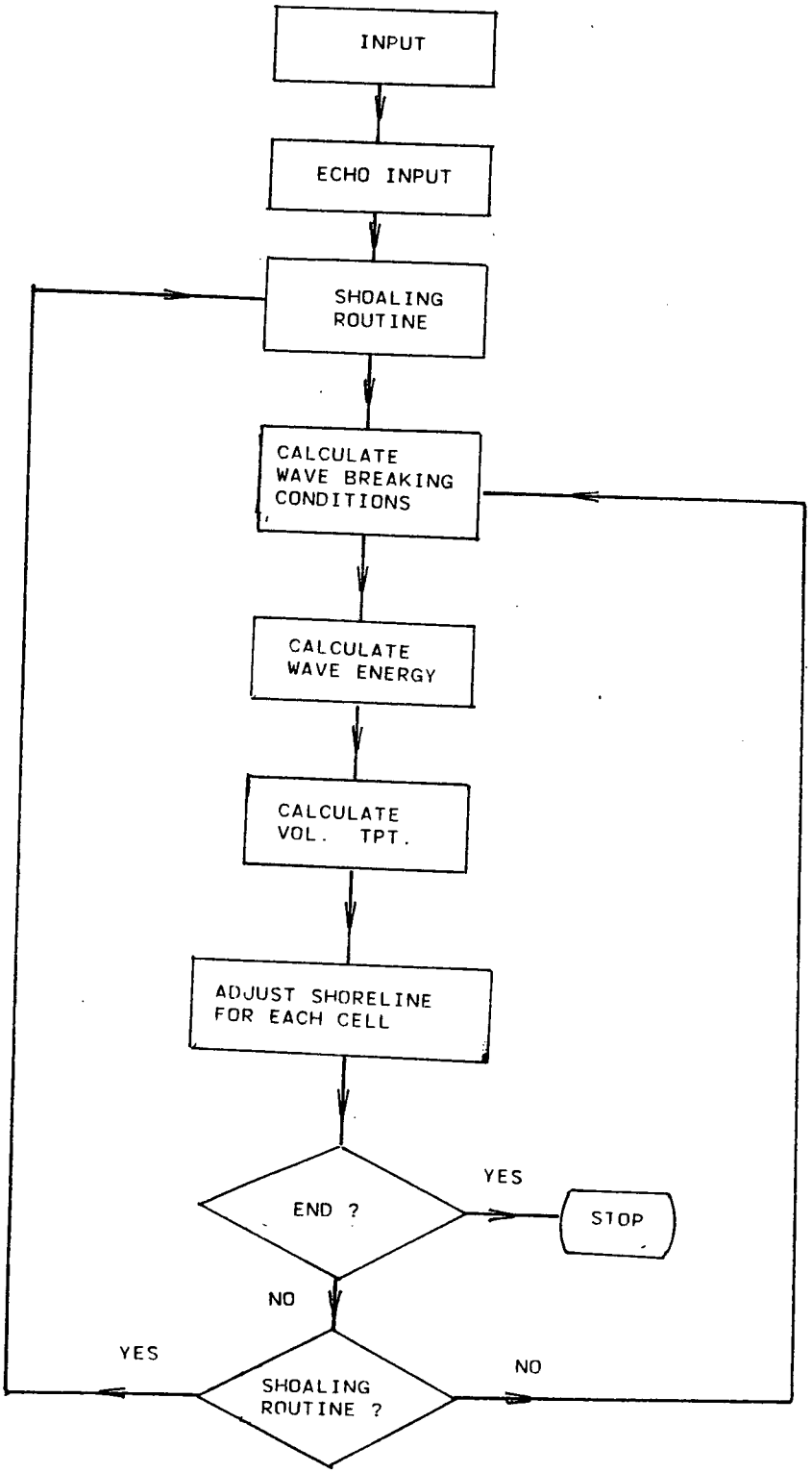

Appendix D

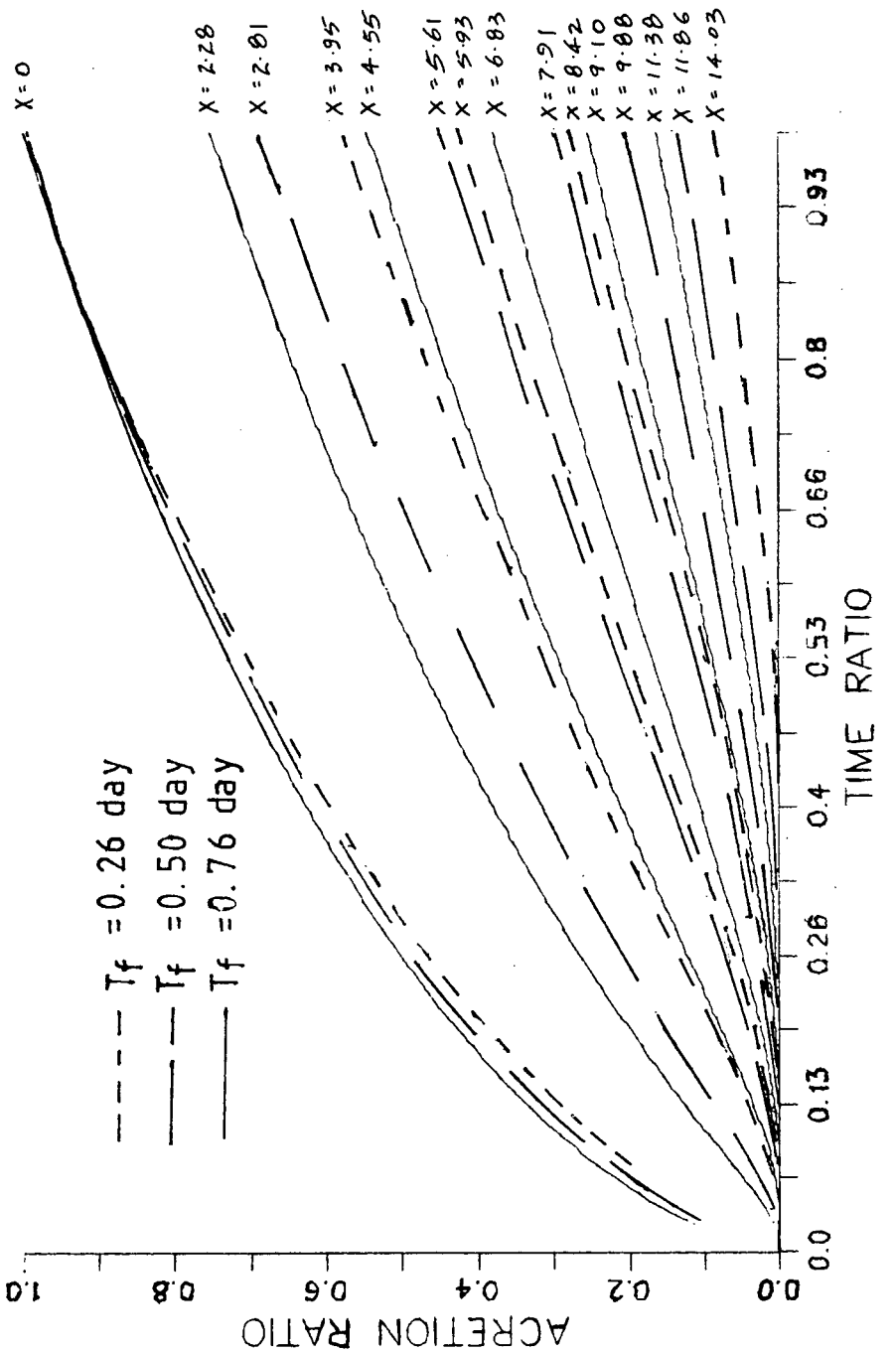
ACRETION RATIO
TIME RATIO
0.0
0.2
0.4
0.6
0.8
1.0
0.0
0.13
0.26
0.4
0.53
0.66
0.8
0.93
X=0
X=2.28
X=2.81
X=3.95
X=4.55
X=5.61
X=5.93
X=6.83
X=7.91
X=8.42
X=9.10
X=9.88
X=11.38
X=11.86
X=14.03
Tf =0.26 day
Tf =0.50 day
Tf =0.76 day

Appendix E

Criteria for selecting Time Ratio

The value of 4.2 used in the example has to be correctly inferred. From figure 4.12, it can be seen that as the time ratio increases, the accretion ratio reaches an asymptotic value. Hence any value of time ratio can be used instead of 4.2. To achieve some consistency in approach, a reasonable criteria will have to be adhered to. A suggested criteria is by defining an acceptable 'terminal' accretion rate as sufficent accuracy for answer. Then using this accretion rate as control, a unique value of time ratio can be read off from any curve in figure 4.12. (See figure E1).

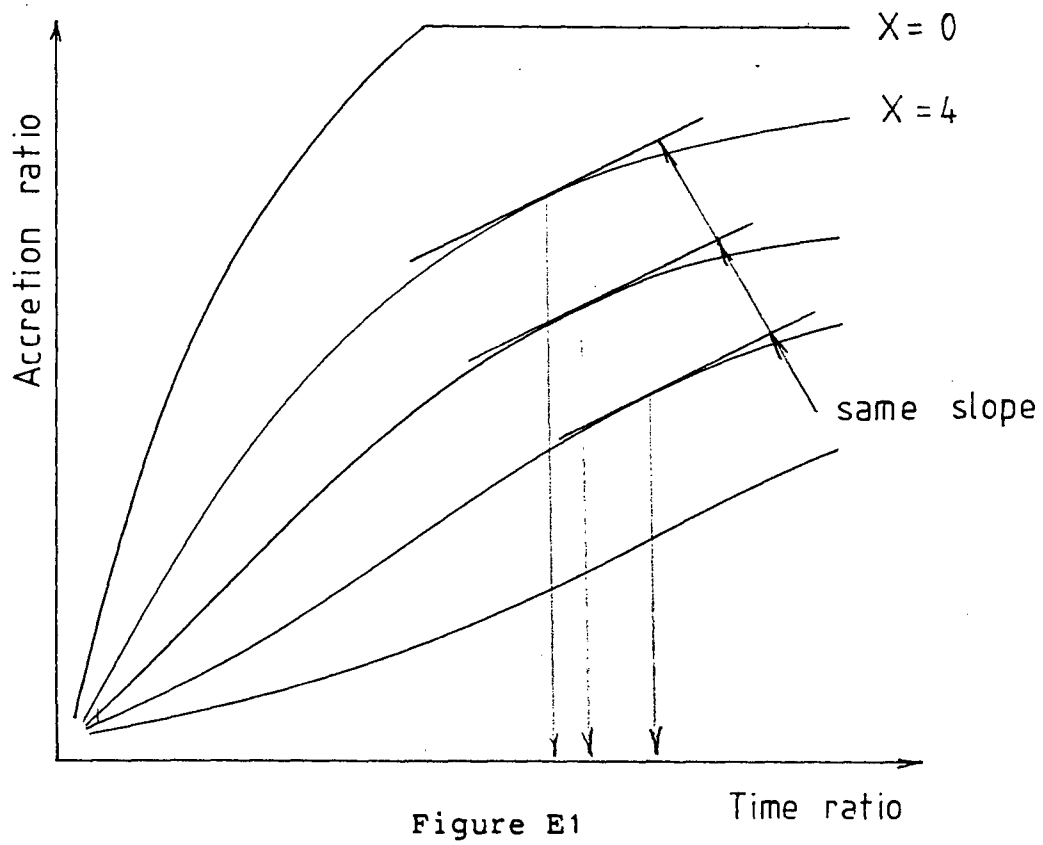

Figure E1

Appendix F

GRAIN SIZE DISTRIBUTION

FRASER RIVER SAND

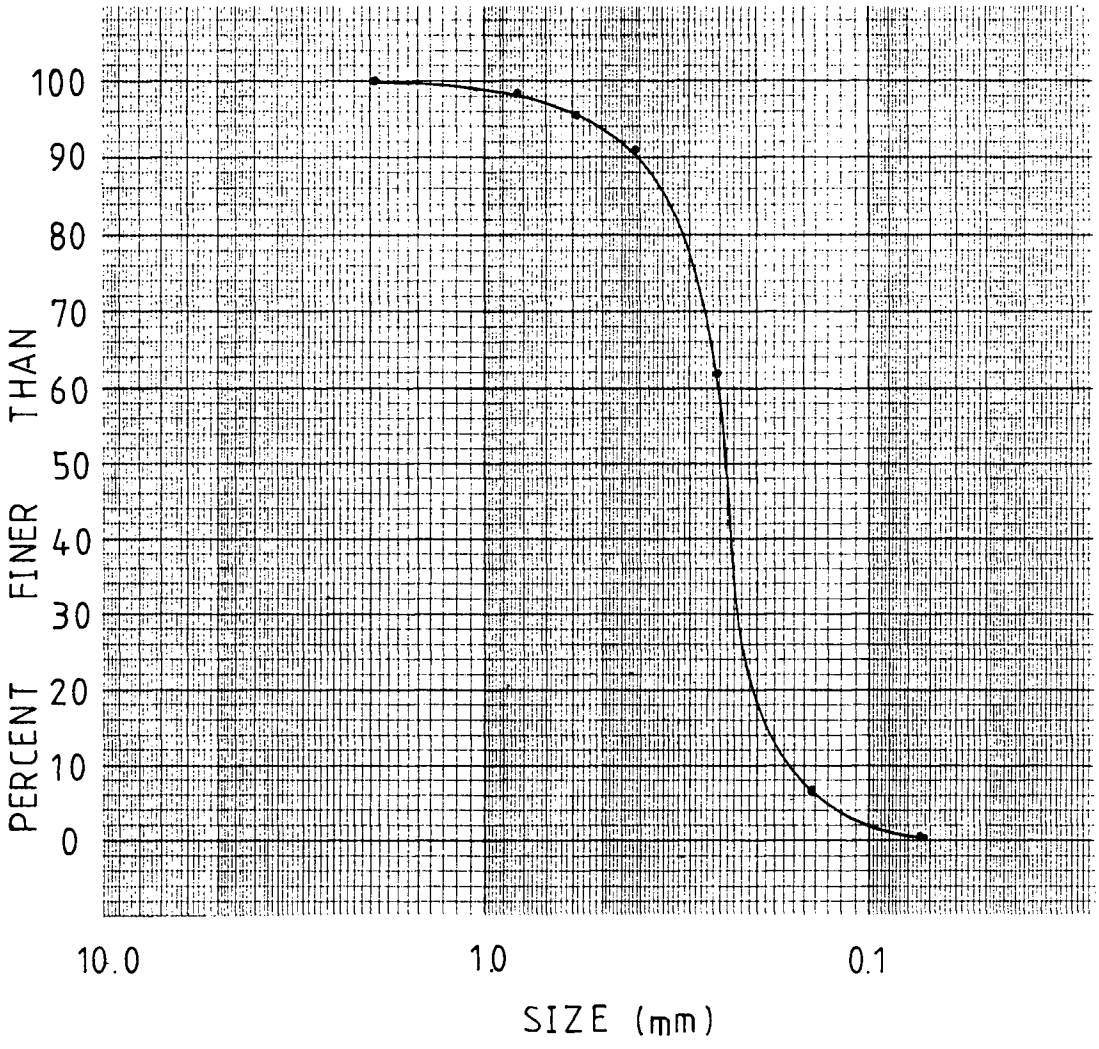

Appendix G

Program descriptions

The maximum dimensions of the study are are:

NX = 100
NY = 100

Input of the program consists of program option and data. The units used in the program are in SI. (ie metre, kilogram, second).

Card 1 NX,NY,DX,DY,T,SWL,DT

NX,NY - are two integers specifying the maximum number of cells in the study area. The definitions are shown in figure 3.2.

DX,DY - are the cell width and length.

T - the wave period of the imposed wave condition.

SWL - the still water level from shore datum as shown in figure G1.

DT - the modelling time interval.

Card 2 PERL,PERR

PERL - the permeability of the barrier on the upstream boundary.

PERR - the permeability of the barrier on the downstream boundary.

The value of 1.0 would indicate full permeability, ie no sediment will be retained, while 0.0 indicates full impermeability with no sediment moving across the barrier.

Card 3 KOUT,END,KALREF,OPTION,KJOFF

KOUT - this integer indicate the number of iterations before output of the shoreline results is printed. The purpose of this option is to reduce unwanted intermediate iterative output.

END - this is the final 'Time' in which the model will terminate its program.

KALREF - This integer is for controlling the routing of the program through the wave refraction and shoaling routine. This integer indicates the number of iterations before the refraction and shoaling routine is called. The primary purpose of this is to study the effect of wave refraction and shoaling on the results.

OPTION - this is a program option variable where 1.0 indicates a detailed output which includes wave refraction results and shoreline change results. The output file is attached to I/O unit 6. Any other number would yield only the shoreline change results, the output is then to I/O unit 7.

KJOFF - this integer controls the looping of the on-offshore routine in the program. The integer for this variable will result in calling the on-offshore routine after 'KJOFF' interations.

Card 4 ANGLE,WAVEHT

ANGLE, WAVHT - this two arrays will define the offshore wave angle and wave height. The program input card is formatted to read 10 number per card (ie five pairs of ANGLE and WAVEHT). If the value of NY is say 30, then there should be 6 cards to define all the offshore wave angle and wave height.

Card 5 RDEPTH

RDEPTH - this is an array which defines the topographical depth of the study area with respect to the shore datum (see figure G1). For every point in the overall grid, there is one RDEPTH. The input of this RDEPTH begins at I = 1, J=1 and ends at I = XN, J = YN (see figure 3.2). The number of variables per card is formatted at 10 in the program.

Card 6 WHI,WAI,TI

WHI - the initial offshore wave height.

WAI - the initial offshore wave angle.

TI - the initial wave period.

These variables are different from those wave height, wave angle and period mentioned earlier. These variables are the initial condition and are use to calibrate the initial equilibrium profile in the on-offshore routine (see chapter 6).

Card 7 FV,BD

FV - is the fall velocity of the D size of the sediment.

BD - is the decay constant of the profile change (see chapter 5 and 6).

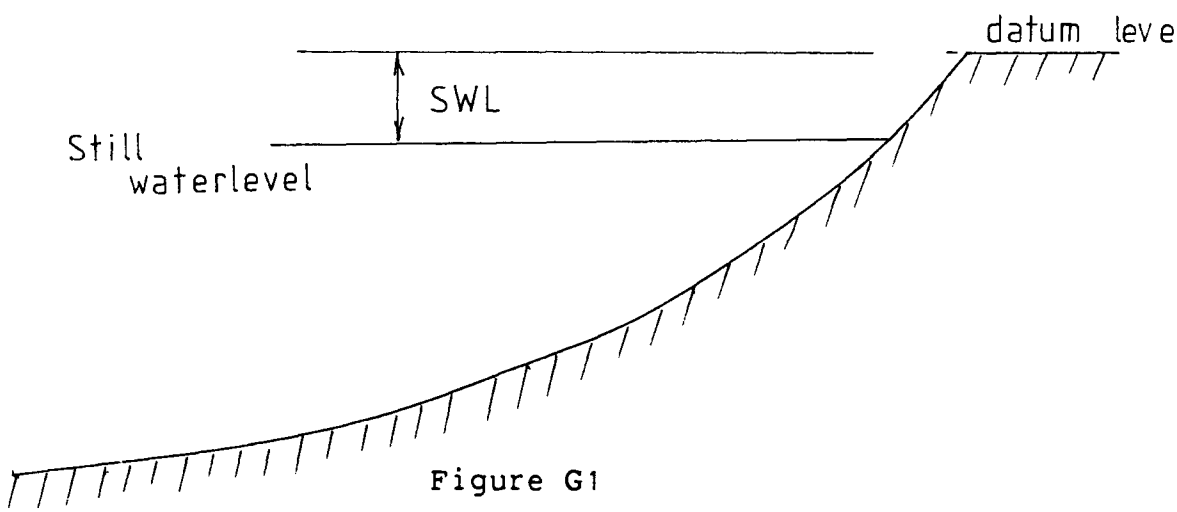

Figure G1

The uncompiled and compiled versions of the program are available in the Civil Engineering department program library, University of British Columbia. The file names are

SHOREC - for the compiled version and
SHORE - for the uncompiled version.

To run the program type the following command:

```
$RUN SHOREC 5=DATA 6=-6 7=-7
```

DATA - is the data file containing all the data as described in the earlier section.

-6 - is the output file when the variable 'option' is specified as 1.0.

-7 - is the output file when the variable 'option' is specified as otherwise.

To obtain a listing of the program or the output file, type:

```
$LIST 'Filename'
```

'Filename' is the name of the file, (eg SHORE or -6).